

THE KINETICS OF COLLOIDAL AGGREGATION

by

MARK STANDER BOWEN

Department of Physics
Massachusetts Institute of Technology
Cambridge, Massachusetts

February 1985

THE KINETICS OF COLLOIDAL AGGREGATION

by

MARK STANDER BOWEN

B.S. Physics, Massachusetts Institute of Technology
(1980)

SUBMITTED IN PARTIAL FULFILLMENT OF THE

REQUIREMENTS FOR THE DEGREE OF

DOCTOR OF PHILOSOPHY

at the

MASSACHUSETTS INSTITUTE OF TECHNOLOGY

February 1985

© Massachusetts Institute of Technology 1985

Signature of Author:.....
Department of Physics, January 11, 1985

Certified by:.....
Professor Richard J. Cohen
Thesis Supervisor

Accepted by:.....
Professor George F. Koster
Chairman, Graduate Committee
Department of Physics

THE KINETICS OF COLLOIDAL AGGREGATION

by

MARK STANDER BOWEN

Submitted to the Department of Physics on January 11, 1985, in partial fulfillment of the requirements for the degree of Doctor of Philosophy.

ABSTRACT

In this thesis I discuss the detailed form of the cluster size distribution as it evolves during the salt-induced aggregation of colloidal polystyrene microspheres. I also present a new experimental tool: an optical pulse particle size analyzer, which has made it possible to observe the microscopic size distribution in this system for the first time.

The optical pulse particle size analyzer is specifically designed to measure cluster size distributions in colloidal dispersions. In this instrument individual clusters pass single file through an optical flow channel, a portion of which is illuminated by a uniform laser beam. Clusters passing through the illuminated region scatter pulses of light, which are collected at angles of less than three degrees and imaged at the surface of a photomultiplier tube. Multichannel pulse-height analysis yields a histogram of the cluster size distribution.

The distinguishing feature of this instrument is its specific use of low angle light scattering for cluster size analysis. I demonstrate - both experimentally and theoretically - that at sufficiently low angles, pulse height is not only proportional to the square of the number of monomeric units in a cluster, but also quite insensitive to cluster shape and orientation. These two effects combine to give this instrument very high resolution in determining size differences between sub-micron clusters.

In experiments with salt-induced aggregation, I find that von Smoluchowski's kinetic theory of colloid flocculation describes both the shape and temporal evolution of the cluster size distribution at short times. This theory assumes that aggregation is irreversible and diffusion limited. The two particle association rate coefficient is a constant, independent of the size of the interacting clusters, and its magnitude may be deduced from the theory of Brownian motion with small corrections for inter-particle potentials (DLVO theory) and hydrodynamic interactions.

At very close to three reaction half-lives there is a sharp departure from von Smoluchowski theory. This departure is manifested by a change in the functional form of the cluster size distribution and a

decrease in the rate of aggregation in the sol. These effects are particularly strong at high particle concentrations. As the system approaches equilibrium it appears that a transition - quite reminiscent of a sol-gel transition in polymer systems - takes place: the total concentration of spheres in the sol steadily decreases, and some anomalously large clusters appear.

This later stage of the reaction may be interpreted in terms of an approach to equilibrium. If the bonds between spheres are weak, cluster fragmentation will be significant, and the equilibrium Flory-Stockmayer theory, applied to this colloidal system by Cohen and Benedek, may apply. This theory predicts a sol-gel transition. Assuming that von Smoluchowski theory gives the correct association coefficients, I deduce fragmentation coefficients from the Flory-Stockmayer equilibrium distribution and propose a rigorous theory to describe the complete temporal evolution of the cluster size distribution.

Recent developments in the kinetic theory of cluster formation have led to a deeper understanding of the connections between the kinetic and equilibrium theories. At the same time, there has been renewed interest in the critical properties of gelation and in the fractal nature of very large aggregates. Relevant aspects of these theories are discussed in detail.

Thesis Supervisor: Dr. Richard J. Cohen

Title: Hermann von Helmholtz Associate Professor
Harvard-MIT Division of Health Sciences and Technology
MIT Department of Physics

ACKNOWLEDGEMENTS

I consider myself extremely fortunate to have had an advisor with the humane wisdom and scientific insight of Richard Cohen. Ever since I stumbled into his office six years ago, I have been impressed with his sometimes uncanny abilities in dealing with the people in his laboratory. In every potentially difficult situation he has displayed such a basic good nature that conflicts have dissolved before they ever had the chance to amount to anything serious. It has been a pleasure to work with him. Richard's disarmingly laissez-faire attitude toward his students has sometimes made life difficult for me; but, in retrospect, I believe it has enhanced my ability to think critically and to solve problems creatively, and I wouldn't have had it any other way. I don't mean to imply that he has ignored my work. He has always helped me see the 'big picture'; and of course, many of the insights voiced in this thesis are his. Finally, I would like to thank him for the financial support, in the form of a Research Assistantship, that he has provided for my entire graduate education.

In a sense this thesis was written for my colleague, Michael Broide. He did a large part of the work described here; he is certainly my most discriminating reader; and I hope that he will benefit from the literature survey of chapter II and the proposals for future

experiments in chapter V. Michael's insistence upon understanding things to his own satisfaction has contributed to every aspect of our work. I mention here just a few of the numerous details he has attended to: he discovered the reason behind the 'ripple' on the signal; he worked out the bugs in the laminar flow cell; he first stated in logical terms the reason for the high resolution of low angle light scattering; and he conducted many experiments. He continues to improve the instrument, and I am sure that his meticulous approach to experimental physics will answer many important questions about colloidal aggregation. I wish him the best of luck in conducting experiments and in writing his thesis, and I know that I leave this project in good hands.

In many ways, this thesis springs out of the work of George Benedek. His analysis of antigen-antibody agglutination with Gustav von Schulthess provided a point of departure for these studies; his theoretical work with Richard Cohen informs most of chapters II and V; I built the prototype for the present instrument in his lab with his equipment; and I benefited greatly from working closely with his group for the first four years of this project. I acknowledge many useful discussions with him over the years.

I would also like to thank the various people who have helped me enjoy the sometimes frantic life here at MIT. Thea Paneth not only typed a significant portion of this text, but also provided entertaining (and refreshingly un-scientific) conversation and camaraderie as I procrastinated in the morning. Liz Connors fixed coffee and helped keep my spirits up during the desperate rush before my defense. Ron

Berger, Bo Saxberg, Solange Axelrod, Amy Ritzenberg, Jeff Madwed, Joe Smith, and in fact all of the people involved in Richard Cohen's various cardiovascular projects have helped create a stimulating and friendly research environment, in which there has been much cross-fertilization. And Joy Peetermans, John Clark, Loretta Mengel, George Thurston, and Zoran Djordjević, provided the same sort of esprit de corps when I first worked in George Benedek's lab.

A few of my friends helped me get my mind off my thesis when it was really necessary. In fact, I might even say that I finished this project in spite of their efforts. I was sorely tempted to go big wall climbing in Yosemite Valley with Joe Landry and Mike Tennican in late September. Next time I will. Other friends who have helped me keep my feet on (or off?) the ground are Paul Duval, Kevin and Alicia Shea, Marshall Randolph, Karen McLaughlin, and Glenna Shannon. I have appreciated their interest in my progress, and I plan to spend more time with all of them now that this thesis is out of the way.

I would like to express my deep gratitude to my parents for their steadfast support and continued good advice. They have always helped me keep a sense of priorities.

And finally, I would like to thank my wife, Craigen. I don't know why, but she always seems to believe in me, and this belief has had a profound effect. She has enriched so many aspects of my life that it is easy to face dry times in the lab, and she has seen to many particulars that may not pertain directly to my work, but that certainly improve its quality.

TABLE OF CONTENTS

	<u>PAGE</u>
ABSTRACT.....	i
ACKNOWLEDGEMENTS.....	iii
FIGURES.....	viii
TABLES.....	ix
CHAPTER I: INTRODUCTION.....	1
REFERENCES - CHAPTER I.....	7
CHAPTER II: KINETIC AND EQUILIBRIUM THEORIES OF AGGREGATION.....	10
2.1 Solutions to the Irreversible Coagulation Equations.....	12
2.1.1 Reaction Limited and Mobility Limited Reactions.....	14
2.1.2 The Bilinear Kernel.....	15
2.1.3 Cases A, B and C.....	19
2.1.3.1 Case A: von Smoluchowski's Theory of Diffusion Controlled Coagulation.....	21
2.1.3.2 Case B: Shear Flow and The A-R-B _∞ Polymer System.....	29
2.1.3.3 Case C: The R-A _∞ Polymer System.....	31
2.1.4 Critical Exponents and Scaling Relations.....	35
2.1.4.1 Values of the Exponents.....	42
2.1.5 Surface Bonding: $a_{ij} \propto (ij)^w$	46
2.1.6 Numerical Solutions to the Irreversible Equations.....	50
2.1.7 Computer Simulations.....	52
2.1.7.1 Cluster-Cluster Aggregation.....	53
2.2 Equilibrium Theories.....	59
2.2.1 Flory-Stockmayer Theory.....	60
2.2.1.1 The Most Probable Distribution.....	61
2.2.1.2 Gelation and Cyclic Bond Formation.....	67
2.2.2 Equilibrium Kinetics: the Reversible Coagulation Equations.....	70
2.2.3 Percolation Theory.....	75
2.3 Conclusions.....	79
REFERENCES - CHAPTER II.....	81
CHAPTER III: EXPERIMENTAL METHODS.....	84
3.1 The Optical Pulse Particle Size Analyzer.....	84
3.1.1 Light Scattering Theory.....	86
3.1.1.1 Scattering from Single Particles.....	87
3.1.1.2 Scattering from Clusters.....	91
3.1.2 Description of Instrument.....	95
3.1.2.1 Flow Cells.....	98
3.1.2.2 Signal Processing.....	100
3.1.3 Light Scattering Results.....	102

3.1.4 Discussion of Instrument.....	108
3.2 Materials and Experimental Procedures.....	113
REFERENCES - CHAPTER III.....	117
CHAPTER IV - RESULTS.....	119
4.1 The Shape of the Distribution.....	119
4.2 Average Cluster Size and the Bond Parameter b.....	126
4.3 Total Sphere Concentration and the Growth of Very Large Clusters.....	129
4.4 Relative Concentrations.....	132
4.5 Colloid Stability.....	134
CHAPTER V: DISCUSSION AND FUTURE PROSPECTS.....	137
5.1 The Nature of the Transition.....	139
5.2 Other Experimental Results.....	148
5.3 Future Experiments.....	152
REFERENCES - CHAPTER V.....	155
APPENDIX I: A Short Review of Colloid Stability Theory.....	157
APPENDIX II: Solution of Case A with Arbitrary Initial Conditions....	173
APPENDIX III: Coincidence Analysis.....	177
BIOGRAPHY.....	180
PUBLICATIONS.....	180

FIGURES

<u>Figure</u>	<u>Page</u>
3.1 Geometry for Rayleigh-Gans-Debye scattering	89
3.2 Comparison of Mie and Rayleigh scattering at 0°	92
3.3 Schematic illustration of the instrument	96
3.4 A closeup showing the range of scattering angles	97
3.5 A histogram of aggregated 450nm spheres	103
3.6 A histogram with a coincidence peak	104
3.7 A histogram of three different sized spheres	106
3.8 Monomer and dimer peaks of 710nm, and 1091nm spheres	107
3.9 A sequence of histograms illustrating aggregation	114
4.1 Time dependence of goodness of fit, E, for cases A, B, and C	120
4.2 Normalized mass fraction, nc_n/c_1 , at short times	121
4.3 The cluster size distribution early in the reaction	122
4.4 The cluster size distribution at intermediate times	123
4.5 The cluster size distribution at late times	124
4.6 The histogram for Figure 4.5	125
4.7 Time dependence of average cluster size at low concentration	127
4.8 Time dependence of average cluster size at higher concentration	128
4.9 Time dependence of bond parameter b at low concentration	129
4.10 Time dependence of bond parameter b at higher concentration	130
4.11 Time dependence of total sphere concentration c_o	131
4.12 Time dependence of c_n/c_1 at low concentration	133
4.13 Time dependence of c_n/c_1 at higher concentration	134
5.1 Fragmentation kernels for a 20-mer	143
A.2.1 Geometry for colloid stability theory	161
A.2.2 The potential at low salt concentration	164
A.2.3 The potential at the critical coagulation concentration	165
A.2.4 The potential at high salt concentration	166
A.2.5 Log(W) versus log(C)	168

TABLES

<u>Table</u>	<u>Page</u>
2.1 Monodisperse solutions to Cases A, B, and C.	20
2.2 Asymptotic forms for c_n/c_0 in Cases A, B, and C.	44
2.3 Exponent values for Cases A, B, and C, and the Bilinear kernel.	45
4.1 Experimental conditions and stability factors for four different preparations.	135

CHAPTER I

INTRODUCTION

Colloidal aggregation is a diverse phenomenon in and of itself, but it also serves as a model for the study of aggregation in all its forms. The theories of cluster formation and gelation described in this thesis have been applied with small changes in detail to processes as diverse as star formation in galaxies¹ and the aggregation of red cells in the blood to form rouleaux - long, cylindrical, occasionally branched, objects that - when viewed through a microscope - look very similar to rolls of coins.² The basic theoretical structures were originally developed for the subject of this thesis, colloidal flocculation,³ and for organic polymer formation,^{4,5} but important contributions have been made by mathematicians, aerosol chemists, meteorologists, astrophysicists, physical chemists, and condensed matter physicists. Specific processes include the formation of rain droplets in clouds,⁶ antigen-antibody agglutination reactions in immunology,^{7,8} the gelation of hemoglobin in sickle cell anemia,⁹ and the growth of porous rocks by mineral deposition. The effect of self polymerization on the catalytic activity of certain enzymes has also been studied.¹⁰ This gives some idea of the pervasiveness of aggregation phenomena.

Although the kinetic theory of polymerization was first formulated near the turn of this century and the equilibrium theory was developed in the 1940's, only recently have the connections between these theories been made rigorous.¹¹ Also, with the development of renormalization group theory and a growing interest in critical phenomena, there has been renewed interest in aggregation, because certain aggregating systems exhibit a phase transition. Some theorists have proposed that gel formation in polymeric systems might lie in the same universality class as the formation of an infinite cluster in percolation theory.¹²

As theory has evolved, so have the quality of experimental tests. Electron microscopy has produced actual pictures of the very large aggregates;¹³ static scattering measurements have determined the scaling properties of polymers and colloidal aggregates over a wide size range;¹⁴ dynamic light scattering has been used to observe both the structure of the particles and the kinetics of the reaction;^{15,16} and single particle techniques, similar to the one used here, have measured the detailed cluster size distribution itself in antigen-antibody systems.⁸ Also, in the gray area between theory and experiment, a variety of computer simulations have modeled addition reactions and cluster-cluster aggregation in irreversible systems.¹⁷

In this thesis, I describe experimental measurements of the detailed cluster size distribution as it evolves during so-called rapid coagulation: the salt induced aggregation of colloidal microspheres. It was precisely this phenomenon that first motivated von Smoluchowski to develop a kinetic theory for cluster formation in

1916.³ Even today his basic equations are the subject of much theoretical work. It was Zsigmondy, a coinventor of the ultramicroscope and one of the early experimentalists in colloid science, who suggested the physical model which von Smoluchowski eventually used to explain colloidal coagulation.¹⁸ In fact, this was one of the earliest applications of the modern theory of Brownian motion. Zsigmondy verified the general details of the coagulation theory by measuring the half-life of the reaction - actually counting, by eye with an ultramicroscope, the total concentration of particles as it decreased with time in a coagulating gold sol.¹⁹

Since the beginnings of colloid science, a major goal has been to develop a quantitative explanation for the stability of sols. When the dissolved concentration of electrolyte reaches a certain sharply defined level, known as the critical coagulation concentration, the initially distinct units in certain sols flocculate, some eventually producing visible precipitates. It had been known since the turn of the century that these lyophobic sol particles are charged and that the critical coagulation concentration depends strongly upon the valency of the dissolved electrolyte,²⁰ but it was not until the 1940's that a quantitative theory for stability, based upon the shape of the potential between two particles, emerged.²¹

Although methods less tedious than Zsigmondy's eventually evolved for testing colloid stability theory,²² they generally measured the rate of change of the particle concentration, just as he did, or some other weighted average of the cluster size distribution. Since one must assume a particular mathematical form for the distribution in

order to draw information from these bulk quantities, the verification of colloid stability theory has always rested tacitly upon von Smoluchowski's original coagulation theory. Only with the development of single particle techniques, such as ours, is it possible to test von Smoluchowski's theory and probe the monomer-monomer interaction directly. The monomer-monomer interaction is the only one that colloid stability theory analyzes explicitly. With bulk techniques higher order interactions complicate the data; hence, our instrument may be used to test stability theory more precisely. In fact, I find in this thesis that von Smoluchowski theory is accurate for the first three half-lives of the reaction, so the assumptions of stability theory seem valid - at least at the low particle concentrations considered here.

In the so-called modern theories of aggregation and gelation¹³ one assumes a 'scaling' form for the cluster size distribution. It is possible to account for polydispersity in bulk scattering if this scaling form holds,¹⁶ but it is still important to determine the form independently.

Recently, Cohen and Benedek²³ have drawn the connection between a coagulating colloidal sol and a condensing polymer system consisting of f -functional ($R-A_f$) monomeric units in the limit of high functionality ($f \rightarrow \infty$). They suggest that the canonical form of the cluster size distribution might change dramatically as the system evolves from a state of kinetic evolution to thermodynamic equilibrium. Flory⁴ and Stockmayer⁵ first proposed the equilibrium theory which has traditionally been applied to the polymer system. I will discuss the

equilibrium state in the context of Flory-Stockmayer theory, as it has been cast into the language of statistical mechanics by Cohen and Benedek.

If there are sufficiently strong interparticle bonds, Flory-Stockmayer theory predicts a sol-gel transition in the isomorphic polymer system at high monomer concentrations. Critical exponents may be used to characterize the cluster size distribution, the growth of the gel fraction, and many other features of the system near the gel point.^{12,23} Also, von Smoluchowski's original coagulation equations become singular in certain regimes, and these singularities are precisely analogous to the growth of a gel phase in the equilibrium theory.²⁴ With appropriate choices for the association and dissociation coefficients, solutions to the coagulation equations correspond precisely to the well-known equilibrium solutions of Flory and Stockmayer.

Although most computer simulations are concerned with the static structure of large aggregates, the recent work of Jullien, Kolb, and Botet²⁵ on so-called cluster-cluster aggregation has focussed upon the cluster size distribution as well. Under certain conditions this model gels. Cluster size distributions from simulations agree with numerical solutions to the coagulation equations. The association kernel is based upon a phenomenological model that includes the effects of diffusion and structure. The presence of a gel changes the shape of the cluster size distribution, and the gel has a different fractal dimension than the finite sized clusters.

In this thesis, I present what I think is convincing evidence that a transition similar to the sol-gel transition takes place in this colloidal system. The shape of the cluster size distribution changes - as Cohen and Benedek and Jullien et al. suggest it might; and some anomalously large clusters appear late in the reaction. It seems that the cluster size distribution becomes bimodal at late times. The system is particularly rich for study, since different mechanisms control the clustering process during its early and late stages, and since our experimental instrument allows us to observe the kinetics of the phase transition in detail. I discuss the early stages of the reaction in terms of kinetics and the late stages in terms of equilibrium. I also discuss the applicability of cluster-cluster aggregation and propose methods for understanding the particularly interesting intermediate regime.

In the next chapter, I review the various kinetic and equilibrium theories in detail. This serves three purposes: it provides a physical motivation for the mathematical forms against which I compare my results later; it allows me to discuss them in a broad context; and it will hopefully provide motivation for future theoretical and experimental work - mostly in my laboratory, but perhaps elsewhere as well. Chapter III consists of a thorough description of the optical pulse particle size analyzer and my experimental methods, with a short theoretical section on light scattering. Chapter IV presents experimental results, and Chapter V concludes with a discussion and some suggestions for future work.

REFERENCES - CHAPTER I

1. Barrow, J.D., J. Phys. A: Math. Gen., **14**, 729 (1981).
Silk, J. and White, S.D., Astrophys. J., **223**, L59 (1978).
2. Samsel, R.W. and Perelson, A.S., Biophys. J., **37**, 493 (1982).
Perelson, A.S. and Wiegel, F.W., Biophys. J., **37**, 515 (1982).
Wiegel, F.W. and Perelson, A.S., J. Stat. Phys., **29**, 813 (1982).
Samsel, R.W. and Perelson, A.S., Biophys. J., in print.
Hendriks, E.M. and Ernst, M.H., J. Colloid Interface Sci., **97**, 176 (1984).
Perelson, A.S. and Samsel, R.W., in Reference 17.
3. von Smoluchowski, M., Phys. Z., **17**, 585 (1916).
von Smoluchowski, M., Z. Phys. Chem., **92**, 129 (1917).
4. Flory, P.J., J. Am. Chem. Soc., **63**, 3083 (1941).
Flory, P.J., J. Am. Chem. Soc., **63**, 3091 (1941).
Flory, P.J., J. Am. Chem. Soc., **63**, 3096 (1941).
Flory, P.J., "Principles of Polymer Chemistry", Cornell University Press, Ithaca, 1953.
5. Stockmayer, W.H., J. Chem. Phys., **11**, 45 (1943).
Stockmayer, W.H., J. Chem. Phys., **12**, 125 (1944).
6. Fuchs, N.A., "The Mechanics of Aerosols", Pergamon Press, Oxford, 1964.
Drake, R.L., in "Topics in Current Aerosol Research" (G.M. Hidy and J.R. Brock, Eds.), Vol. 3, Pergamon Press, New York, 1972.
7. Goldberg, R., J. Am. Chem. Soc., **74**, 5715 (1952).
Singer, J.M., Oreskes, I., Hutterer, F., and Ernst, J., J. Ann. Rheumat. Disease, **22**, 424 (1963).
Cohen, R.J. and Benedek, G.B., Immunochemistry, **12**, 349 (1975).
von Schulthess, G.K., Cohen, R.J., Sakato, N., and Benedek, G.B., Immunochemistry, **13**, 955 (1976).
von Schulthess, G.K., Cohen, R.J. and Benedek, G.B., Immunochemistry, **13**, 963 (1976).
Cohen, R.J., von Schulthess, G.K. and Benedek, G.B., Ferroelectrics, **30**, 185 (1980).
8. von Schulthess, G.K., Benedek, G.B. and De Blois, R.W., Macromolecules, **13**, 939 (1980).
von Schulthess, G.K., Benedek, G.B., and De Blois, R.W., Macromolecules, **16**, 434 (1983).
von Schulthess, G.K., Ph.D. Thesis, M.I.T. (unpublished), 1979.
Johnston, D.F., Ph.D. Thesis, M.I.T. (unpublished), 1983.
Johnston, D.F. and Benedek, G.B., in Reference 17.
9. Cheetham, R.C., Huehns, E.R., and Rosemeyer, M.A., J. Mol. Biol., **129**, 45 (1979).

10. Cohen, R.J. and Benedek, G.B., J. Mol. Biol., **108**, 129 (1976).
Cohen, R.J. and Benedek, G.B., J. Mol. Biol., **108**, 151 (1976).
Cohen, R.J. and Benedek, G.B., J. Mol. Biol., **129**, 37 (1979).
11. Spouge, J.L., Macromolecules, **16**, 121 (1983).
Spouge, J.L., J. Stat. Phys., **31**, 363 (1983).
Spouge, J.L., J. Phys. A: Math. Gen., **16**, 767 (1983).
Van Dongen, P. and Ernst, M.H., J. Phys. A: Math. Gen., **16**, L327 (1983).
Van Dongen, P. and Ernst, M.H., in Reference 17.
Hendriks, E.M., "Cluster Size Distributions in Equilibrium",
preprint, 1984.
Van Dongen, P. and Ernst, M.H., "Kinetics of Reversible Polymerization",
preprint, 1984.
12. Stauffer, D., J. Chem. Soc., Faraday Trans. 2, **72**, 1354 (1976).
de Gennes, P.G., "Scaling Concepts in Polymer Physics", Cornell
University Press, Ithaca, 1979.
Stauffer, D., Phys. Reps., **54**, 1 (1979).
Stauffer, D., Coniglio, A., and Adam, M., Adv. Poly. Sci., **44**,
103 (1982).
13. Forrest, S.R. and Witten, T.A., Jr., J. Phys. A: Math. Gen., **12**,
L109 (1979).
Weitz, D.A. and Oliveria, M., Phys. Rev. Lett., **52**, 1433 (1984).
Weitz, D.A. and Huang, J.S., in Reference 17.
14. Shaeffer, D.W., Martin, J.E., Wiltzius, P.W., and Cannell, D.S.,
in Reference 17.
Shaeffer, D.W., Martin, J.E., Wiltzius, P.W., and Cannell, D.S.,
Phys. Rev. Lett., **52**, 2371 (1984).
Shaeffer, D.W. and Keefer, K.D., Mat. Res. Soc. Symp. Proc., **32**, 1
(1984).
Shaeffer, D.W. and Keefer, K.D., "Origin of Fractal Structures
in Amorphous Materials", preprint, 1984.
Sinha, S.K., Freltoft, T., and Kjems, J., in Reference 17.
15. Weitz, D.A., Huang, J.S., Lin, M.Y., and Sung, J., Phys. Rev. Lett.,
53, 1657 (1984).
Cummins, P.G., Staples, E.J., and Thompson, L.G., J. Colloid Interface
Science, **92**, 189 (1983).
16. Martin, J.E. and Schaefer, D.W., "Dynamics of Fractal Colloidal
Aggregates", preprint, 1984.
Martin, J.E. and Ackerson, B.J., "Static and Dynamic Scattering
from Fractals", preprint, 1984.
17. Family, F. and Landau, D.P., eds., "Kinetics of Aggregation and
Gelation", North Holland, Amsterdam, 1984.
18. Chandrasekhar, S., Rev. Mod. Phys., **15**, 1 (1943), p. 60.
19. R. Zsigmondy, Z. Phys. Chem., **92**, 600 (1917).
20. Kruyt, H.R., "Colloid Science", Vol. I, Elsevier, Amsterdam, 1952,

- Chap. I, section 1.b.2, and references therein.
21. Derjaguin, B.U. and Landau, L., *Acta Physicochim. URSS*, **14**, 633 (1941).
Verwey, E.J. and Overbeek, J. Th. G., "Theory of the Stability of Lyophobic Colloids", Elsevier, Amsterdam, 1948.
 22. Lichtenbelt, W. Th., Pathmamanoharan, C., and Wiersema, P.H.,
J. Colloid Interface Sci., **49**, 281 (1974).
Lips, A., Smart, C., and Willis, E., *Trans. Faraday Soc.*, **67**,
2979 (1971).
Lips, A. and Willis, E., *J. Chem. Soc. Faraday*, **69**, 1226 (1973).
 23. Cohen, R.J. and Benedek, G.B., *J. Phys. Chem.*, **86**, 3696 (1982).
 24. Ziff, R.M., *J. Stat. Phys.*, **23**, 241 (1980).
Ziff, R.M. and Stell, G., *J. Chem. Phys.*, **73**, 3492 (1980).
 25. Meakin, P., *Phys. Rev. Lett.*, **51**, 1119 (1983).
Kolb, M., Botet, R., Jullien, R., *Phys. Rev. Lett.*, **51**, 1123 (1983).
Botet, R. and Jullien, R., *J. Phys. A: Math. Gen.*, **17**, 2517 (1984).
Jullien, R., Kolb, M., and Botet, R., in Reference 17.
Botet, R., Jullien, R. and Kolb, M., *J. Physique Lettres*, **45**,
L211 (1984).
Kolb, M., *Phys. Rev. Lett.*, **53**, 1653 (1984).
Botet, R., Jullien, R., and Kolb, M., *Phys. Rev.*, **A30**, 2150 (1984).

CHAPTER II

KINETIC AND EQUILIBRIUM THEORIES OF AGGREGATION

As I pointed out in the introduction, colloid flocculation was originally formulated in terms of kinetics. This chapter emphasizes kinetics more than equilibrium, primarily because it is easiest to interpret my experimental results in this context. Also, there is no clear indication that the process studied here ever reaches equilibrium.

However, the statistical Flory-Stockmayer theory, as reformulated by Cohen and Benedek, provides a compelling equilibrium model. Moreover, the kinetic analogue of Flory-Stockmayer theory has been explored in such great detail that it has shed light on the basic assumptions of the equilibrium theory. The best paradigm for this 'unified' theory is polymer formation. Hence, I will often use a sort of chemical language to describe colloidal aggregation when, in fact, chemistry may have little actual bearing. Despite the clear parallels in many aggregating systems, the 'universality classes' or 'relevant fields' of this problem - to borrow from the terminology of thermodynamic phase transitions - have yet to be defined.

Unfortunately, there has been such an emphasis upon the intriguing mathematical connections between kinetics and equilibrium that the

physical differences between these two regimes have been largely overlooked. A very delicate kinetic balance obtains at equilibrium. Recent solutions to the reversible kinetic equations have assumed that this balance applies at all times, but there is no physical reason for this to be true. Since one of the most important results of this thesis is the fact that different kinetic mechanisms operate during the early and late stages of colloidal aggregation, I emphasize in this chapter the differences as well as the interrelations between kinetics and equilibrium.

Most theoretical advances in the kinetic theory have been obtained with the irreversible coagulation equations. Explicit solutions of the reversible case have added little in the way of new physics; they merely rescale time. For this reason, most of this chapter regards the irreversible case. Connections are made with Flory-Stockmayer theory through out, and reversibility is discussed after the equilibrium theory - essentially because no one has yet solved the reversible equations without knowing the solution before hand from the equilibrium theory.

I discuss percolation, scaling, and critical exponents, but not in great depth, because these concepts concern primarily very large aggregates and the gel phase - precisely the features of the system which my experiments don't measure. The emphasis through out this chapter is upon theories of the cluster size distribution.

2.1 SOLUTIONS TO THE IRREVERSIBLE COAGULATION EQUATIONS

At low enough particle concentrations, two primary processes contribute to the kinetic evolution of the cluster size distribution: the collision of two clusters to form a larger cluster containing the sum of the particles in each, and the dissociation of a large cluster into two smaller ones. At high concentrations three body interactions and restricted mobility come into play. I will estimate the levels at which these effects become important later, but throughout this section I will take the dilute approximation.

When the bonds formed between particles have effectively infinite strength, coagulation will be unidirectional, and dissociation may be ignored. The kinetics are then determined by the following infinite set of coupled differential equations, first proposed by von Smoluchowski in 1916.^{1,2} The rate of change of c_n , the concentration of clusters of size n , will be given by

$$\frac{dc_n}{dt} = 1/2 \sum_{k=1}^{n-1} a_{n-k,k} c_{n-k} c_k - \sum_{k=1}^{\infty} a_{nk} c_n c_k \quad [2.1]$$

where a_{ij} is the two particle association coefficient or kernel, which determines the rate at which i -mers and j -mers react to form $(i+j)$ -mers. The matrix a_{ij} is symmetric under the exchange of indices i and

j. I will often refer to equations [2.1] as the discrete coagulation equations.

The first term represents the formation of n-mers, due to the coagulation of smaller clusters; the factor of 1/2 accounts for the fact that each possible combination is counted twice in the sum. The second term represents the disappearance of n-mers due to coagulation with all other species in solution.

In some systems, such as condensing water droplets in clouds, aggregates may have a continuous range of sizes. Then the continuous analogue of [2.1] is used:

$$\frac{\partial f(x,t)}{\partial t} = \frac{1}{2} \int_0^x a(x-y,y) f(x-y,t) f(y,t) dy - \int_0^\infty a(x,y) f(x,t) f(y,t) dy$$

$$\text{with } f(x,0) = g(x) \quad [2.2]$$

where $f(x,t)$ is the number of particles with mass x at time t . Equation [2.1] is the special case of [2.2] with $g(x)$ set to a series of delta-functions in x .

After the coagulation equations are specified, virtually all of the physics of the problem is contained in the association coefficients. Their dependence upon i and j is the most important factor in determining both the mathematical form of the cluster size distribution and the possibility for gel formation. Various physical models dictate the form of a_{ij} , but they have been kept relatively simple in order to facilitate solution of the coagulation equations themselves.

2.1.1 - Reaction Limited and Mobility Limited Reactions

Von Smoluchowski deduced a_{ij} for colloidal flocculation utilizing the theory of Brownian motion; he then solved [2.1]. In his original model (described in section 2.1.3.1), clusters stick each time they collide, but diffusion determines the rate at which they collide. He also considered diffusion in shear flow (section 2.1.3.2), where he found a different functional form for a_{ij} . Since coagulation rates are determined entirely by mobility in these models, I refer to them as mobility limited reactions.

On the other hand, polymer chemists generally assume that molecules collide several times before finding the correct orientation for bonding. In this case reaction times increase, because they are limited by stoichiometry. Taking the limit of infinite mobility, polymer chemists construct the kernel using two basic assumptions:⁴

- 1) all unbonded functional groups on an i -mer will bind with equal probability to any unbonded group on a j -mer, and
- 2) the total probability that an i -mer and a j -mer will bind is proportional to the number of ways the two can form a bond.

These two assumptions provide the fundamental connection between reaction limited kinetic theories and Flory-Stockmayer theory. They essentially restate Flory's principle of equal reactivity (section 2.2.1) in a language more appropriate to kinetics.

It is difficult to estimate the absolute magnitude of a_{ij} in reaction limited reactions - only that it will be smaller than in the mobility limited case. The functional form of the kernel is the distinguishing feature of the reaction.

Noyes' shows that when both mobility and chemical bonding control the reaction, the absolute rate coefficient is given by

$$a_{ij} = \frac{a_{ij}^r \cdot a_{ij}^m}{a_{ij}^r + a_{ij}^m} \quad [2.3]$$

where a_{ij}^r is the appropriate reaction limited kernel, and a_{ij}^m is the appropriate mobility limited kernel. In other words, the two effects add in parallel. If a_{ij}^r is much larger than a_{ij}^m then $a_{ij} \approx a_{ij}^m$ and vice versa. Unfortunately, the coagulation equations have only been solved in one or the other limiting case.

In the next few sections, we treat specific forms for a_{ij} ; some pertain directly to colloid flocculation, and others have helped elucidate fundamental properties of the coagulation equations themselves.

2.1.2 - The Bilinear Kernel

The most general form for a_{ij} that has ever been solved exactly is the so-called bilinear kernel:

$$a_{ij} = A + B(i+j) + Cij \quad [2.4]$$

where A, B, and C are positive constants.[†]

In reaction limited polymeric systems, the bilinear kernel corresponds to the general A_g-R-B_{f-g} model, in which monomers have g A-type functional groups and f-g B-type functional groups, and bonding occurs between A's and B's only. Two of the three polymer systems I will discuss are special cases of the A_g-R-B_{f-g} model, and the third has the same critical behavior as the A_g-R-B_{f-g} model. Also, the diffusion limited theory of colloid flocculation is a special case of the bilinear kernel, so a general solution for this kernel is of great practical interest.

Even though Flory⁷⁻¹⁰ and Stockmayer^{11,12} had discussed gel formation in aggregating systems in the early 1940's, and Stockmayer¹¹ had even outlined the connections between the equilibrium equations and the coagulation equations, it seems that it wasn't until 1972¹³ that irregularities in solutions to the coagulation equations were first identified with gel formation.

To solve the coagulation equations one first solves the moment equations obtained by summing (or integrating) [2.1] (or [2.2]). The k^{th} power moment $M_k(t)$ is defined as

[†] These constants may depend upon other factors besides i and j, such as time - in which case the variable t may have to be renormalized throughout this section, but everything else will remain unchanged.*

$$M_k(t) = \sum_{n=1}^{\infty} n^k c_n(t) \quad [2.5]$$

or, in the continuous case,

$$M_k(t) = \int_0^{\infty} x^k f(x,t) dx \quad [2.6]$$

The zeroth moment corresponds to the total number of particles in the system, while the first corresponds to the total mass, which one might naively expect to remain constant.

If the coefficient C in [2.4] is non-zero, the total mass in the sol will begin to drop at some finite time, which we shall call the critical time t_c . At the same time, the second and higher moments diverge. This happens in both the continuous and discrete cases. Early workers^{3,14,15} thought that kernels of the form $a_{ij} = Cij$ were unphysical because they lead to such events. Later, these events were identified with the appearance of a gel phase.

Ziff¹⁶ explicitly calculates the rate (per unit volume) at which clusters smaller than size L form clusters greater than size L :

$$- \frac{d}{dt} \sum_{k=1}^L k c_k \quad [2.7]$$

Taking the limit $L \rightarrow \infty$, he shows that a superparticle with infinite mass begins to form at the critical time.

The discrete coagulation equations were first solved with

monodisperse initial conditions ($c_n(t=0) = c_0 \delta_{n1}$) and arbitrary, positive A, B, and C by Trubnikov¹⁷ in 1971. His results are difficult to use, and it is also unclear whether all possible values of A, B, and C are accounted for in his solution. Trubnikov also considers case C to be unphysical because of the irregularities previously mentioned. In a series of three papers, Spouge¹⁸⁻²⁰ has recently presented a complete pre-gelation solution with critical times for all positive values of A, B, and C. He also makes some very interesting connections, which I touch upon in section 2.2.2, between the reaction limited kinetic theory and Flory-Stockmayer theory. Van Dongen and Ernst^{21,22} have found a solution that is valid both before and after gelation. (We will consider various kinetic models for gelation in section 2.1.3.3) They have also included reversible processes.

Drake³ first calculated critical times (although he was then unaware of their precise meaning) for the continuous coagulation equations. Although he also presents a formal solution for some cases, his results are generally difficult to use for computation. Spouge²³ has recently presented computationally useful pregelation solutions as well as critical times and has also completed a solution using the theory of branching processes.²⁴

Generally, expressions for the cluster size distribution in both the discrete and continuous cases are not in closed form. Also, since this kernel has three variable parameters, it is probably possible to fit these solutions to a wide range of experimental findings, and it is unclear what the physical significance of the result will be. However, we do have ample physical motivation for considering the

following special cases of the bilinear kernel:

$$\text{Case A: } a_{ij} = A \quad [2.8a]$$

$$\text{Case B: } a_{ij} = B(i+j) \quad [2.8b]$$

$$\text{Case C: } a_{ij} = Cij \quad [2.8c]$$

Cases A and C are particularly interesting to us, because - as I shall show - case A corresponds to diffusion controlled coagulation, and case C is the reaction limited kernel for our possible equilibrium system.

The general bilinear case is most useful for its broad features: the conditions necessary for gelation, its close relationship to Flory-Stockmayer theory, and its critical properties. Near the critical time, it leads to the same universal behavior as case C, which is discussed in section 2.1.3.3.

2.1.3 - Cases A, B, and C

With monodisperse initial conditions each of these cases produces a unique form for the cluster size distribution (see Table 2.1).² The distributions are parameterized by two variables: c_0 , the total concentration of monomeric units initially introduced into solution, and b , the bond parameter. All of the time dependence is contained in b ,

Case	A	B	C
a_{ij}	A	$B(i+j)$	Cij
c_n	$c_0(1-b)^2 b^{n-1}$	$c_0(1-b)e^{-nb} \frac{(nb)^{n-1}}{n!}$	$c_0 e^{-2nb} \frac{(2nb)^{n-1}}{n \cdot n!}$
$b(t)$	$(t/\tau_A)/(1+\tau_A)$	$1-e^{-t/\tau_B}$	t/τ_C
range of b	$0 < b < 1$	$0 < b < 1$	$0 < b < 1/2$
time constant	$\tau_A = 2/(Ac_0)$	$\tau_B = 1/(Bc_0)$	$\tau_C = 2/(Cc_0)$

Table 2.1

Solutions to the irreversible coagulation equations for cases A, B, and C with monodisperse initial conditions ($c_n(t=0) = c_0 \delta_{n1}$).

so that in each case the functional form of the cluster size distribution is time invariant. In cases A and B, b increases monotonically with time and asymptotically approaches unity. In case C, the gel point occurs when b reaches a value of 1/2. The kinetic equations must be modified to include interactions between the sol and gel phases, but the functional form of the cluster size distribution in the sol remains unchanged in all known post-gelation models (see section 2.1.3.3).

For cases A and B, and for case C below the gel point, b is given by

$$b = \frac{\sum_{n=1}^{\infty} (n-1)c_n}{\sum_{n=1}^{\infty} nc_n} = 1 - \frac{\sum_{n=1}^{\infty} c_n}{\sum_{n=1}^{\infty} nc_n} = 1 - 1/\bar{n} \quad [2.9]$$

where \bar{n} is the mean cluster size in the sol. For a system composed entirely of monomers, $b = 0$.

The kinetic theory makes no assumption regarding the structure of the evolving clusters; however, if one were to assume that the clusters contain no intra-cluster bonds or cycles, then Equation [2.9] would provide a simple physical interpretation for b . Since there are $n-1$ bonds in an acyclic n -mer, b would represent the ratio of the total number of bonds to the total number of monomeric units in the system. In fact, b is exactly the minimum value of this ratio. This final assumption is an integral part of Flory-Stockmayer theory.

2.1.3.1 - Case A: Von Smoluchowski's Model For Diffusion Controlled Coagulation

In this first quantitative model for coagulation,^{1,2} particles undergo Brownian motion, unhindered by other particles until they come within some 'sphere of influence' of each other, at which point they adhere. In the dilute approximation, only two particle collisions are considered. Although the physics behind the sphere of influence was not well understood when this model was introduced, von Smoluchowski's simple treatment explains a large part of the phenomenology of colloidal

aggregation, even predicting the reaction rate to within a factor of two.

Dostal and Raff²⁶ were the first to show that case A also describes the reaction limited linear aggregation of bifunctional (R-A₂) polymers. Since there are always two free ends on such linear polymers - no matter what their size - the association kernel remains constant under the two assumptions of section 2.1.1. Perelson²⁷ has also applied this case to antigen-antibody reactions.

To determine a_{ij} for this model, we consider the relative diffusion of non-interacting particles in an isotropic medium. This problem is also treated in detail by Drake² and Chandrasekhar.²⁸ Clusters will be treated as spheres with a radius given by, say, the average radius of gyration for that particular cluster size. First we choose a test particle - an i -mer with radius r_i - centered at the origin, and calculate the rate at which j -mers, with radius r_j and concentration c_j , diffuse toward its surface. The radius R_{ij} of the 'sphere of influence' will be given by:[†]

$$R_{ij} = r_i + r_j \quad [2.10]$$

It is entirely equivalent to give the test particle a radius R_{ij} and consider j -mers as point particles. First we must solve the spherically symmetric diffusion equation:

$$\frac{\partial \tilde{c}_j}{\partial t} = -\vec{\nabla} \cdot \vec{j} = D_j \frac{1}{r^2} \frac{\partial}{\partial r} \left[r^2 \frac{\partial \tilde{c}_j}{\partial r} \right] \quad [2.11]$$

[†] At this point Chandrasekhar (in his equation 452) introduces an erroneous factor of 1/2, which propagates to the end of his treatment.

subject to the boundary conditions

$$\tilde{c}_j(\vec{r}) = c_j; \quad r > R_{1j}; \quad t=0 \quad [2.12a]$$

$$\tilde{c}_j(\vec{r}) = 0; \quad r \leq R_{1j}; \quad 0 \leq t \leq \infty \quad [2.12b]$$

$$\tilde{c}_j(\vec{r}) = c_j; \quad r = \infty; \quad 0 \leq t \leq \infty \quad [2.12c]$$

Here $j(r)$ is the net radial flux of j -mers relative to the test particle:

$$j(r) = -D_j \frac{\partial \tilde{c}_j}{\partial r} \quad [2.13]$$

and D_j is the diffusion coefficient of j -mers in the surrounding medium. The tilde distinguishes the localized value of c_j from its average. The value of the diffusion coefficient is given by the Stokes-Einstein relation:

$$D_j = kT/6\pi\eta r_j \quad [2.14]$$

where k is Boltzmann's constant, T is absolute temperature, and η is the viscosity of the solvent. Boundary conditions [2.12b] and [2.12c] state that the test particle acts as a perfect sink at $r = R_{1j}$ and that the concentration of j -mers remains constant extremely far from the test particle.

Since we are searching for steady state solutions, we could set the left hand side of the diffusion equation to zero, but it is illuminating to examine time dependence as well. The solution with boundary conditions

[2.12] is

$$\tilde{c}_j = c_j \left[1 - \frac{R_{1j}}{r} \left[1 - 2/\pi^{1/2} \int_0^{(r-R_{1j})/2(D_j t)^{1/2}} \exp(x^2) dx \right] \right] \quad [2.15]$$

The integral drops to zero in the steady state ($t \rightarrow \infty$). Evaluating expression [2.13]:

$$j(r) = -D_j \frac{R_{1j}}{r^2} c_j \left[1 + R_{1j}/(\pi D_j t)^{1/2} \right] \quad [2.16]$$

The total rate at which j-mers collide with the test particle is given by

$$-4\pi r^2 j = 4\pi D_j R_{1j} c_j \left[1 + R_{1j}/(\pi D_j t)^{1/2} \right] \quad [2.17]$$

So far, we have assumed that the test particle is stationary. If we allow it to describe a Brownian walk with its own diffusion coefficient D_1 , the previous analysis remains unchanged except that the single particle diffusion coefficient D_j is replaced with a relative diffusion coefficient given by:

$$D_{1j} = D_1 + D_j \quad [2.18]$$

This is only possible if the motions of the diffusing particles are entirely uncorrelated. In fact, this expression must be modified to include hydrodynamic interactions, which become increasingly important at small particle separations. This effect is discussed in Appendix I.

With the final observation that the i-mer test particles have a concentration c_i , the rate at which i-mers and j-mers collide to give (i+j)-mers is given by

$$K_{ij} = 4\pi D_{ij} R_{ij} c_i c_j \left[1 + R_{ij} / (\pi D_{ij} t)^{1/2} \right] \quad [2.19]$$

The second term in brackets defines the relaxation time over which the distribution of i-mers and j-mers in space approaches equilibrium:

$$t_{\text{relax}} = R_{ij}^2 / \pi D_{ij} \quad [2.20]$$

It is important that this process approach equilibrium much faster than the concentrations of i-mers and j-mers change due to coagulation. Since this is generally the case, we will drop this term. Later we will determine when it is valid to do so by comparing the relaxation time to the coagulation time.

Using expressions [2.10], [2.14], and [2.18], our explicit form for the two-particle association kernel ($K_{ij}/c_i c_j$) now becomes:

$$a_{ij} = 4\pi D_{ij} R_{ij} = 2kT/3\eta \left[(r_i + r_j)^2 / r_i r_j \right] \quad [2.21]$$

At this point von Smoluchowski made another assumption that takes on increased importance in view of recent evidence²⁹⁻³¹ that colloidal aggregates are ramified, fractal structures. He assumed that clusters are hexagonally dense-packed - in which case $r_i \sim i^{1/3}$, and

$$a_{ij} = 2kT/3\eta \left[2 + (i/j)^{1/3} + (j/i)^{1/3} \right] \quad [2.22]$$

This weak dependence of the kernel upon particle size led von Smoluchowski to propose that a_{ij} is independent of i and j . While actual structures probably are ramified, the dependence is still evidently weak especially at the beginning of the reaction. The reason for this weak dependence is found in the Stokes-Einstein relation, equation [2.14]: the greater collision cross-section of larger clusters is approximately offset by their slower diffusion. Von Smoluchowski set i equal to j to find the kernel for this process:

$$a_{ij} = 8kT/3\eta = A \quad [2.23]$$

The first line of Table 2.1 gives the half-life (or coagulation time) for reactions with a constant association kernel:

$$\tau = 2/(Ac_0) = 3\eta/4kTc_0 \quad [2.24]$$

This is the time it takes the total number of clusters to drop to 1/2 of its initial value. Comparing τ with the relaxation time in [2.20] (using $i=j=1$), we see that this analysis is valid as long as the average volume per particle in the solution is much larger than the particle volume, or

$$c_0 \ll \frac{1}{32a^3} \quad [2.25]$$

In my studies, for instance, the radius of an individual sphere is 225 nm so that the initial concentration is restricted to values below

$2.7 \times 10^{12} \text{ cm}^{-3}$. Another, probably more important, factor that comes into play at high concentrations is the three body interaction, which would invalidate the coagulation equations [2.1]. Both of these effects speed up aggregation.

Experimentally, it is often difficult to produce an entirely monomeric sample, but it is straightforward to solve the coagulation equations for case A with arbitrary initial conditions. This solution is presented in Appendix II.

It can be shown that with $a_{ij} = A$ all of the moments of the cluster size distribution are well behaved for $0 < t < \infty$. No sol-gel transition occurs in this model. According to Table 2.1, the cluster size distribution is a simple geometric series in n . Its functional form remains invariant in time, because all time dependence is contained in the parameter b .

In this analysis of the coagulation kernel, I have posited a very simplified interaction between diffusing particles. There are no hydrodynamic coupling effects, and the two-particle pair potential is simply a square well, rising from minus infinity to zero at R_{ij} . In fact, colloid scientists have developed a very detailed model of the actual interaction. In this model, the pair potential is made up of an attractive term, which arises from van der Waals forces, and a repulsive term, which arises from partially shielded like charges on the colloidal surfaces. The relative diffusion coefficient D_{ij} (equation [2.18]) is also modified to include repulsive hydrodynamic forces. These effects are discussed more thoroughly in Appendix I.

Although stability theorists have modified the pair interaction, they have continued to assume that von Smoluchowski's kinetic arguments are valid: that aggregation is irreversible and that a_{ij} is a constant as in case A. They analyze only the monomer-monomer interaction, determining how potentials and hydrodynamic effects modify the value of A in equation [2.23]. The net contribution of these effects is expressed in terms of a stability factor W, the ratio of the actual half-life to τ as computed in equation [2.24].

A variety of techniques which measure some average degree of aggregation have been used to measure reaction half-life. These include measurements of the turbidity of the suspension,⁴⁰ the mean intensity of the scattered light,^{41,42} and its temporal correlation function.⁴³ Such measurements have generally confirmed the predictions of colloid stability theory, as embodied in the parameter W. They have also shown that equation [2.24] provides a reasonable estimate of the actual half-life in so-called rapid coagulation, which takes place at high salt concentrations. I point out the reason for this in Appendix I: in this regime the attractive van der Waals force is approximately cancelled by the repulsive viscous force. To interpret bulk measurements, however, it is necessary to assume that von Smoluchowski's form for the cluster size distribution is correct. This prediction has rarely been questioned. Since our instrument measures the cluster size distribution itself, we can observe the monomer-monomer interaction directly and, thereby, test stability theory more precisely.

2.1.3.2 - Case B: Shear Flow and the A-R-B_∞ Polymer System

This case is closely tied to the A-R-B_{f-1} polymer system, in which monomeric units have one A-type functional group and f-1 B-type functional groups, with bonding between A's and B's only. If this system is reaction limited, Ziff¹⁶ and Cohen and Benedek⁴ have shown that the form of a_{ij} is expected to be:

$$a_{ij} = (f-2)(i+j) + 2 \quad [2.26]$$

The essential features of the aggregation process remain unchanged in the limit of large f:

$$\begin{aligned} a_{ij} &\approx (f-2)(i+j) \\ &\approx B(i+j) \end{aligned} \quad [2.27]$$

Von Smoluchowski, in his original paper on Brownian coagulation,¹ also studied the coagulation of colloids in a fluid undergoing laminar shear flow. Assuming dense packed structures, he found that the mobility limited kernel for this process goes as $(i^{1/3} + j^{1/3})^3$, but he never solved the coagulation equations for this difficult kernel. Golovin⁴⁴ and Scott⁴⁵ approximated this as $(i+j)$ in order to solve the coagulation equations. Swift and Friedlander⁴⁶ have investigated this case experimentally.

While there is no obvious reason to suspect that colloid flocculation will behave as either the $A-R-B_{f-1}$ or the shear flow system, case B does provide another exact solution with which to compare my results. Besides, unexpected things do happen: although a statistical mechanical treatment of antigen-antibody agglutination⁴⁷ shows that it corresponds to case C, von Schultess et al.⁴⁸⁻⁵⁰ and Johnston et al.^{51,52} have found distribution B in experiments with antigen coated latex microspheres cross-linked by antibody.[†] These workers also showed that aggregation is irreversible and that reaction rate is several orders of magnitude slower than von Smoluchowski's theory of Brownian coagulation would predict. In this system, the cross-linking process involves two steps: first, a free antibody quickly binds to an antigen on the surface of a sphere, and, second, the singly bound antibody slowly binds to an empty site on the surface of another sphere. It is suspected that the second step determines not only the aggregation rate, but also the form of the association matrix, which evidently corresponds to case B. The results can also be explained if the polymeric clusters are fractal and binding occurs only at the surface of these clusters.^{51,52} I discuss surface bonding in section 2.1.5.

The disparity between experimental results and equilibrium predictions in the antigen-antibody system led Cohen et al.^{4,53} to observe that systems could behave quite differently when kinetics rather than

[†] This is an $R-A_f$ (large f), B_2 system, which reduces to the $R-A_f$ system if the number of B_2 's attached to only one $R-A_f$ is ignored. The $R-A_f$ system is closely tied to case C as I show in the next section.

energetics control the reaction. In fact, kinetic factors could prevent the system from ever reaching thermodynamic equilibrium.

The explicit form for the solutions is found in Table 2.1. Once again, all of the time dependence is contained in the parameter b . The moments of the cluster size distribution are well behaved for all times; there is no sol-gel transition in this system.

2.1.3.3 - Case C: The $R-A_{\infty}$ Polymer System

The polymer system that corresponds to this case is the $R-A_f$ system, in which monomers have f identical functional groups. Cohen and Benedek⁴ show that under reaction limited conditions the form of a_{ij} in this system is expected to be

$$a_{ij} \simeq (i(f-2)+2)(j(f-2)+2) \quad [2.28]$$

which in the high functionality limit becomes

$$\begin{aligned} a_{ij} &\simeq (f-2)^2 ij \\ &\simeq Cij \end{aligned} \quad [2.29]$$

They also point out that the essential features of both the aggregation process and the phase transition are unchanged in this limit, while the mathematics is greatly simplified. The high functionality

limit represents the case in which clusters interact not at discrete sites but via continuous potentials. Cohen and Benedek point out that this limit may be particularly appropriate in describing our colloidal system, in which van der Waals and electrostatic potentials - rather than chemical bonds - lead to coagulation. In section 2.2.1.1 I discuss the Flory-Stockmayer approach to this case.

It is difficult to imagine a physically meaningful system in which a bimolecular (or two-particle) rate coefficient could have a stronger ij dependence than it does here in case C. Every free site on a cluster - even if it is deep within a very large aggregate - is given equal probability of reaction. In realistic systems, steric hindrance and limited rotational mobility will tend to decrease the reactivity of larger clusters. The form $a_{ij} \approx (ij)^\omega$ ($0 \leq \omega \leq 1$), which I discuss in section 2.1.5, is often used to account for these effects. On the other hand, large clusters may have enhanced mobility in a gravitational field. I discuss this effect in Chapter V.

As I pointed out in the discussion of the bilinear kernel, kernels of the type C_{ij} lead to a sol-gel transition at a finite time t_c . From Table 2.1 we see that with monodisperse initial conditions the gel appears when b reaches a value of $1/2$ - at $t_c = 1/Cc_0$. Examining the essentially identical $R-A_3$ system, Ziff¹⁶ shows explicitly that at the critical instant t_c a cascading growth process leads to the formation of an infinitely large cluster, which corresponds to the gel.

Exactly how the system should be treated after gelation has been a topic for debate ever since Flory and Stockmayer originally studied this problem.¹¹ Ziff and Stell¹⁴ have recently examined the basic

assumptions of both Flory and Stockmayer and explained their differing post-gel solutions in the context of the coagulation equations. Considering units with finite functionality, they present several post-gelation models: one in which the sol and gel interact and cyclical bonding occurs in the gel (the Flory model), a second in which there is no sol-gel interaction (the Stockmayer model), and a third in which the sol and gel interact, but no cycles form in the gel. In the high functionality limit the first and third models are identical.

In the Flory model, the coagulation equations must be modified past the gel point to account for sol-gel interactions. Ziff and Stell identify a specific term in the post-gel equations with this interaction and another with cyclical bond formation in the gel. Cascading growth occurs only at the instant t_c . Past this point the gel grows only by interacting with the sol. In a very detailed article discussing kernels of type C, Ziff, Ernst, and Hendricks²² show that in the Flory model the cluster size distribution in the sol maintains its pre-gel functional form:

$$c_n = c_0 e^{-2nb} (2nb)^{n-1} / (n \cdot n!) \quad [2.30]$$

and that the bond parameter b continues to grow linearly with time:

$$b = t/\tau_C \quad [2.31]$$

$$\text{where } \tau_C = 2/Cc_0 \quad [2.32]$$

The difference after gelation is that this value of b no longer

applies to the sol. Cohen and Benedek⁴ (who consider only Flory's post-gel model) show that the total mass in the sol, obtained by explicitly calculating the sum $\sum c_n$, begins to drop as b exceeds $1/2$. Also, for every value of b larger than $1/2$, there corresponds a value smaller than $1/2$ which gives precisely the same relative cluster size distribution. Thus b_s , the effective bond parameter in the sol, increases linearly with time before the critical point and then drops - monotonically, but not linearly - as the gel grows. The instrument I use measures only b_s ; hence, a drop in the apparent degree of aggregation in my experiments could indicate interaction between the sol and gel phases.

While the Flory model applies to systems in which comparatively small sol particles penetrate the macroscopic particles of the gel, the Stockmayer model applies to systems in which the phases separate spatially, by precipitation of the gel or some other mechanism. In the Stockmayer model there is no modification of the coagulation equations past the gel point. Since there are no sol-gel interactions, the only way that very large gel particles form is by continued cascading growth. For this reason, the gel forms more slowly in this model. Ziff and Stell point out that the rate of gel growth in an experiment may indicate which post-gelation model applies. Cascading growth only takes place when $b = 1/2$; thus, the cluster size distribution 'sticks' past the gel point. It retains its shape at criticality (characterized by a b -value of $1/2$), but all n -mer concentrations (and, therefore, the mass in the sol) begin to drop as $1/t$:

$$c_n(t > t_c = 1/Cc_0) = c_n(t_c)/tCc_0 = c_0 n^{n-2} e^{-n}/n! t, \quad [2.33]$$

where $t' = 2t/\tau_c$.

For experimental purposes it is most important to realize that the functional form of the cluster size distribution in the sol remains unchanged in both the Flory and Stockmayer solutions even after the gel point. This is a direct result of the fact that fragmentation is not allowed and the aggregation process is reaction limited at all times. These are very special kinetic conditions. Later in this chapter and in chapter V I discuss mechanisms that may cause the form of the distribution to change.

2.1.4 - Critical Exponents and Scaling Relations

I have already pointed out that the second moment of the cluster size distribution, for instance, diverges as b approaches its critical value b_c . For case C, this divergence exhibits the power law dependence: $M_2(b) \propto (b_c - b)^{-\gamma}$, where $b_c = 1/2$ and $\gamma = 1$. The critical point shifts with the bilinear kernel or kernels of the form [2.28], corresponding to the $R-A_f$ system with finite f , but the value of the critical exponent γ does not change.⁴ It is also insensitive to the form of the initial cluster size distribution, as long as the third moment of the initial distribution is not divergent.⁵⁵ This insensitivity to details of the system is called universality in the parlance of thermal phase transitions, where one of the major aims is to determine the 'relevant fields' in a problem: parameters that change universal characteristics - which usually means the exponents - of the

phase transition. Groups of apparently diverse phenomena exhibiting the same critical exponents are then sorted into so-called universality classes.

The physical principal underlying universality is scale invariance: at the critical point in the phase diagram of a material the behavior of its microscopic constituents is often correlated over a macroscopic length, so that microscopic details recede in importance. Observed over a wide range of length scales - often many orders of magnitude - the material appears self similar. In our system, scaling takes three basic forms: first, the random clusters may themselves be self-similar or fractal;⁵⁶ second, the cluster size distribution may scale with size as $n^{-\tau}$; and third, larger clusters may diffuse more slowly than smaller ones, with a diffusion coefficient that scales with mass.⁵³ If these three forms of scaling hold, a sol near criticality would look exactly the same through a microscope - no matter what the magnification. The third form of scaling may be called dynamic scaling. Actually, there may be another form of dynamic scaling in which the features of the sol scale with time - for instance \bar{n} may grow as t to some power.^{57,58}

These concepts of scale invariance and universality, which had been applied with great success to thermal critical phenomena in the late 1960's and early 1970's, led polymer chemists to look more closely at the sol-gel transition beginning in roughly 1974.⁵⁹ Shortly thereafter, percolation theory, which I discuss in section 2.2.3, was proposed^{60,61} as an alternative to Flory-Stockmayer theory.

Critical exponents and universal properties generally refer to the features of very large aggregates or the gel itself. But the instrument I have used investigates only the sol, measuring the concentrations of relatively small aggregates (with $n \leq 25$), so in this thesis I present no experimental values for critical exponents. Nevertheless, I feel that a discussion of scaling concepts is necessary to any review of aggregation theory and should be an important part of future work on this system, so I define here the various critical exponents, critical amplitudes, and scaling functions commonly used to describe the sol-gel transition. For a more thorough discussion of these concepts, the reader is referred to a recent review article by Stauffer et al.⁶² whose notation I use.[†] It should be noted, however, that in the absence of a rigorous equation of state for the percolation model, all of these scaling forms and scaling relations are essentially conjectures, based upon analogies to liquid-gas phase transitions, the numerical results of percolation theory, and the generalization of exact solutions to the kinetic equations and Flory-Stockmayer theory. Indeed, at this point, there is very little experimental evidence backing up these conjectures.

In polymer chemistry the quantity associated with the second moment of the cluster size distribution is the so-called weight average degree of polymerization, the DP_w , defined as

[†] - except that their p (the ratio of the actual number of bonds to the maximum possible number of bonds) becomes my b . In situations where cyclization is allowed, equation [2.9] no longer accurately describes b , but b still stands for the ratio of the actual number of bonds to the number of monomeric units in the system.

$$DP_w \equiv M_2(b)/M_1(b) = \frac{\sum n^2 c_n}{\sum c_n} \quad [2.34]$$

The exponent characterizing the divergence of this quantity is γ :

$$\begin{aligned} DP_w &= C(b_c - b)^{-\gamma} & b \rightarrow b_c^- \\ DP_w &= C'(b - b_c)^{-\gamma'} & b \rightarrow b_c^+ \end{aligned} \quad [2.35]$$

where a '+' or '-' superscript denotes the direction from which the critical point is approached. Thus, generally, the weight average degree of polymerization may diverge differently before and after gelation. Since the denominator in [2.34] is simply the mass of the sol, which has the stationary value c_0 at b_c , the exponent γ also applies to the second moment $M_2(b)$. Aharony⁶³ has shown that the 'critical amplitude ratio' C'/C - and others that I don't mention here - may also be universal.

The order parameter in cluster formation is the gel fraction G . It is analogous in liquid-gas phase transitions to Δ , the difference in density between the gas and liquid phases along the coexistence curve, and to the spontaneous magnetization in ferromagnets. Rigorously, G may be defined as the probability that a monomeric unit belongs to an infinite cluster. Below the gel point $G = 0$. Above it G is expected to grow with a power law dependence given by

$$G = B(b - b_c)^\beta \quad b \rightarrow b_c^+ \quad [2.36]$$

Expressions [2.35] and [2.36] together give the dependence of the weight average degree of polymerization upon gel fraction:

$$DP_w \propto G^{1-\delta} \quad G \rightarrow 0 \quad [2.37]$$

where $\delta = 1 + (\gamma'/\beta)$.

The z average degree of polymerization is defined as

$$DP_z \equiv M_3(b)/M_2(b) \quad [2.38]$$

This quantity is expected to diverge with the characteristic exponent σ :

$$DP_z \propto |b - b_c|^{-1/\sigma} \quad b \rightarrow b_c \quad [2.39]$$

The 'cluster number scaling hypothesis' unifies these apparently fragmentary conjectures. Close to the gel point the distribution is expected to approach the form

$$\frac{c_n(b)}{c_0} = q_0 n^{-\tau} f((b - b_c)n^\sigma) \quad b \rightarrow b_c^+, n \rightarrow \infty \quad [2.40]$$

where q_0 is a constant critical amplitude. The scaling function $f(z)$ rapidly approaches zero as its argument z goes to plus or minus infinity, while $f(0) = 1$. If expression [2.40] is true, then all of the previously mentioned critical exponents may be expressed in terms of the fundamental exponents σ and τ :

$$\beta = (\tau-2)/\sigma$$

$$\gamma = \gamma' = (3-\tau)/\sigma \quad [2.41]$$

$$\delta = 1/(\tau-2)$$

These expressions are known as 'scaling relations'. The cluster number scaling hypothesis also implies that at the critical point the cluster size distribution scales with n :

$$\frac{c_n(b=b_c)}{c_0} = q_0 n^{-\tau} \quad n \rightarrow \infty \quad [2.42]$$

Scaling forms may also obtain away from criticality. Far below the gel point the postulated scaling form for the distribution is

$$c_n(b) \propto n^{-\theta} \exp(-\text{const} \cdot n^{\delta}) \quad b \neq b_c, n \rightarrow \infty \quad [2.43]$$

Recently, there has been a great interest in the geometric features of very large clusters and the gel.³⁰ Electron micrographs of large colloidal clusters,^{39,36,37} light scattering results on aggregated colloidal silicates,^{31,32} many computer simulations,^{30,64-69} and renormalization group calculations⁷⁰ indicate that clusters are often highly ramified as well as fractal. The radius of gyration, R_n , of a fractal aggregate will scale with its mass as

$$R_n^2 = \frac{1}{n} \sum_{i=1}^n r_i^2 \propto n^{2\rho} \quad n \rightarrow \infty; b \text{ fixed} \quad [2.44]$$

where r_i is the distance to particle i from the center of mass of the aggregate. The exponent ρ is inversely proportional to the fractal dimension d_f of the aggregate:

$$\rho = 1/d_f \quad [2.45]$$

The correlation function within a fractal scales with the distance r from its center of mass:

$$C(\vec{r}) = \frac{1}{m} \left\langle \sum_{\vec{r}'} \rho(\vec{r}') \rho(\vec{r} + \vec{r}') \right\rangle \propto r^{-A} \quad [2.46]$$

where $\rho(\vec{r}) = 0,1$ is the density at \vec{r} and the brackets indicate averaging over configurations. The fractal dimension and A are related through the dimension d of space:

$$A + d_f = d \quad [2.47]$$

The correlation length ξ of the sol is the z average radius of gyration:

$$\xi^2 \equiv \frac{\sum n^2 c_n R_n^2}{\sum n^2 c_n} \equiv \langle R_n^2 \rangle_z \quad [2.48]$$

Not unexpectedly, the correlation length also diverges at criticality:

$$\begin{aligned}\xi &= \xi_0 (b_c - b)^{-v} & b \rightarrow b_c^- \\ &= \xi'_0 (b - b_c)^{-v'} & b \rightarrow b_c^+\end{aligned}\quad [2.49]$$

With the cluster number scaling hypothesis, ρ becomes our third fundamental exponent:

$$v = v' = \rho/\sigma \quad [2.50]$$

Finally, in percolation, but apparently not in the classical theories, 'hyperscaling' holds: ρ is related to the the dimensionality d :

$$\rho(b=b_c) = (1+1/\delta)/d \quad [2.51]$$

$$\text{or} \quad dv = 2\beta + \gamma = \beta(\delta+1) \quad [2.52]$$

2.1.4.1 - Values of the Exponents

The exponents and critical amplitudes in Flory-Stockmayer theory depend upon bonding rules, while in kinetic theories they depend upon the interaction kernel. Just as there has been correspondence between equilibrium and kinetic theories so far, there is a correspondence in the exponents. Moreover, the gelation model of Flory in both case C

and the bilinear case, gives the same exponents as percolation in six or more dimensions. On the other hand, at lower dimensionality percolation and various Monte Carlo simulations of aggregation by diffusion on a lattice give different exponents. In fact, there is such a variety of the latter³⁰ that it is hard for a non-specialist to keep track of the accepted values. I discuss two lattice models in section 2.1.7. Current values for percolation are tabulated in the review by Stauffer et al.⁶² Here I consider only the kinetic kernels I have discussed.

Cases A and B are often said to produce phase transitions when b reaches its maximum possible value of one - an infinite time after aggregation is initiated. This is similar to the Ising model in one dimension, where a transition takes place at zero temperature. These 'transitions' are hardly universal, however, and it is only by stretching definitions that it is possible to give values to most of the exponents. Examining Table 2.2, which details the behavior of cluster size distributions near b_c , we could assign τ values of 0 and $3/2$ to cases A and B respectively. In neither case does the cluster size distribution ever approach the scaling form [2.40], so it is not really possible to find σ . However, the second moment of the cluster size distribution does diverge at $b = 1$ in both cases, giving values of 1 and 2, respectively, for γ . Since cluster number scaling does not hold, scaling relations [2.41] also break down.

The critical behavior of case C and the bilinear kernel are identical, and analytic values have been found for most of the critical exponents and amplitudes. This is a good example of universality,

Case	b_c	c_n/c_0
A	1	$\varepsilon^2(1-n\varepsilon)$
B	1	$(2\pi)^{-1/2}n^{-3/2}\frac{\varepsilon}{(1-\varepsilon)}(1-n\varepsilon^2/2)$
C	1/2	$(2\pi)^{-1/2}n^{-5/2}(1-2n\varepsilon^2)$

Table 2.2.

Asymptotic values of concentrations c_n for Cases A, B, and C as $n \rightarrow \infty$ and $\varepsilon \rightarrow 0$ with $n\varepsilon \ll 1$. The variable $n\varepsilon$ is defined as $(b_c - b)$.

because critical behavior in the bilinear case is entirely dominated by the coefficient C_{ij} . Case C is discussed very thoroughly in a paper by Ziff et al.²² They also show that critical behavior below the gel point is insensitive to initial conditions as long as the third moment of the initial distribution is not divergent ($M_3(t=0) < \infty$). The bilinear case is covered by van Dongen and Ernst.^{21,22} Since the critical behavior is identical insofar as it is known, I discuss only case C.

Here it is important to distinguish between the Flory and Stockmayer gelation models, which behave identically until the critical point. The Stockmayer model is not universal, primarily because past the gel point the parameter b sticks at a value of 1/2, breaking the symmetry of the transition. In the Flory model b begins to drop immediately after t_c , so that symmetry is preserved. Known results are tabulated in Table 2.3.

Case	A	B	C and Bilinear			
Gel model			Flory		Stockmayer	
			$b < b_c$	$b > b_c$	$b < b_c$	$b > b_c$
τ	0	3/2	5/2	5/2	5/2	5/2
σ	-	-	1/2	1/2	1/2	-
β	-	-	-	1	-	1
γ	1	2	1	1	1	-
δ	-	-	-	2	-	-
θ	0	3/2	5/2	5/2	5/2	5/2
ζ	0	1	1	1	1	-
ρ	-	-	1/4	1/4	1/4	1/4
ν	-	-	1/2	1/2	1/2	-

Table 2.3.
Exponent values for Cases A, B, and C and the bilinear kernel.

Although the kinetic theory makes no assumption regarding the structure of clusters, it is possible to calculate ρ for the sol particles in both models, assuming only that all similar sites have equal a priori probabilities of bonding at a given time and that no cycles form.⁷¹⁻⁷³ This second assumption comes from Flory-Stockmayer theory. One finds that $\rho=1/4$.

For the Flory model, all of the scaling relations [2.41] hold even past the gel point. This is a direct result of the symmetry of the cluster size distribution on either side of the transition. In the Stockmayer model the moments M_2 , M_3 , etc. remain infinite, and such quantities as σ , γ and δ are meaningless. To calculate β , which describes the growth of the gel, it is necessary to transform from b to t as a dynamical variable in the Stockmayer model.

Dimensionality is not a variable in either the coagulation equations or Flory-Stockmayer theory, so hyperscaling does not apply. I shall return to this and other questions of universality later when I discuss equilibrium theories, but now I consider an association kernel for which only approximate solutions - with interesting scaling properties - have been found.

2.1.5 Surface Bonding: $a_{ij} \propto (ij)^\omega$

In reaction limited reactions, this form of the association kernel may account for steric hindrance or even cyclical bond formation in large aggregates if we assume that only sites close to the surface of a cluster may form bonds. For this kernel ω becomes a fundamental exponent, since it turns out that all exponents except perhaps ρ and ν can be expressed in terms of it. If one asserts that the association kernel has the form $a_{ij} = s_i \cdot s_j$, where $s_i \propto i^\omega$ is the number of sites on the surface of an i -mer, then $a_{ij} \propto (ij)^\omega$. Since there may be some interpenetration, ω should fall in the range

$$(d_f-1)/d_f \leq \omega \leq 1 \quad [2.53]$$

the lower limit corresponds to surface interactions between clusters with fractal dimension d_f ; and the upper limit corresponds to total interpenetration, where reactivity is proportional to cluster volume (case C).

Leyvraz has questioned the validity of this simplified picture, in which surface area is the only determinant of reactivity:

...such assumptions...are at best dubious, since it is, for example, not obvious that a small cluster 'sees' the same area of a large cluster as a large cluster...⁷⁴

A small cluster may penetrate where a larger cluster may not, for instance, or it may lack the mobility to bond to all the surface sites that a larger cluster might encounter simply due to its breadth. Ziff et al.⁷⁵ also point out that ω more accurately reflects the interaction of large clusters with each other than it does the interaction between large and small clusters. Whatever the validity of this model, it is certainly a refinement of case C, and it has yielded some interesting results.

Considering kernels of the related form $a_{ij} \propto i^\mu j^{\nu+1} j^\mu$, White⁷⁶ proved that gelation does not occur for $\mu \leq \nu \leq 1/2$, which corresponds in the present case to $\omega \leq 1/2$. Considering much more general questions about

gelation, Ziff¹⁶ conjectured that gelation would occur only if the diagonal elements of the association matrix scale as $a_{ii} \sim i^\alpha$, with α larger than one - corresponding again to $\omega > 1/2$. And finally, Leyvraz and Tshudi¹⁷ and Ziff et al.¹⁸ proved that gelation occurs for $a_{ij} \sim (ij)^\omega$ only when ω exceeds $1/2$.

There are no exact solutions for $c_n(t)$ for all times, but asymptotic and approximate solution have been found - often by testing the scaling ansatzes [2.40] and [2.43]. In this fashion, a number of new scaling relations have been found.

For the relatively uninteresting range $0 < \omega \leq 1/2$, a 'transition' takes place at infinite time and $c_n(b_c) \sim n^{-\tau}$ with $\tau = 1 + 2\omega$ (see [2.42]).

For $0 < \omega < 1$ and far below the gel point, Ernst et al.¹⁹ show that

$$c_n \simeq n^{-2\omega} \xi^n \quad [2.54]$$

where ξ is a constant. Thus the scaling ansatz [2.43] holds for this model with $\theta = 2\omega$ and $\zeta = 1$. Note that at $\omega = 1$ this kernel corresponds to case C, where $\theta = 5/2$ ($\neq 2\omega$). Hence θ is discontinuous in ω at this point.

For $1/2 < \omega \leq 1$ - close to and below the transition - the cluster size distribution approaches the scaling form [2.40] with

$$\tau = \omega + 3/2 \quad ; \quad \sigma = \omega - 1/2 \quad 15, 17, 19-21 \quad [2.55]$$

These expressions replace the former fundamental exponents with ω . Hendricks et al.²¹ confirm scaling relations [2.41], at least below the gel

point, by showing that $\gamma=(3/2-\omega)/(\omega-1/2)$ and $\beta=1$. In considering the continuous coagulation equations [2.2] with $a(x,y) = xy^\omega$, Ernst et al.⁸² show that scaling is insensitive to initial conditions. In fact, virtually every result mentioned in this section holds in the continuous case.[†]

After gelation, results have been found^{75,79,82} only for the Stockmayer model, and they are similar to the results for case C. The distribution sticks at its critical shape [2.42] with $\tau=\omega+3/2$, and moments M_2 , M_3 , etc. remain divergent above the gel point. Thus the cluster size distribution behaves differently on either side of the transition and scaling breaks down. The exponent β retains its classical value of one because scaling relations [2.41] make it independent of ω .

It is tempting to connect the critical exponents, τ , σ , and so on to the structural exponents, ρ and ν or to dimensionality through ω and hyperscaling. Unfortunately, this leads to contradictory results. However, Ziff et al.⁷⁵ and Ernst et al.⁷⁸ have attempted to utilize scaling relations in estimating fractal dimension as a function of dimensionality. The results compare reasonably well with those of exact and numerical lattice theories, but this is probably a coincidence; the cluster-cluster model (section 2.1.7.1) provides a more plausible physical motivation for the connection between ω and d .

[†] - It is also interesting to note that the criterion for gelation, $\omega > 1/2$, and the relations for τ in this model conform to the general criterion for gelation established by Cohen and Benedek (Reference 4, section III): gelation occurs only for systems in which τ exceeds 2.

This concludes my discussion of exact solutions to the irreversible coagulation equations. I have only scratched the surface of the vast literature on the subject. What is surprising is the lack of experimental testing of these theories; perhaps this thesis will help rectify this imbalance.

2.1.6 Numerical Solutions to the Irreversible Equations

By numerical solutions I mean iterative methods (like the Runge-Kutta method) of solving the set of equations [2.1]. It is, of course, necessary to truncate the infinite set at some point - usually at 100 or so. By far, the largest field of application for this technique has been meteorology and aerosol physics. Here, complex effects such as turbulence, sedimentation, the addition of a Cunningham 'slip' factor to Brownian motion, and others have been added to the coagulation kernel. Often, the goal has been to prove the existence of so-called self-preserving solutions, according to the predictions of Friedlander.³³ Drake³ reviews various numerical techniques as well as results.

In section 2.1.3.2 I mentioned the fact that antigen coated latex spheres cross-linked by antibody molecules produce distribution B experimentally.⁴⁸⁻⁵² At long times the distribution approaches the form $c_n \propto n^{-\tau}$ with $\tau \simeq 3/2$. In attempting to provide an explanation for this behavior (since Flory-Stockmayer theory indicates that Case C should apply to this problem), Johnston⁵² solved the discreet

coagulation equations numerically starting from monodisperse initial conditions with the following forms for a_{ij} :

$$a_{ij} = i^{\omega'} + j^{\omega'} \quad [2.56a]$$

$$a_{ij} = [i^{\omega'/2} + j^{\omega'/2}]^2 \quad [2.56b]$$

$$a_{ij} = (ij)^{\omega'/2} \quad [2.56c]$$

He found that at long times each of these kernels produced asymptotic cluster size distributions of the form $c_n \sim n^{-\tau}$. He also found that in each case a value of $\omega' \sim 1$ gave $\tau \sim 3/2$ and noted that the diagonal exponent ($a_{ii} \sim i^{\omega_d}$) might be the factor that determines τ , since ω_d appeared to be the same in each case.

In the previous section I reviewed analytic results, obtained subsequent to Johnston's analysis, for [2.56c] (note that ω' in [2.56c] becomes the ω of the previous section). It is now known that gelation occurs in [2.56c] for $\omega' > 1$. There are two scaling relations connecting ω' and τ : $\tau = 1 + \omega'$ for $0 < \omega' \leq 1$, and $\tau = \omega'/2 + 3/2$ for $1 < \omega' \leq 2$. Both give $\tau = 2$ at $\omega' = 1$, in contradiction with Johnston's numerical results. Johnston also used the lower limit in [2.53] to estimate the fractal dimension of antigen-antibody clusters. With $\omega' = 1$ (which becomes $\omega = 1/2$) he deduced $d_f = 2$. The analytic solutions would give $\omega' = 1/2$ (or $\omega = 1/4$) for $\tau = 3/2$, hence the fractal dimension would be $4/3$.

Analytic results have also been obtained for [2.56a].³⁰ Here the results agree with Johnston's:

$$\text{for } a_{ij} \propto i^{\omega'} + j^{\omega'} \quad (0 < \omega' \leq 1); \quad \tau = 1 + \omega'/2 \quad [2.57]$$

Hence, τ would equal 3/2 at $\omega' = 1$. (Note that τ is discontinuous in ω' at $\omega' = 0$, because the kernel in [2.57] becomes a constant (as in case A), in which case $\tau = 0$.)

Recently, Kolb, Botet, and Jullien have coupled numerical and analytic solutions to the coagulation equations with computer simulations. These results are discussed two sections hence.

2.1.7 Computer Simulations

Judging from the wide number of papers being published on the subject, it seems that Monte Carlo methods are particularly appropriate in modeling growth processes of all kinds.³⁰ There are two models that may be applicable to our system: The Witten-Sander model and the Cluster-Cluster model.[†]

The Witten-Sander^{64,65} model was proposed after electron

† - One must be careful with terminology nowadays, because these models have very specific meaning in the simulation industry. The words "diffusion limited aggregation" are virtually a synonym for the Witten-Sander model. While we might think of the Cluster-Cluster model or even actual colloidal flocculation as diffusion limited aggregation, we had best refer to them by their real names if we wish to be understood.

micrographs of smoke particles formed by a variety of substances (zinc, iron and silicon dioxide) revealed that large aggregates are quite ramified, with a fractal dimension of somewhere from 1.7 to 1.9.²⁹ Witten and Sander suggested that this dimension is universal since it is independent of the substance being used. As long as the inter-particle potential is short range and bonds are rigid and unbreakable, the fractal geometry of large aggregates seems to depend only upon dimensionality.

In the Witten-Sander model, a seed particle is placed at the center of a d-dimensional lattice, and monomers are introduced one at a time at a randomly chosen site on the lattice perimeter. The monomers describe a random walk until they visit a lattice point adjacent to the seed, at which point they become a part of the seed particle. This is clearly an addition reaction and will not give accurate cluster size distributions. However, it may yield the appropriate fractal dimension for an addition reaction. The fact that smoke formation is not an addition reaction appears relevant to fractal geometry, because simulations in three dimensions³⁴ give $d_f \approx 2.5$ for the Witten-Sander model - in poor agreement with experimental results. Mean-field treatments of Witten-Sander have also been proposed.^{35,36}

2.1.7.1 Cluster-Cluster Aggregation

This model^{38,39} is a variation on Witten-Sander. Here the process seems quite similar to the subject of this thesis: N_0 particles are

placed on random sites in a hypercubic d -dimensional lattice of volume $V_0 = L^d$. They then diffuse just as in the Witten-Sander model and when two occupy neighboring sites they adhere and diffuse together. The velocity of a diffusing cluster scales with its mass as

$$v(m) = m^\alpha \quad [2.58]$$

where α is usually negative. This mass dependent velocity is implemented in the simulation by choosing clusters to move at random but only allowing them to move with a probability proportional to m^α . The clusters neither rotate nor restructure.

There is also a 'hierarchical' model⁸⁷⁻⁸⁹ for cluster-cluster aggregation, in which all particles are grouped into pairs, then one pair of particles is allowed to diffuse until they adhere - without interaction with other particles. Pairs are fused in this way until the original N_0 monomers become $N_0/2$ dimers; then the dimers are grouped into pairs and the process is repeated. Hence at each step all clusters have the same size.

The fact that interacting clusters are roughly the same size in both models apparently plays a dominant role in determining the structure of the resulting clusters. As long as there is no gelation in the regular model, the fractal dimension of large aggregates is the same in both the hierarchical and regular models.⁸⁷ In three dimensions $d_f = 1.75$.^{87,88} Recalling that $d_f = 2.5$ in the Witten-Sander model, we see that aggregates are much more ramified here. The essential reason is that small monomers in Witten-Sander can penetrate the large seed cluster more deeply than a cluster of the same size would. It is also

interesting to note that in the regular version d_f is independent of α as long as $\alpha < 1$.⁸⁷

Kolb⁹⁰ distinguishes between two regimes in this model. He defines the 'cluster density' as

$$\rho = N/V = \rho_0 \bar{m}^{(d-d_f)/d_f} \quad [2.59]$$

where N is the total number of clusters, $\bar{m} = N_0/N$, and $V \equiv R^d$. V is the volume of the lattice measured in units of the average radius of a particle. Relation [2.59] results from the observation that $R \sim \bar{m}^{1/d_f}$. When $\rho \ll 1$ the average distance between clusters is much larger than their radius; whereas, when $\rho \simeq 1$ the two are roughly equivalent, and gelation occurs. With ramified clusters, this effective density always grows as aggregation proceeds.

In simulations, the relations $R \propto \bar{m}^{1/d_f}$ and $C(\vec{r}) \propto r^{-A}$ are found to hold with $d_f + A = D$, as expected (see Equations [2.44] - [2.47], section 2.1.4). Also, d_f and A are independent of time. This time dependence leads Jullien et al.⁸⁷ to postulate dynamical scaling of the form:

$$\bar{m}(t) \propto t^{-\gamma} \quad [2.60]$$

Then, renormalizing time and space[†] they show that

[†] - The procedure for renormalization which leads to scaling relation [2.61] assumes that the positions of clusters are uncorrelated in both time and space and that clusters are all the same size.⁹⁰ Since correlations and fluctuations are neglected, this is

$$\gamma = (1 - \alpha - (d-2)/d_f)^{-1} \quad [2.61]$$

These last two relations are also verified in simulation.

The aspect of this model that makes it especially relevant to our studies is the fact that the Orsay group has also investigated the cluster size distribution. By applying the coagulation equations to this model, and assuming that $a_{ij} \propto (ij)^\omega$ (or, equivalently, that $a_{\lambda i, \lambda j} = \lambda^{2\omega} a_{ij}$) they connect ω to the previously defined exponents:

$$2\omega = \alpha + (d-2)/d_f \quad * \quad [2.62]$$

Hence, in two dimensions $2\omega = \alpha$, and since α is generally negative so is ω . Botet et al.^{9,1} show analytically that for $\omega < 0$ the cluster size distribution exhibits a maximum at

$$(m/\bar{m})_{\max} = \frac{-2\omega}{1-2\omega} \frac{N}{N_0} \quad [2.63]$$

When $\omega = 0$ the peak is found at the origin, as we would expect for case A.

In three dimensions, $\omega = 0$ corresponds to $\alpha = -1/d_f$. In light of von Smoluchowski's analysis, which I described in section 2.1.3.1, we see that ω goes to zero when the hydrodynamic radius of a cluster

a mean-field theory. The coagulation equations also neglect correlations between particles, and this is the physical rationale for connecting α to ω in [2.62].

* - In the factor $(d-2)/d_f$, the '2' is the dimension of a random walk. Generally, it should be replaced by d_w , the dimension of the walk.^{9,1}

(which determines the diffusion coefficient according to the Stokes-Einstein relation [2.14]) grows with mass at the same rate that its 'sphere of influence' does. Although it is hard to justify a kernel of the form $(ij)^\omega$ in the framework of von Smoluchowski's arguments, we might say qualitatively that ω goes negative if the hydrodynamic radius of a cluster grows faster than its cross-section.

One of the most interesting aspects of a paper regarding analytic cluster size distributions by Botet and Jullien⁹¹ is the fact that they rewrite the coagulation equations in order to deal with a finite number of particles. Coagulation equations [2.1] and [2.2] implicitly assume that there is an infinite number of particles. This is the reason that the gel is formally infinite and that the cluster size distribution does not change even after gelation in all of the analytic solutions I have discussed.

For $0 < \omega < 1/2$ the analytic cluster size distribution in finite systems is strictly decreasing, and for $\omega > 1/2$ it actually inverts at some finite time. Thus gelation in this model is distinguished by a distribution that increases with cluster size.

For $\omega < 0$, Kolb⁹⁰ and Botet et al.⁹¹ define a scaling form for a 'reduced' cluster size distribution and show that results of simulations agree with solutions to the coagulation equations for the appropriate ω given by [2.62]. For $\omega < 1/2$, this reduced distribution scales with both time and cluster size for all times. For $\omega > 1/2$ scaling holds only before gelation.

Solutions to the traditional (infinite) coagulation equations

(assuming monodisperse initial conditions and reaction limited kernels) are equivalent to the most probable cluster size distribution in Flory-Stockmayer theory, which also treats infinite systems. Donoghue and Gibbs⁹²⁻⁹⁴ have treated finite systems from an equilibrium standpoint. They show that the average cluster size distribution in a finite system only converges to the most probable distribution in the limit of $N \rightarrow \infty$. In the finite case, the morphology of the distribution does change at gelation: it becomes bimodal, with a peak at large n corresponding to the gel phase. Botet and Jullien⁹¹ consider only the case $\omega < 1/2$, but they do provide the formalism for treating the analytically difficult case in which gelation occurs in a kinetically evolving finite system.

At this date, the cluster size distribution has not been investigated analytically for finite systems after gelation. However, simulations have provided a very interesting qualitative picture.^{87,95} For $\omega > 1/2$, at some point in time a cluster very much larger than all the others begins to form. Not only does this 'gel' cluster effect the cluster size distribution; it also has a different fractal dimension than the smaller clusters. Actually, near its center its fractal dimension is the same as for cluster-cluster aggregation, and near the perimeter it is more dense, with the same fractal dimension as for Witten-Sander. Apparently, it is the great difference in size between the gel cluster and the finite sized clusters that leads to Witten-Sander geometry after gel formation. Also, the gel cluster changes the dynamics of the aggregation process by nature of its structure - through [2.62]; hence, the functional form of the cluster size distribution is expected to change.

2.2 EQUILIBRIUM THEORIES

Although I have not yet discussed the physics of equilibrium, I have already discussed some of the mathematics, because - as I have tried to emphasize - under certain very special conditions, kinetic and equilibrium cluster size distributions are the same. With monodisperse initial conditions and with reaction limited kernels derived for the $A-R-B$, $A-R-B_{f-1}$, $R-A_f$, and A_g-R-B_{f-g} systems using the two principles of section 2.1.1, solutions to the discrete coagulation equations [2.1] correspond precisely to Flory-Stockmayer equilibrium distributions. In section 2.2.2, I discuss special fragmentation kernels that produce the same results.

Since most analytic results for Flory-Stockmayer theory have been covered in the discussions of cases A, B and C and the bilinear kernel, I review just the basic structure of Flory-Stockmayer theory in the next section, where I discuss only case C (and particularly the high functionality limit) specifically. Then, in section 2.2.2, I clarify the rigorous connections between equilibrium and reversible kinetics.

Most of the principles of percolation theory that are appropriate to this problem were reviewed in section 2.1.4 on scaling. Hence, I discuss percolation and related models only enough to show how they

relate to polymer formation and to introduce certain controversies regarding their application.

2.2.1 Flory-Stockmayer Theory

This is not the place to review the theoretical considerations and experimental results that led Flory to propose his principle of equal chemical reactivity. However, before physicists who have little experience in a chemistry laboratory glibly dismiss it as a primitive 'mean-field' assumption, I suggest that they read chapter III of his book Principles of Polymer Chemistry.¹⁰ At the end, he states the principle in this way:

... on the basis of these results together with the assurance provided by theoretical considerations ... we may conclude that at all stages of the polymerization the reactivity of every like functional group is the same ...

I have already underlined the role of equal reactivity in reaction limited kinetic theories. Utilizing this principle, it is also possible to determine the equilibrium size distribution in a polymeric system by the following recipe: first one specifies the bonding rules in a system (A-R-B, etc.), second one specifies the conversion α_i for each type i of functional group in the system, and third one constructs the distribution

using - essentially - combinatorics. The conversion α_i is defined as the fraction of reacted functional groups of type i, and may be interpreted as a probability. Stockmayer¹¹ first showed that this recipe was equivalent to finding the most probable distribution by maximizing the statistical mechanical entropy.

2.2.1.1 The Most Probable Size Distribution

The purpose of this section is to review the basic assumptions of Flory-Stockmayer theory and to show how the statistical mechanical formulation of Cohen and Benedek⁴ allows Flory's assumption of equal reactivity to be relaxed. Spouge¹⁸ uses a very similar approach. In this formulation, one first constructs a canonical partition function to describe the complete system, consisting of solvent and polymer molecules:

$$Z(V, T, \{m_n\}) = z_s(V, T)^N \left[\prod_n z_n(V, T, N)^{m_n} \right] \frac{\Omega(\{m_n\})}{M!} \quad [2.64]$$

where z_s is the partition function of a single solvent molecule, z_n is the partition function of an n-mer, m_n is the number of n-mers, and $\Omega(\{m_n\})$ is the number of distinct ways of combining a total of M distinguishable monomers to form the set $\{m_n\}$. The simple multiplicative dependence of Z upon the single particle partition functions z_s and z_n implies non-interacting particles and no excluded volume effects. Any explicit effect of n-mer translation, rotation, vibration, or

configuration are ignored in the subsequent analysis. In a recent review⁹⁶ of Flory-Stockmayer theory, Gordon discusses these degrees of freedom.

The function $\Omega(\{m_n\})$ depends upon the number of distinct ways W_n that an n-mer can be made from n distinguishable units (i.e., the number of isomers of size n):

$$\frac{\Omega(\{m_n\})}{M!} = \prod_n \frac{1}{m_n!} \left[\frac{W_n}{n!} \right]^{m_n} \quad [2.65]$$

The Gibbs free energy of the system can be calculated from the partition function:

$$G = F + PV = kT \left[\frac{\partial}{\partial \ln V} - 1 \right] \ln Z \quad [2.66]$$

Using general thermodynamic arguments such as the fact that G is an extensive quantity, Cohen and Benedek deduce the chemical potentials of the polymer molecules:

$$\begin{aligned} \mu_n(P, T, X_n) &= \partial G / \partial m_n \\ &= \mu_n^0 + kT \ln X_n \end{aligned} \quad [2.67]$$

where $X_n = m_n/N$ is the mole fraction of n-mers, N is the number of solvent molecules, and μ_n^0 is the standard part of the chemical potential, given by

$$\mu_n^0 = \Phi_n(P, T) - kT \ln(W_n/n!) \quad [2.68]$$

Here Φ is the local change in free energy obtained by adding a single n-mer to the system.

The most probable polymer size distribution is the set $\{m_n\}$ that minimizes the Gibbs free energy under the constraint $\sum_n m_n = M$. This occurs when

$$\mu_n = n\mu_1 \quad [2.69]$$

With [2.67] and [2.68] this gives

$$X_n = X_1^n e^{-(\Phi_n - n\Phi_1)/kT} D_n \quad [2.70]$$

$$\text{where } D_n = W_n/n! \quad [2.71]$$

Here, the first term results from the entropy of mixing and represents the entropic cost (since X_1 is always less than one) of localizing n free monomers. The second term is a Boltzmann factor arising from the energy of bond formation. Since bond energies are always negative, this term promotes the formation of large n-mers. Finally, D_n is called a degeneracy factor since it represents the number of ways an n-mer can be made. The factorial in the denominator accounts for the indistinguishability of the monomeric units under Maxwell-Boltzmann statistics.

Equation [2.70] constitutes a general solution to the equilibrium problem. The basic parameters are $(\Phi_n - n\Phi_1)$, the standard free energy of the bonds in an n-mer, and X_1 , the mole fraction of free monomers. Since X_1 is difficult to control experimentally, one generally transforms to X_0 , the total mole fraction of monomeric units, through the relation $X_0 = \sum_n nX_n$. If a gel has formed, X_0 is the mole fraction of the sol phase.

In considering specific systems, Flory made two simplifying assumptions. The first, and most fundamental, is the assumption of equal reactivity. In order to simplify the calculation of D_n , Flory also required acyclic, or Cayley tree-like polymers, noting that this assumption causes small errors in the calculation of the gel point.⁹⁷ In the next section I show that this second assumption actually results from the first in the thermodynamic limit.

Cohen and Benedek show that equal reactivity corresponds in their formalism to equal standard free energies of bond formation for all equivalent bonds. Since the second assumption ensures that a n-mer will have precisely n-1 bonds, equal reactivity gives

$$\Phi_n - n\Phi_1 = (n-1)g \quad [2.72]$$

where g is the free energy of an individual bond. The simplified polymer distribution then becomes

$$X_n = X_1^n e^{-(n-1)g/kT} D_n \quad [2.73]$$

Applying this result to the A-R-B, A-R-B_{f-1}, and R-A_f systems, Cohen and Benedek show complete correspondence between their formalism and Flory's.

By giving the function $\Phi_{n-n\Phi_1}$ a more general form, we see that it is possible in this framework to relax the equal reactivity assumption. Of course, this will tend to produce more complicated polymer size distributions. Spouge⁹⁸ describes a probabilistic approach to relaxing the assumption.

Cohen and Benedek give solutions for all three polymer systems at arbitrary f . They show that the important features of each system are unchanged in the limit of $f \rightarrow \infty$ and emphasize the mathematical simplicity of this limit.

As I have stated, the R-A_f ($f \rightarrow \infty$) system, which corresponds precisely to case C with monodisperse initial conditions, may describe colloidal systems at equilibrium. In the equilibrium case, b , which is essentially analogous to α , is a deterministic parameter, independent of time. For our purposes it is useful to relate b to the free energy of bond formation.

In the R-A_f system, the degeneracy factor D_n is given by:

$$D_n(f) = \frac{f^n (fn-n)!}{(fn-2n+2)! n!} \quad [2.74]$$

At large but finite f , this expression simplifies to:

$$D_n(f \gg 1) = f^{2n-2} \frac{n^{n-2}}{n!} \quad [2.75]$$

The factor f^{2n-2} may be absorbed into the Boltzmann factor of Equation [2.73], thereby rescaling the free energy of bond formation:

$$g' = g - kT \ln f^2 \quad [2.76]$$

It appears at first that g' , the effective free energy of bond formation, should diverge in the limit $f \rightarrow \infty$; however, one should recognize that g is also a free energy. In the continuum limit the concept of a binding 'site' becomes less useful. The area of a 'site' becomes negligibly small; so that the probability of finding it goes to zero, and entropic effects cause the first term, g , to diverge in the positive direction - offsetting the second term. Therefore, g' is the relevant parameter in the continuum limit.

The simplified degeneracy factor, $D'_n = n^{n-2}/n!$, now represents the number of distinct ways of attaching n indistinguishable monomers with $n-1$ indistinguishable bonds.⁴

Cohen and Benedek show that b is related to g' by

$$b = \frac{X_0}{2} e^{-g'/kT} \quad [2.77]$$

Thus it is possible to estimate the effective strength of a bond by measuring b at equilibrium.

It is worth noting here that Spouge¹⁸⁻²⁰ has used a very similar approach to find pre-gelation solutions and gel points for the general $A-R-B_{f-g}$ polymer system. These solutions reduce with appropriate choices for f and g to the known $A-R-B$ and $A-R-B_{f-1}$ solutions; and if

either g or $f-g$ exceeds 2, gelation may occur. Spouge proves a relation between the number of n -mer isomers W_n and the reaction limited kernel and shows explicitly that equilibrium is a delicately balanced kinetic state. In fact, he uses his paper on equilibrium¹⁸ as part of a general solution²⁵ to the irreversible coagulation equations with bilinear kernel $a_{ij} = A + B(i+j) + Cij$. I discuss the relation in detail in section 2.2.2.

2.2.1.2 - Gelation and Cyclic Bond Formation

I discussed the differing Flory and Stockmayer gelation models in my review of case C (section 2.1.3.3). Here I discuss them in the context of the equilibrium theory.

Flory's first paper concerning gelation,⁹ dealt with the $R-A_3$ polymer system. Assuming equal reactivity and acyclic structures, he calculated the cluster size distribution and gel fraction as a function of α , the fraction of reacted functional groups. Stockmayer¹¹ subsequently generalized Flory's result to arbitrary f . In examining post-gelation relationships, he showed that Flory's method of calculating gel fraction led to cycles in the gel. He concluded by questioning the "fundamental logic involved in Flory's procedure", claiming that it could not be rigorous. Flory responded by asserting that his assumption applied only to "finite species".⁹⁹ This sparked a debate that was finally settled in the computer simulations of Falk and Thomas.¹⁰⁰

Flory and Stockmayer consider infinite systems. As I have shown, the effective value of α (or b) in the sol decreases in Flory's post-gel model, while in Stockmayer's α_s sticks at its gel point value.

Falk and Thomas consider a finite number N of $R-A_f$ monomers, which bind in a stepwise random fashion. In their 'rings allowed' model, all Nf functional groups react two at a time with equal probability until a fraction α are bonded. Their 'rings forbidden' model is essentially the same, except that at each step the newest bond is tested to see if it causes a cycle; the bond is broken if it does. By varying N , Falk and Thomas extrapolate to the thermodynamic limit, $N = \infty$. In this limit the two models agree as long as α stays below the critical value α_c .[†] The cluster size distribution agrees with Flory-Stockmayer theory, and even in the 'rings allowed' model the number of cycles in the sol goes to zero. Above α_c , the 'rings allowed' model gives Flory's cluster size distribution, while the 'rings forbidden' model gives Stockmayer's. This simulation clarifies the assumptions of both models and shows that, indeed, both are consistent.

The question of the thermodynamic limit is an important one. Donoghue and Gibbs²⁻⁴ consider finite systems for which the acyclic assumption is strictly maintained ('rings forbidden' model). They show that in finite systems one must calculate the mean or average cluster size distribution, rather than the most probable as in Flory-Stockmayer theory. In an infinite system, the two are identical.

[†] - Note: $\alpha_c = 1/(f-1)$ for finite f .

Donoghue and Gibbs show that the cluster size distribution becomes bimodal past the critical point. Furthermore, in an asymptotically large system, they show that the Stockmayer distribution holds for all α .

Spouge^{101,102} extends the results of both Donoghue et al. and Falk et al. by examining both the 'rings allowed' and 'rings forbidden' models analytically. He also shows how to incorporate steric hindrance using graph theory. Furthermore, in the thermodynamic limit of the 'rings allowed' model he calculates the number of cycles in the gel, showing that his results agree with the kinetic post-gelation Flory model of Ziff and Stell.⁵⁴ As I mentioned in section 2.1.3.3, the gel reacts with both itself and the sol in the Flory model, while in the Stockmayer model it reacts with neither.

Although these aspects of ring formation may seem more a question of logic and mathematics than physics, the results do indicate the power of Flory's principle of equal reactivity. Since equal reactivity leads to acyclic sol clusters, they need not be a separate postulate in Flory-Stockmayer theory. Cohen and Benedek point out that a finite sized cluster contains an infinitesimal fraction of the free functional groups in a macroscopic system. Hence, under equal reactivity, the probability that a free group on a small cluster will bind to another free group on the same cluster is negligibly small (zero in the thermodynamic limit). On the other hand, a gel particle may form loops since it contains a significant fraction of the free groups in the system at a given time.

2.2.2 Equilibrium Kinetics: the Reversible Coagulation Equations

In writing equations [2.1] and [2.2], I mentioned that they apply only when the bond strengths in a cluster are effectively infinite. In such a case, the aggregation process never actually stops until there is just one huge cluster left containing all of the units in the system. With [2.1] and [2.2] the concentrations c_n of finite species all drop to zero at infinite time, because the gel is infinitely large. After observing that kinetic solutions starting from a monodisperse distribution coincide exactly with equilibrium Flory-Stockmayer solutions, it is natural to attempt to build some process for stopping the reaction into the coagulation equations. Of course this process is cluster dissociation, the most important term of which will describe the separation of a large cluster into two smaller ones. With the addition of this process, equations [2.1] become

$$\frac{dc_n}{dt} = 1/2 \sum_{k=1}^{n-1} (a_{n-k,k} c_{n-k} c_k - b_{n-k,k} c_n) - \sum_{k=1}^{\infty} (a_{nk} c_n c_k - b_{nk} c_{n+k}) \quad [2.78]$$

where b_{ij} is the two particle dissociation coefficient, or kernel which determines the rate at which $(i+j)$ -mers break up into i -mers and j -mers, and $b_{ji} = b_{ij}$. The continuous analogue of this set of equations follows naturally by comparison with [2.2].

Equilibrium is a dynamic state in which association and dissociation processes exactly cancel each other. In the kinetic context the cluster size distribution at equilibrium is determined entirely by the

association and dissociation kernels. Taking the stationary ($dc_n/dt = 0$) solution to [2.78] we find

$$\frac{a_{ij}}{b_{ij}} = \frac{c_{i+j}(\infty)}{c_i(\infty)c_j(\infty)} \quad [2.79]$$

This is essentially the principle of detailed balance. On the other hand we can also look at this equation from right to left and observe that the energetics and stoichiometry of equilibrium fully determine the ratio of a_{ij} to b_{ij} . Since fragmentation may not become significant until the system is highly aggregated, there is no physical reason for the cluster size distribution to have the same shape at all times. Also, it is possible to obtain a Flory-Stockmayer distribution, for instance, at equilibrium even when the association and dissociation kernels are not given by the appropriate reaction limited theories.

I have spent a great deal of time discussing the physics of association kernels, but I can not do the same for dissociation kernels, because there is far less known about them. Blatz and Tobolsky¹⁰³ first solved the reversible equations in 1945 for the reaction limited A-R-B polymer system. In doing so, they introduced the converse to Flory's principle of equal reactivity: in reaction limited systems, every bond has an equal probability of breaking at all stages of the reaction. Progress along the same lines has only resumed in the past two or three years, and even so, only reaction limited dissociation kernels have ever been considered analytically. It is harder to justify reaction limited b_{ij} 's than a_{ij} 's, because diffusion will play an

even larger role in fragmentation than it does in aggregation. The two particles formed after a bond breaks are so close to each other that they will probably collide again. Hence, the rate at which free clusters are actually formed is not necessarily proportional to the rate at which bonds break. I discuss this idea in more depth in chapter V, because cluster fragmentation may explain the results I have obtained for colloid flocculation. Here I cover only reaction limited kernels, where many intriguing results have recently been obtained.

If one already knows the equilibrium cluster size distribution from Flory-Stockmayer theory, it is possible to construct the dissociation (or fragmentation) kernel using equations [2.79] and [2.73]:

$$b_{ij} = \lambda \frac{D_i D_j}{D_{i+j}} a_{ij} \quad [2.80]$$

$$\text{where} \quad \lambda = c_{\text{solvent}} e^{g/kT} \quad [2.81]$$

and c_{solvent} is the concentration of solvent molecules.

Van Dongen and Ernst^{11,22} have recently used [2.80] to solve the reversible equations with general bilinear kernel $a_{ij} = A + B(i+j) + Cij$ and for $a_{ij} = (i(f-2)+2)(j(f-2)+2)$, which corresponds to the reaction limited R-A_f system. They have also treated a special case relating to rouleaux formation.¹⁰⁴ In all three cases, they use reaction limited a_{ij} 's and degeneracy factors from the corresponding equilibrium distributions to calculate b_{ij} . It is easily shown that this yields fragmentation kernels that are entirely determined by the rate of bond breakage. Upon plugging b_{ij} into the coagulation equations

they find that the kinetically evolving distribution is, once again, identical to the equilibrium distribution. Since van Dongen and Ernst have basically used the known solution to construct their problem, this result is not surprising. The mathematics is new in this procedure, but the physics is not. The time dependence of cluster growth is slightly more complicated than in the unidirectional case, but in the limit $t \rightarrow \infty$ the degree of polymerization depends upon λ (or bond strength) exactly as it does in Flory-Stockmayer theory. Van Dongen and Ernst also solve both the Flory and Stockmayer post-gelation solutions, with expected results.

Spouge¹⁸ explores the connection with the equilibrium formulation at a more fundamental level. He shows that reversible kinetics are implicit in the equilibrium formulation by relating the mathematically simple association kernel in a unidirectional system to the degeneracy factors in an equilibrium system. The equation upon which this relationship is based is

$$2(k-1)w_k = \sum_{i=1}^{k-1} \frac{k!}{i!(k-i)!} w_i w_{k-i} a_{i,k-i} ; \quad w_1 = 1 \quad [2.82]$$

Recall that $w_i = i!D_i$ is essentially the number of branched tree isomers of mass i . For reasons of clarity, it is probably best to quote Spouge's explanation of this equation:

...The left side ... is the number of ways of assembling a k -mer, choosing one of its $k-1$ bonds (noncyclic polymers) and then painting one of the

two polymers on either side of the chosen bond black. The right side ... is the sum over i of the number of ways of starting with k units, painting i of them black, assembling a painted i -mer and an unpainted $(k-i)$ -mer, and then choosing a bond through which to combine them into a k -mer...¹⁸

With Blatz and Tobolski's principle, equation [2.82] is an explicit statement of detailed balance for k -mers. Consider the reactions



where R_k represents a k -mer, and i runs from 1 to $k-1$. The left hand side of [2.82] is proportional to the rate at which a uniform distribution of w_k isomeric k -mers breaks apart, assuming that each bond has an equal probability of breaking at a given time. The right hand side is proportional to the aggregation rate for k -mers, assuming that there is a uniform distribution over isomeric configurations for every species. The proportionality constant is determined by the constraints $\sum_n c_n = M_0$ and $\sum_n n c_n = M_1$.

Spouge stresses the fact that all necessary information about an equilibrium polymer system is contained in the reaction limited association kernel a_{ij} . Clearly, van Dongen and Ernst rely upon this fact as they construct their fragmentation kernels. In fact, a_{ij} can also be used to construct degeneracy factors for complicated systems. Botet and

Jullien²¹ use [2.82] to construct degeneracy factors for the $(ij)^{\omega}$ kernel.

Equation [2.82] also explains why it is necessary to start from a monodisperse distribution in order to obtain Flory-Stockmayer distributions. The equation will only describe detailed balance if there is a uniform distribution of isomers for all cluster sizes at all times. This condition is satisfied when aggregation proceeds randomly from monodisperse initial conditions. Van Dongen and Ernst²² point out that the fragmentation kernel [2.80] does depend upon the distribution of isomers and that, in general, a microscopic rate equation must be constructed in terms of the concentrations of each type of isomer. Hendriks¹⁰⁵ outlines these microscopic rate equations in a paper that also considers mean and most probable distributions in finite and infinite systems.

Finally, Ernst¹⁰⁶ discusses relaxation towards equilibrium for general initial conditions in the reaction limited A-R-B polymer system. In the process, he proves the so-called F-theorem: an analogue of Boltzmann's H-theorem in the context of the coagulation equations.

2.2.3 Percolation Theory

Flory-Stockmayer theory and kinetic theories based upon the coagulation equations are mean-field theories in the sense that they neglect correlations and fluctuations in the sol. The principle of equal reactivity ignores steric and excluded volume effects as well as the possible

entropic advantage of cycle formation due to the proximity of free sites on the same n-mer. The coagulation equations [2.1] involve only the mean concentration of n-mers and also imply that their positions are uncorrelated.

Fluctuations and correlations dominate the critical phenomena in liquid-gas and magnetic phase transitions. This observation first led de Gennes⁶⁰ and Stauffer⁶¹ to propose percolation as a model for gelation in polymer systems. Unfortunately, it is difficult to discuss anything but the critical phenomena of gelation in the context of percolation.[†] I have reviewed most of the basic principles of this model in section 2.1.4.

In fact, Flory-Stockmayer theory was the first example of what came to be called percolation. Acyclic Flory polymers are also called Cayley trees, and $R-A_f$ random polycondensation is simply percolation on a so-called Bethe lattice with coordination number f . Percolation comes in many flavors, and other closely related lattice models such as random walks, self-avoiding random walks, lattice animals,^{*} and the computer simulations of section 2.1.7 have all been proposed as models for polymer formation. Reviews by Stauffer,¹⁰⁸ Stauffer et al.⁶² and Stanley et al.⁷⁰

[†] - The one exception I have found is a paper by Kinzel,¹⁰⁷ which utilizes renormalization group theory on a 2-d triangular lattice to investigate the cluster size distribution. Kinzel calculates the values of τ and σ near the gel point, where the cluster number scaling hypothesis [2.40] holds. Far below the gel point $c_n \sim \exp\{n(p_c - p)^{1/\sigma}\}$ with $\sigma = 0.5 \pm 0.01$.

^{*} - A lattice animal is simply a cluster on a lattice. The basic problem is to determine the number of unconstrained configurations such a cluster may have. All configurations are assumed equally likely. In percolation, some configurations are more likely than others, so average properties of percolation clusters differ from those of lattice animals. The name 'lattice animal' refers to the highly theoretical biological question: How many different multicellular organisms can be constructed from n cells?¹⁰⁹

serve as references for this vast subject.

In site percolation, the sites on a lattice are randomly occupied with probability p . At some well defined critical value $p = p_c$, a connected cluster of occupied nearest neighbor sites suddenly spans the lattice. This phenomenon is clearly quite similar to gelation. The critical exponents that I have defined in section 2.1.4 are independent of the details of the lattice and even whether there is a lattice at all. They depend only upon dimensionality. This universality also extends to bond percolation, site-bond percolation, and correlated site-bond percolation.⁶² Above the upper critical dimension $d = 6$, the exponents maintain the Flory-Stockmayer values of Table 2.3.

Flory¹¹⁰ observes that experimental gel points generally occur above the values he would predict. He attributes this to cyclical bond formation, which should be more prevalent at low initial concentrations c_0 . Stockmayer and Weil¹¹¹ have measured the gel point as a function of c_0 . By extrapolating to the limit $c_0 = \infty$, they have obtained precise agreement with predicted values.

But the gel point is not a universal characteristic. Partisans of percolation claim that the absence of ring formation is a drastic approximation that will effect critical exponents severely. Unfortunately, very few experiments exist to test these claims. Some experiments give percolation values and others Flory-Stockmayer.⁶²

On the other hand, proponents of Flory-Stockmayer theory,⁹⁶ suggest that percolation errs in the other direction, predicting too many cycles. Experimentally,¹¹² it is observed that steric effects rarely allow

anything but 5, 6, and 7 membered rings to form.

Stauffer et al.⁶² also discount Flory-Stockmayer theory by claiming that it leads to infinite particle density in the interior of the gel. A close scrutiny of their argument, however, reveals that they assume the gel has the same internal structure as large sol aggregates. They are apparently not aware of Flory's suggestion that the gel forms rings and is therefore more compact.

The concept of universality was brought to the polymer problem almost as an assumption by percolation theorists. Now that a few years have passed, it is clear that the relevant parameters in gelation have yet to be defined. There is a bewildering variety of exponents, and there are few well-defined universality classes. Most likely, both the lattice theories and Flory-Stockmayer theory will have to be modified to provide the true theory. The only answers to questions about critical exponents will lie in experiments - most likely with polymer systems, in which diffusion may not play as important a role as it does with colloids.

2.3 CONCLUSIONS

In this review, I have attempted to cover the theories that I think are most relevant to colloidal aggregation. The general structure of this chapter betrays my basic prejudice that in the future a kinetic approach will prove more appropriate to this problem than an equilibrium one.

Colloidal aggregation presents some interesting questions: How can diffusion controlled aggregation (Case A) be reconciled with the equilibrium $R-A_{\infty}$ model, which gives the same cluster size distribution as Case C (see Table 2.1)? And will there be a cross-over between a kinetic and an equilibrium regime?

In the initial stages of cluster growth, aggregation processes dominate fragmentation. For colloidal flocculation aggregation is diffusion controlled. As the reaction proceeds, fragmentation gains in importance, and the system approaches equilibrium. At equilibrium energetics and stoichiometry fully determine the state of the system according to the principle of detailed balance (equation [2.79]). Therefore, different physical mechanisms dictate the form of the cluster size distribution at short and long times. These same mechanisms dictate whether or not it is possible for a gel phase to form. For colloidal flocculation I expect the distribution to evolve in time

from Case A to Case C. Distribution A precludes sol-gel coexistence while distribution C permits such coexistence; thus a gel phase could form as equilibrium is approached.

In Chapter V - after presenting my data - I propose a framework based on detailed balance for determining the complete evolution of the cluster size distribution over time. This framework is fundamentally different from the approach of van Dongen and Ernst (see section 2.2.2) in that a change in the shape of the cluster size distribution is specifically built in. Van Dongen and Ernst build the kinetic mechanisms of equilibrium into their theory from the very start.

The gelation theories that I have described have seen little testing of any kind; and, since I measure only the concentrations of finite sized species here, I do not analyze gelation quantitatively. The most interesting unanswered questions involving gelation regard finite systems. The work on cluster-cluster aggregation (section 2.1.7.1), including the analytical work of Botet and Jullien,⁹¹ appears to hold the most promise in this regard. This work as well as the work of Donoghue and Gibbs⁹²⁻⁹⁴ on the finite Stockmayer model indicates that gelation should have a profound effect upon kinetics among the finite sized species.

REFERENCES - CHAPTER II

1. von Smoluchowski, M., Phys. Z., **17**, 585 (1916).
2. von Smoluchowski, M., Z. Phys. Chem., **92**, 129 (1917).
3. Drake, R.L., in "Topics in Current Aerosol Research", Vol. 3, G.M. Hidy and J.R. Brock, eds., Pergamon Press, New York, 1972.
4. Cohen, R.J. and Benedek, G.B., J. Phys. Chem., **86**, 3696 (1982).
5. Noyes, R.M., Prog. Reaction Kinetics, **1**, 129 (1961).
6. Johnston, D.F., Ph.D. Thesis, M.I.T. (unpublished), 1983, section 1.3.
7. Flory, P.J., J. Am. Chem. Soc., **63**, 3083 (1941).
8. Flory, P.J., J. Am. Chem. Soc., **63**, 3091 (1941).
9. Flory, P.J., J. Am. Chem. Soc., **63**, 3096 (1941).
10. Flory, P.J., "Principles of Polymer Chemistry", Cornell University Press, Ithaca, 1953.
11. Stockmayer, W.H., J. Chem. Phys., **11**, 45 (1943).
12. Stockmayer, W.H., J. Chem. Phys., **12**, 125 (1944).
13. Drake, R.L., J. Atmos. Sci., **29**, 537 (1972)
14. McLeod, J.B., Quart. J. Math., **13**, 119, 193, 283 (1962).
15. McLeod, J.B., Proc. London Math. Soc., **14**, 445 (1964).
16. Ziff, R.M., J. Stat. Phys., **23**, 241 (1980).
17. Trubnikov, B.A., Sov. Phys. Doklady, **16**, 124 (1971).
18. Spouge, J.L., Macromolecules, **16**, 121 (1983).
19. Spouge, J.L., J. Stat. Phys., **31**, 363 (1983).
20. Spouge, J.L., J. Phys. A: Math. Gen., **16**, 767 (1983).
21. Van Dongen, P. and Ernst, M.H., J. Phys. A: Math. Gen., **16**, L327 (1983).
22. Van Dongen, P. and Ernst, M.H., "Kinetics of Reversible Polymerization", preprint, 1984.
23. Spouge, J.L., J. Phys. A: Math. Gen., **16**, 3127 (1983).
24. Spouge, J.L., Adv. Appl. Prob., **16**, 56 (1984).
25. Solutions may be found in Reference 3. For solutions in terms of the variable b see Reference 4.
26. Dostal, H. and Raff, R., Z. Phys. Chem. B, **32**, 117 (1936).
27. Perelson, A.S., in "Mathematical Models in Molecular and Cellular Biology", L.A. Segal, ed., Cambridge University Press, Cambridge, 1979.
28. Chandrasekhar, S., Rev. Mod. Phys., **15**, 1 (1943).
29. Forrest, S.R. and Witten, T.A., Jr., J. Phys. A: Math. Gen., **12**, L109 (1979).
30. Family, F. and Landau, D.P., eds., "Kinetics of Aggregation and Gelation", North Holland, Amsterdam, 1984.
31. Shaeffer, D.W., Martin, J.E., Wiltzius, P.W., and Cannell, D.S., Phys. Rev. Lett., **52**, 2371 (1984).
32. Shaeffer, D.W., Martin, J.E., Wiltzius, P.W., and Cannell, D.S., in Reference 30.
33. Martin, J.E. and Schaefer, D.W., "Dynamics of Fractal Colloidal Aggregates", preprint, 1984.
34. Shaeffer, D.W. and Keefer, K.D., Mat. Res. Soc. Symp. Proc., **32**, 1 (1984).
35. Shaeffer, D.W. and Keefer, K.D., "Origin of Fractal Structures in Amorphous Materials", preprint, 1984.
36. Weitz, D.A. and Oliveria, M., Phys. Rev. Lett., **52**, 1433 (1984).

37. Weitz, D.A. and Huang, J.S., in Reference 30.
38. Weitz, D.A., Huang, J.S., Lin, M.Y., and Sung, J., Phys. Rev. Lett., **53**, 1657 (1984).
39. Sinha, S.K., Freltoft, T., and Kjems, J., in Reference 30.
40. Lichtenbelt, W. Th., Pathmamanoharan, C., and Wiersema, P.H., J. Colloid Interface Sci., **49**, 281 (1974).
41. Lips, A., Smart, C., and Willis, E., Trans. Faraday Soc., **67**, 2979 (1971).
42. Lips, A. and Willis, E., J. Chem. Soc. Faraday, **69**, 1226 (1973).
43. Cummins, P.G., Staples, E.J., and Thompson, L.G., J. Colloid Interface Science, **92**, 189 (1983).
44. Golovin, A.M., Bull. Acad. Sci. USSR, Geophys. Ser., No. 5, 482 (1963).
45. Scott, W.T., J. Atmos. Sci., **25**, 54 (1968).
46. Swift, D.L. and Friedlander, S.K., J. Colloid Sci., **19**, 621 (1984).
47. Goldberg, R., J. Am. Chem. Soc., **74**, 5715 (1952).
48. von Schulthess, G.K., Benedek, G.B. and De Blois, R.W., Macromolecules, **13**, 939 (1980).
49. von Schulthess, G.K., Benedek, G.B., and De Blois, R.W., Macromolecules, **16**, 434 (1983).
50. von Schulthess, G.K., Ph.D. Thesis, M.I.T. (unpublished), 1979.
51. Johnston, D.F. and Benedek, G.B., in Reference 30.
52. Johnston, D.F., Ph.D. Thesis, M.I.T. (unpublished), 1983.
53. Cohen, R.J., von Schulthess, G.K. and Benedek, G.B., Ferroelectrics, **30**, 185 (1980).
54. Ziff, R.M. and Stell, G., J. Chem. Phys., **73**, 3492, (1980).
55. Ziff, R.M., Ernst, M.H., and Hendriks, E.M., J. Phys. A: Math. Gen., **16**, 2293 (1983).
56. Mandelbrot, B.B., "The Fractal Geometry of Nature", Freeman, New York, 1982.
57. Vicsek, T. and Family, F., in Reference 30.
58. Vicsek, T. and Family, F., Phys. Rev. Lett., **52**, 1669 (1984).
59. Gordon, M., in Gels, Gelling Processes (conf. proc.): Faraday Disc. **57**, 1 (1974).
60. de Gennes, P.G., J. Physique, **37**, L1 (1976).
61. Stauffer, D., J. Chem. Soc., Faraday Trans. 2, **72**, 1354 (1976).
62. Stauffer, D., Coniglio, A., and Adam, M., Adv. Poly. Sci., **44**, 103 (1982).
63. Aharony, A., Phys. Rev., **B22**, 400 (1980).
64. Witten, T.A. Jr., and Sander, L.M., Phys. Rev. Lett., **47**, 1400 (1980).
65. Witten, T.A. Jr., and Sander, L.M., Phys. Rev., **B27**, 5686 (1983).
66. Meakin, P., Phys. Rev., **A27**, 1495 (1983).
67. Meakin, P., Phys. Rev., **A27**, 604 (1983).
68. Meakin, P., Phys. Rev. Lett., **51**, 1119 (1983).
69. Kolb, M., Botet, R., and Jullien, R., Phys. Rev. Lett., **51**, 1123 (1983).
70. Stanley, H.E., Reynolds, P.J., Redner, S., and Family, F., in "Real Space Renormalization", T.W. Burkhardt and J.M.J. van Leeuwen, eds., Springer-Verlag, Heidelberg, 1982.
71. Zimm, B.H. and Stockmayer, W.H., J. Chem. Phys., **17**, 1301 (1949).
72. Dobson, G.R. and Gordon, M., J. Chem. Phys., **41**, 2389 (1964).
73. de Gennes, P.G., Biopolymers, **6**, 715 (1968).
74. Leyvraz, F., J. Phys. A: Math. Gen., **16**, 2861 (1983).
75. Ziff R.M., Hendriks, E.M., and Ernst, M.H., Phys. Rev. Lett., **49**, 593 (1982).

76. White, W., Proc. Am. Math. Soc., **80**, 273 (1980).
77. Leyvraz, F. and Tshudi, H.R., J. Phys. A: Math. Gen., **15**, 1951 (1982).
78. Ernst, M.H., Hendriks, E.M., and Leyvraz, F., J. Phys. A: Math. Gen., **17**, 2132 (1984).
79. Ernst, M.H., Hendriks, E.M., and Ziff, R.M., J. Phys. A: Math. Gen., **15**, L74 (1982).
80. Leyvraz, F., Phys. Rev., **A29**, 854 (1984).
81. Hendriks, E.M., Ernst, M.H., and Ziff, R.M., J. Stat. Phys., **31**, 519 (1983).
82. Ernst, M.H., Ziff, R.M., and Hendriks, E.M., J. Colloid Interface Sci., **97**, 266 (1984).
83. Friedlander, S.K., "Smoke, Dust and Haze", Wiley, New York, 1977.
84. Meakin, P., J. Colloid Interface Sci., **102**, 491, 505 (1984).
85. Muthukumar, Phys. Rev. Lett., **50**, 686 (1983).
86. Hentschel, N.G.E., Phys. Rev. Lett., **52**, 212 (1984).
87. Jullien, R., Kolb, M., and Botet, R., in Reference 30.
88. Botet, R., Jullien, R., and Kolb, M., J. Physique Lettres, **45**, L211 (1984).
89. Botet, R., Jullien, R., and Kolb, M., J. Phys. A: Math. Gen., **17**, L75 (1984).
90. Kolb, M., Phys. Rev. Lett., **53**, 1653 (1984).
91. Botet, R. and Jullien, R., J. Phys. A: Math. Gen., **17**, 2517 (1984).
92. Donoghue, E. and Gibbs, J., J. Chem. Phys., **70**, 2346 (1979).
93. Donoghue, E., J. Chem. Phys., **77**, 4236 (1982).
94. Donoghue, E., in Reference 30.
95. Botet, R., Jullien, R., and Kolb, M., Phys. Rev., **A30**, 2150 (1984).
96. Gordon, M., Macromolecules, **17**, 514 (1984).
97. Reference 10, p. 354 ff.
98. Spouge, J.L., Macromolecules, **16**, 831 (1983).
99. Flory, Chem. Rev., **38**, 137 (1946), p. 192.
100. Falk, M. and Thomas R.E., Can. J. Chem., **52**, 3285 (1974).
101. Spouge, J.L., "Analytic Results for Finite Systems of Ringed Flory Polymers", preprint, 1984.
102. Spouge, J.L., "Polymers and Random Graphs: Asymptotic Equivalence to Branching Processes", preprint, 1984.
103. Blatz, P.J. and Tobolsky, A.V., J. Chem. Phys., **49**, 77 (1945).
104. Van Dongen, P. and Ernst, M.H., in Reference 30.
105. Hendriks, E.M., "Cluster Size Distributions in Equilibrium", preprint, 1984.
106. Ernst, M.H., in "Studies in Statistical Mechanics", vol. X, E.W. Montroll and J.L. Lebowitz, eds., North Holland, Amsterdam, 1983.
107. Kinzel, W., Z. Phys., **B34**, 79 (1979).
108. Stauffer, D., Phys. Reps., **54**, 1 (1979).
109. Reference 108, p. 52.
110. Reference 10, pps. 354-356.
111. Stockmayer, W. H., in "Advancing Fronts in Chemistry", S. B. Twiss, ed., Reinhold, New York, 1945.
112. Reference 10, chapter III.

CHAPTER III

EXPERIMENTAL METHODS

3.1 The Optical Pulse Particle Size Analyzer

The determination of size distributions in dispersions of sub-micron particles is important not only to colloid science, but also to a number of problems in physics, chemistry, biology and engineering. The size distribution determines many bulk properties of a dispersion and - as I show in this thesis - provides detailed information about the mechanisms governing both the kinetics and thermodynamics of aggregation.

A number of techniques have been developed to characterize such size distributions. The most prevalent is light scattering, which has mainly been used to measure bulk properties of colloidal dispersions and aerosols. Various weighted averages of the particle size distribution may be deduced from the turbidity of the solution,¹ the mean intensity of the scattered light,²⁻⁷ or its temporal correlation function.⁸⁻¹² With more polydisperse samples, it becomes increasingly difficult to characterize the distribution using these techniques. Consequently, single particle techniques - which measure the distribution itself - have emerged.

Resistive pulse analysis, invented by Coulter in 1949,¹³ is the most widely used single particle sizing method. While commercial Coulter counters are designed for particles larger than one micron, a Nanopar resistive pulse analyzer developed by Deblois and Bean in 1970^{14,15} has been used to detect the aggregation of 235 nm latex spheres.¹⁶⁻²⁰ Since the resistive pulse technique requires electrolytic solvents, it is of limited utility when salt is an experimental parameter - such as in studies of colloid stability. Alternatively, some single particle counters measure fluorescence²¹ or scattered light intensity.²¹⁻²⁴ Flow cytometry²⁵ has combined all three detection techniques with digital signal processing and hydrodynamic focussing in an extensive effort to characterize and sort individual mammalian cells - particles larger than one micron.

In this section I discuss an optical pulse particle size analyzer that I have designed to study colloid flocculation. This instrument is distinguished from similar optical devices by its explicit use of a simple relation, derived below, between low angle scattered light intensity and cluster size. In the low angle limit, we expect intensity to be proportional to n^2 , the square of the number of spheres in a cluster. I demonstrate that this n^2 dependence holds with remarkable precision and is independent of cluster shape and orientation. While this might be expected for very small particles in the Rayleigh-Gans-Debye regime, I show here that it is true even when the individual spheres are Mie scatterers - with diameters up to three times the wavelength of the incident light.

The fact that coherent, low angle light scattering is insensitive

to cluster shape and orientation, gives this instrument extremely high resolution in the measurement of cluster size distributions - much higher, in fact, than it is possible to obtain with either fluorescence detectors or resistive pulse analyzers, because shape and orientation have an effect even for small cluster numbers with these techniques.

3.1.1 Light Scattering Theory

The problem of scattering from single particles of arbitrary size and shape differs fundamentally from the problem of scattering from clusters of identical sub-units. Although exact solutions exist for single spheres,²⁶⁻²⁸ cylinders, and other simple shapes^{29,30} and for clusters of spheres,^{31,32} the mathematical complexity of these solutions sometimes obscures the simpler physical properties of scattering which are clarified in various approximations. For single particles small compared to the wavelength of the incident light, the scattered light intensity at low angles is proportional to V^2 , where V is the volume of the particles. When a single sphere is larger than 3 or 4 times the incident wavelength, low angle intensity is directly proportional to V .^{34,35-37} For clusters, scattered intensity at low angles will be proportional to n^2 even when the individual sub-units are too large to yield V^2 intensity dependence individually. In this section, I briefly review both kinds of scattering and establish criteria for V^2 intensity dependence in the case of single particles and for n^2

dependence in the case of clusters.

3.1.1.1 Scattering from Single Particles

The exact solution for the scattering of a plane electromagnetic wave by a sphere of arbitrary size is commonly referred to as the Mie solution.²⁶ While it is possible to obtain an analytic expansion for the small particle (Rayleigh) limit,²⁶ it is quite difficult to find a simple small angle approximation that will apply to spheres of arbitrary size. Nevertheless, the numerical solution to the low angle scattering problem may be easily constructed from tabulated values of the Mie solution.²⁷⁻⁴⁰ In this review, I discuss small particle approximations first, because insights gained in this limit provide a useful context for interpreting the exact solution.

Rayleigh's theory of scattering by a small dielectric sphere⁴¹ assumes that the diameter of the scatterer is less than one twentieth the wavelength of the incident light, so that the incident field is essentially constant over the volume of the scatterer. If the incident light is linearly polarized, the scattered wave has a dipole radiation pattern, and the intensity of the scattered light is proportional to v^2 .

For slightly larger particles with arbitrary shape, in which the incident field varies over the volume of the scatterer, simple Rayleigh scattering is superceded by the Rayleigh-Gans-Debye

approximation.⁴¹⁻⁴⁶ This approximation is analogous to the first Born approximation in quantum theory in that one assumes that the incident plane wave remains essentially unperturbed by the scatterer. The scatterer is treated as a collection of Rayleigh dipoles that oscillate in phase with the incident wave. A superposition of dipole radiation patterns, interfering according to the relative positions of the continuous distribution of point scatterers, makes up the scattered light. The approximation is considered valid only when the 'phase shift' induced by the scatterer is small, or

$$2kd(m-1) \ll 1 \quad [3.1]$$

where d is the longest linear dimension of the particle.

In this approximation, for linearly polarized incident light, the differential scattering cross section (power per unit solid angle scattered in the direction \vec{n} per unit incident flux in the direction \vec{n}_0) is given by:

$$\frac{d\sigma}{d\Omega} = \frac{9k^4}{16\pi^2} \left| \frac{m^2-1}{m^2+2} \right|^2 V^2 P(\theta) \sin^2 \phi \quad [3.2]$$

where $k = 2\pi/\lambda$

λ = the wavelength of the incident light in the surrounding medium

V = the volume of the particle

m = the ratio of the dielectric constant of the sphere to that of the surrounding medium

ϕ = the angle between \vec{n} and the polarization vector of
the incident light
and θ = scattering angle

The angles ϕ and θ are defined in Figure 3.1.

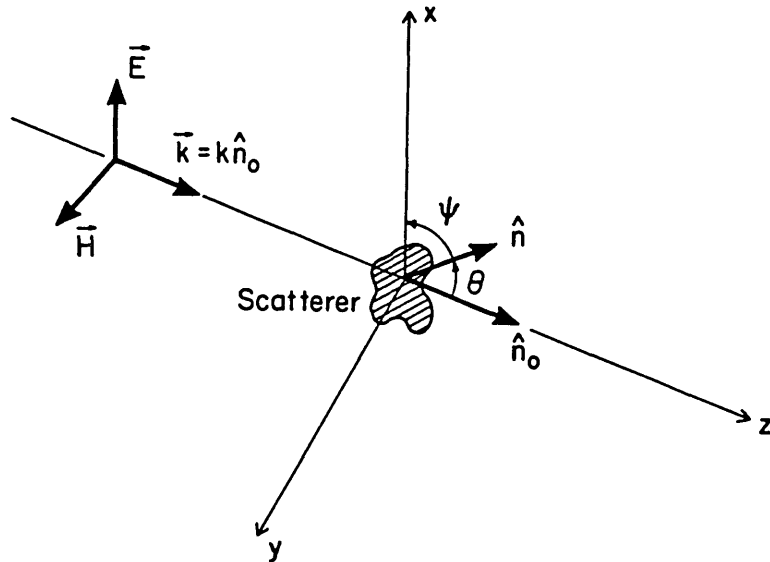


Figure 3.1
Geometry for Rayleigh-Gans-Debye Scattering.

The form factor $P(\theta)$ is defined as

$$P(\theta) = \frac{1}{V^2} \left| \int_V e^{i\vec{q} \cdot \vec{r}} d^3r \right|^2 \quad [3.3]$$

$$\text{where } \vec{q} = k(\vec{n}_0 - \vec{n})$$

$$q = 2k \sin(\theta/2)$$

Here, the integral extends over the volume of the scatterer, and the origin for the vector \vec{r} is the center of mass of the scatterer.

If $\vec{q} \cdot \vec{r}$ remains small throughout the volume of the scatterer, the exponential in [3.3] may be expressed as a power series. Thus,

$$P(\theta) \simeq 1 - \frac{1}{V} \int_V (\vec{q} \cdot \vec{r})^2 d^3r \quad [3.4]$$

When $P(\theta)$ approaches unity, Equation [3.2] reduces to the Rayleigh result, and the scattered light intensity is simply proportional to V^2 . This occurs when

$$\frac{1}{V} \int_V (\vec{q} \cdot \vec{r})^2 d^3r \ll 1 \quad [3.5]$$

This may be accomplished with small particles, long wavelengths, and/or small scattering angles. This analysis shows that in the Rayleigh-Gans-Debye approximation V^2 intensity dependence will be obtained for small particles of arbitrary shape and orientation, and for larger particles at small, scattering angles. For spheres criterion [3.5] becomes

$$(qa)^2 \ll 5 \quad [3.6]$$

It would be incorrect to deduce from this analysis of the form factor that the scattered light from a particle of arbitrary size will be proportional to V^2 at arbitrarily small angles. For large particles, the fundamental assumption of Rayleigh-Gans-Debye theory (Equation [3:1]) is violated and the entire analysis becomes invalid. The theory applies to arbitrarily large particles only when the relative refractive index m approaches unity.

For larger particles we expect a departure from the V^2 dependence mentioned above. To observe this departure, I have divided zero angle scattered intensity, taken from tables⁴⁰ of the Mie solution, by the Rayleigh result and plotted it against sphere diameter in Figure 3.2. For this graph, I chose $\lambda = 386.8$ nm (the 514.5 nm argon ion line corrected for refraction in water) and $m = 1.2$, corresponding to the actual values in my system. For spheres smaller than 700 nm I find that scattered intensity varies even more strongly with diameter than we would expect from Rayleigh theory. Past this point, scattered intensity increases more slowly than V^2 . In my system, the Rayleigh limit will be accurate to within 10% only for spheres smaller than roughly 100 nm.

3.1.1.2 Scattering from Clusters

The general theory of scattering by a collection of particles³² is formulated similarly to Mie theory: Maxwell's equations are solved with the appropriate boundary conditions. Once again small particle

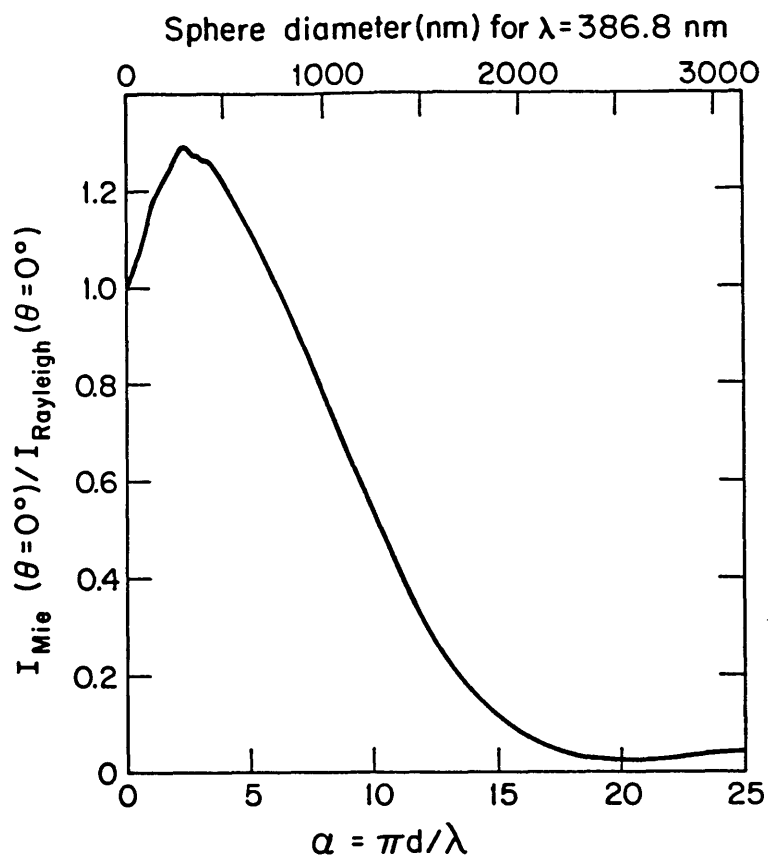


Figure 3.2
Comparison of Mie and Rayleigh Scattering at 0° .

approximations are possible, but an analytic, small angle approximation is difficult to obtain. However, if the scattered light is much less intense than the incident light or, equivalently, if secondary scattering is negligible, an approximate solution can be constructed.[†]

[†] - In my analysis, I develop a criterion under which secondary scattering can be ignored. I do not explicitly consider, however, the mutual interaction of the internal polarization fields of neighboring particles.^{31,32,49} This effect could be important for

Scattered waves from individual elements within a cluster will then interfere exactly as dipole wavelets interfere in Rayleigh-Gans-Debye theory. The major differences here are that individual elements may themselves have complex scattering properties, which depend on orientation of the element, and that the elements are discretely distributed in space. To simplify the analysis and to make it more directly applicable to my experimental system, I consider clusters of spheres. Then secondary scattering may be ignored as long as the average scattered intensity one diameter away from the center of a particular sphere is smaller than, say, one tenth the incident intensity, or

$$\frac{\sigma}{16\pi a^2} \lesssim 0.1 \quad [3.7]$$

where σ is the total scattering cross section of the sphere, which has radius a . Using the values of λ and m mentioned above, I find that in my system secondary scattering may be ignored for particle diameters as large as 580 nm.¹⁷

In further analogy to Rayleigh-Gans-Debye theory, we may express the differential scattering cross section of a cluster as:

$$\frac{d\sigma_n}{d\Omega} = \frac{d\sigma_1}{d\Omega} n^2 P_n(\theta) \quad [3.8]$$

immediately adjacent spheres in a cluster, but does not seem to alter the predicted and observed n^2 dependence at low angles. Averaging over orientations, as I do, might minimize this effect, leaving n^2 dependence intact while broadening the peaks in the measured histograms.

$$\text{where } P_n(\theta) = \frac{1}{n^2} \left| \sum_{k=1}^n e^{i\vec{q} \cdot \vec{r}_k} \right|^2 \quad [3.9]$$

n = the number of spheres in the cluster

and \vec{r}_k = the position of the k^{th} sphere

Hence, $d\sigma_n/d\Omega$ is proportional to $d\sigma_1/d\Omega$. This is true whenever the differential scattering cross section for all sub-units is identical; the units themselves may be Rayleigh, Rayleigh-Gans-Debye, or Mie scatterers. It should also be pointed out that $P_n(\theta)$ does not contain all of the angular dependence of the cluster cross section since $d\sigma_1/d\Omega$ will also vary with scattering angle. Lips et al.^{2,3} were the first to use this formulation in the analysis of bulk scattering from sols of aggregating spheres.

Debye has shown^{42,47} that, if we average over all orientations of the cluster in the incident field, we obtain

$$\langle P_n(\theta) \rangle = \frac{1}{n^2} \sum_{i=1}^n \sum_{j=1}^n \frac{\sin qr_{ij}}{qr_{ij}} \quad [3.10]$$

where r_{ij} is the distance between the centers of spheres i and j in the aggregate. Expanding in powers of qr_{ij} , we find

$$\langle P_n(\theta) \rangle \simeq 1 - \frac{q^2}{3} R_g^2 \quad [3.11]$$

$$\text{where} \quad R_g^2 = \frac{1}{2n^2} \sum_{i=1}^n \sum_{j=1}^n r_{ij}^2 \quad [3.12]$$

R_g would be the radius of gyration of the cluster if the spheres were replaced by point particles.^{4*} We see from Equation [3.11] that scattered intensity from a cluster of n spheres will be proportional to n^2 if

$$(qR_g)^2 \ll 3 \quad [3.13]$$

Note the similarity between this expression and the criterion for v^2 dependence in the case of Rayleigh-Gans-Debye spheres (Equation [3.6]). Again in the case of clusters, small angles yield the desired dependence as long as secondary scattering is negligible.

3.1.2 Description of the Instrument

In the schematic illustration presented in Figure 3.3, the dispersion passes through an optical flow cell, a portion of which is illuminated by the focussed beam of an argon-ion laser (Spectra-Physics model 164-06). The elliptically shaped beam is 150 μm by 30 μm with its major axis perpendicular to the particle stream. Since the stream is never wider than 50 μm , this ensures uniform illumination of the particles. Two lenses located on the axis of the beam project a magnified image of the cell onto a variable slit, which serves with an iris diaphragm as the aperture for a photomultiplier tube (EMI model

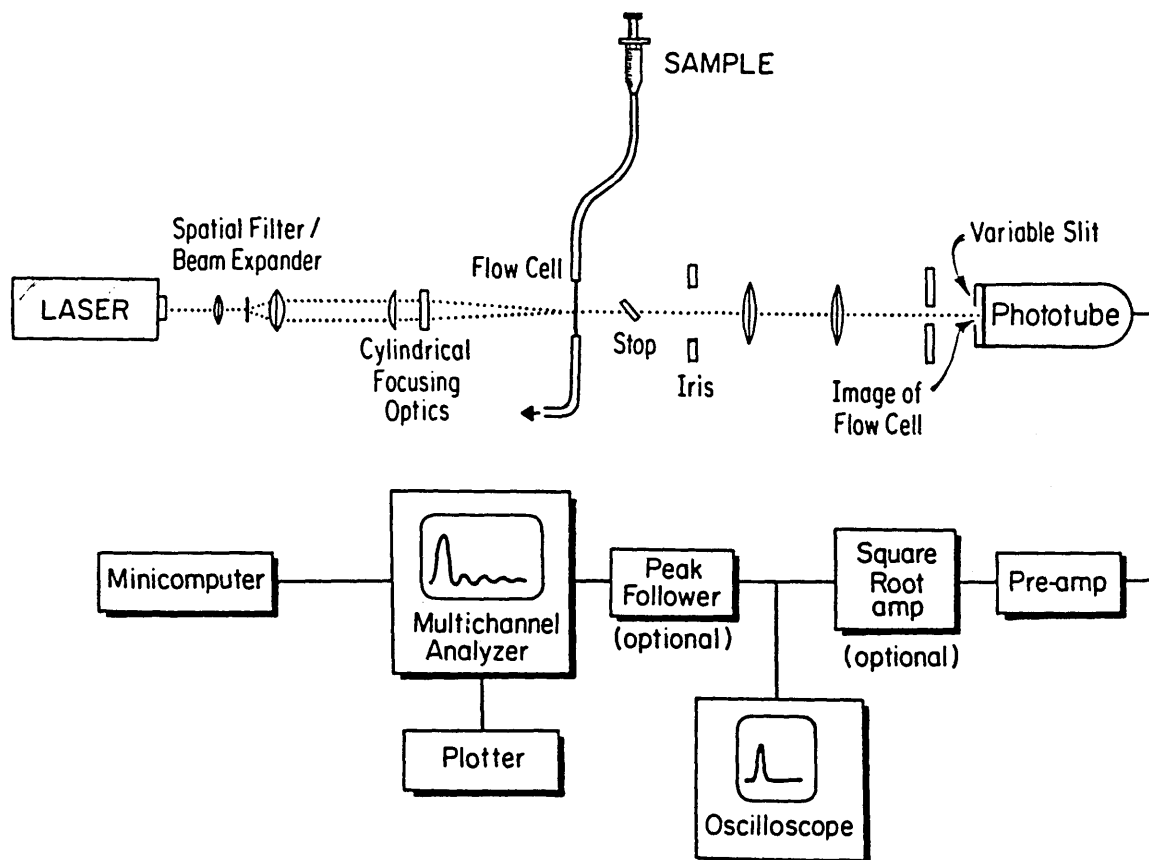


Figure 3.3
A schematic illustration of the instrument.

9789b). The width of the variable slit and the diameter of the iris diaphragm define the small section of the flow cell viewed by the phototube, which I shall call the 'scattering volume'. A rectangular mirror (the stop) reflects the transmitted laser beam away from the optical axis, so that only scattered light is trained upon the phototube.

As it passes through the scattering volume, each suspended particle produces an optical pulse, which is converted to a current pulse by the phototube. This raw signal is processed and then fed to a multichannel analyzer (Norland Corp. model IT-5400), which constructs a histogram of the pulse-height distribution. Various peripherals record and analyze the results.

The range of angles over which light is collected is defined by the width of the stop as well as the diameter of the iris diaphragm immediately adjacent to it (see Figure 3.4).

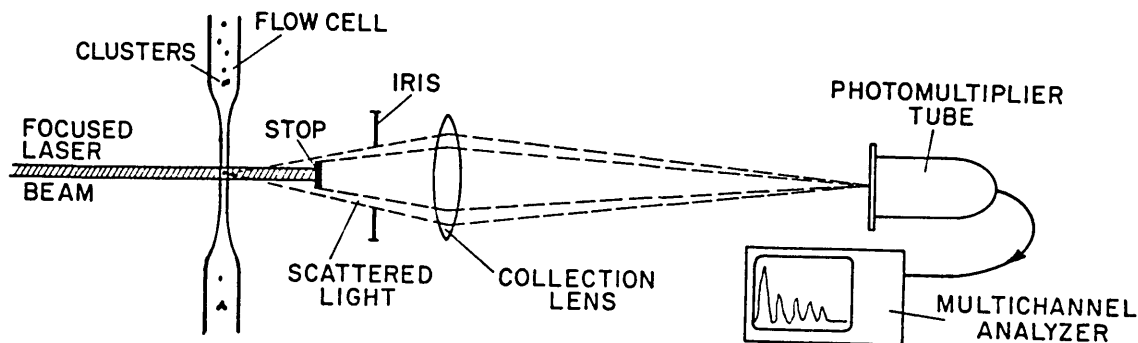


Figure 3.4
A closeup showing the range of scattering angles.

Scattered light is collected between 1.5 and 3 degrees, yielding an average value of $6.4 \times 10^{-4} \text{ nm}^{-1}$ for the scattering vector q . Using this value of q in Equation [3.13] we see that n^2 intensity dependence should obtain for clusters with radii of gyration smaller than about

860 nm.

It is important to minimize the scattering volume, because two or more clusters passing through it at the same time will cause an anomalous 'coincidence' count. As I show in Appendix III, the maximum particle concentration that may be observed with an acceptable level of coincidences is inversely proportional to the size of the scattering volume. In our system, scattering volumes are typically 3×10^{-9} cc. At a concentration of 2×10^6 particles/cc this will yield roughly one coincidence for every 1000 counts.

3.1.2.1 Flow Cells

I have used two kinds of optical flow cells with this instrument. The first is a simple 10 μ l glass micropipette, stretched to an internal diameter of anywhere from 10 to 50 microns over a bunsen burner. These capillaries are essentially disposable and are stretched to different diameters depending on the concentration and degree of aggregation of the sample being studied. A vacuum pump is attached to one end of the tube in order to draw the sample through it. The second kind of optical cell is a commercially produced laminar flow cell (Ortho Diagnostic Systems, part number 300-0511-000), which employs hydrodynamic focussing¹⁰ to produce particle streams as narrow as five microns.

In capillaries, shear forces exerted upon clusters suspended in

the fluid will grow with increasing pressure and decreasing capillary radius. In the thinnest portion of a capillary, the Reynolds number is typically less than 5, well below the critical value of about 2000 at which laminar flow gives way to turbulence. In my experiments, changes in pressure and capillary radius have had no noticeable effect upon histograms obtained from highly aggregated samples. I take this as evidence that shear forces within a capillary are not strong enough to break larger clusters apart.

Optically, glass capillaries cause two major problems. First, due to their cylindrical shape, they distort both the incident and scattered waves. Inhomogeneities in the incident wave ultimately lead to broadened peaks in the final histogram. Distortion of the scattered wave allows scattered light from angles larger than 3° to enter the phototube and also makes it difficult to image particles within the tube. Proper imaging is essential in obtaining well shaped pulses. Secondly, the air/glass interface at the surface of the capillary causes an intense specular reflection to emerge from the scattering volume in a plane perpendicular to the capillary axis. The reflection itself is not a serious problem, since it is confined to very small angles, and it is easily removed by the stop. However, to remove it the stop must be oriented perpendicular to the capillary - which means perpendicular to the direction of particle flow. As particles flow past, their scattered light is diffracted at the edges of the stop, causing a high frequency 'ripple' to be superposed upon what would have been a smooth, roughly bell shaped pulse. With the laminar flow cell, which has flat exterior walls and causes no off-axis specular reflection, I can orient the stop parallel to the direction of

particle flow and remove the ripple.

While the laminar flow cell has many optical advantages over capillaries, it has one disadvantage that presently makes it difficult to study coagulation with it. I have observed significant shearing of clusters at certain flow rates and fluid pressures in this cell. Samples that clearly contained significant numbers of large clusters (up to $n = 8$) when viewed with a capillary often showed only small clusters (up to $n = 3$) with the laminar cell.

In this cell, the sample is injected into the center of a tube of sheath fluid, which is undergoing laminar flow. The diameter of the sheath decreases past the point of injection, and the particle stream is focussed correspondingly. The sheath pressure determines the overall velocity of the particles, while the sample pressure determines the diameter of the focussed stream. At normal operating pressures, the Reynolds number may reach a value of 500. By reducing fluid pressures, I have brought the Reynolds number as low as it is in the capillary, roughly 5; but I have still observed significant shearing. Therefore, I used the laminar cell only to study scattering from single spheres and the capillary to study aggregation.

3.1.2.2 Signal Processing

The first stage of the interface consists of an inverting bandpass filter which produces a positive voltage pulse, proportional to the

anode current from the phototube. The voltage supplied to the phototube determines the overall gain. Since flow rates differ between capillaries and the laminar cell, I use different filters for each. With capillaries the pass band is 27 Hz - 1000 Hz and with the flow cell it is 600 Hz - 332 KHz. A switch gives me the option of sending the filtered signal through a square root amplifier (Analog Devices model AD533). With dispersions of aggregated latex spheres, I usually use the square root mode since it gives linearly spaced peaks in the histogram and increases the dynamic range of the instrument with no effect upon its intrinsic resolution. With clusters in the square root mode, the instrument would have enough of a dynamic range to see up to 25 peaks if light scatter response went strictly as n^2 .

The filtered signal is displayed on an oscilloscope. With the capillary pulses are typically 0.2 ms wide; whereas, with the laminar flow cell they are roughly 20 μ s wide. Pulses from the laminar cell are smooth, and may be fed directly to the multichannel analyzer. The ripple on pulses from the capillary makes interfacing difficult since the A/D converter on the multichannel analyzer triggers as its input signal drops, usually mistaking the first or second local maximum as the height of a pulse. A specifically designed analog peak follower sends a square voltage pulse with the true height of the filtered signal to the multichannel analyzer.

3.1.3 Light Scattering Results

The smallest spheres that I was able to resolve had diameters of 380 nm.[†] With $m = 1.2$ and $\lambda = 386.8$ nm, spheres of this diameter violate criterion [3.1] for Rayleigh-Gans-Debye scattering; they are clearly in the Mie regime. I could not observe smaller particles with the laminar flow cell than I could with a capillary, despite the apparent optical superiority of the laminar flow cell.

The histogram in Figure 3.5 was collected in the square root mode using a glass capillary. The sample consisted of 450 nm polystyrene spheres in the late stages of salt induced aggregation. Eight peaks are easily distinguished. In the inset, mean channel number is plotted against peak number for each visible peak. The remarkably linear spacing of all eight peaks confirms that clusters of spheres may exhibit simple scattering behavior even though the individual spheres do not.

With extremely aggregated samples, the quality of histograms generally deteriorated: peaks became broad, and even the first two would often overlap. Deteriorating histograms generally coincided with the appearance of some extremely large pulses, which often lasted 20 times the length of a monomeric pulse and exhibited many oscillations. These anomalous, oscillating pulses, which probably arose from clusters many times the size of the scattering volume, caused a random background distribution of pulse-heights which certainly contributed to the

[†] - Spheres are manufactured by Dow Chemical Co. and Polysciences, Inc.

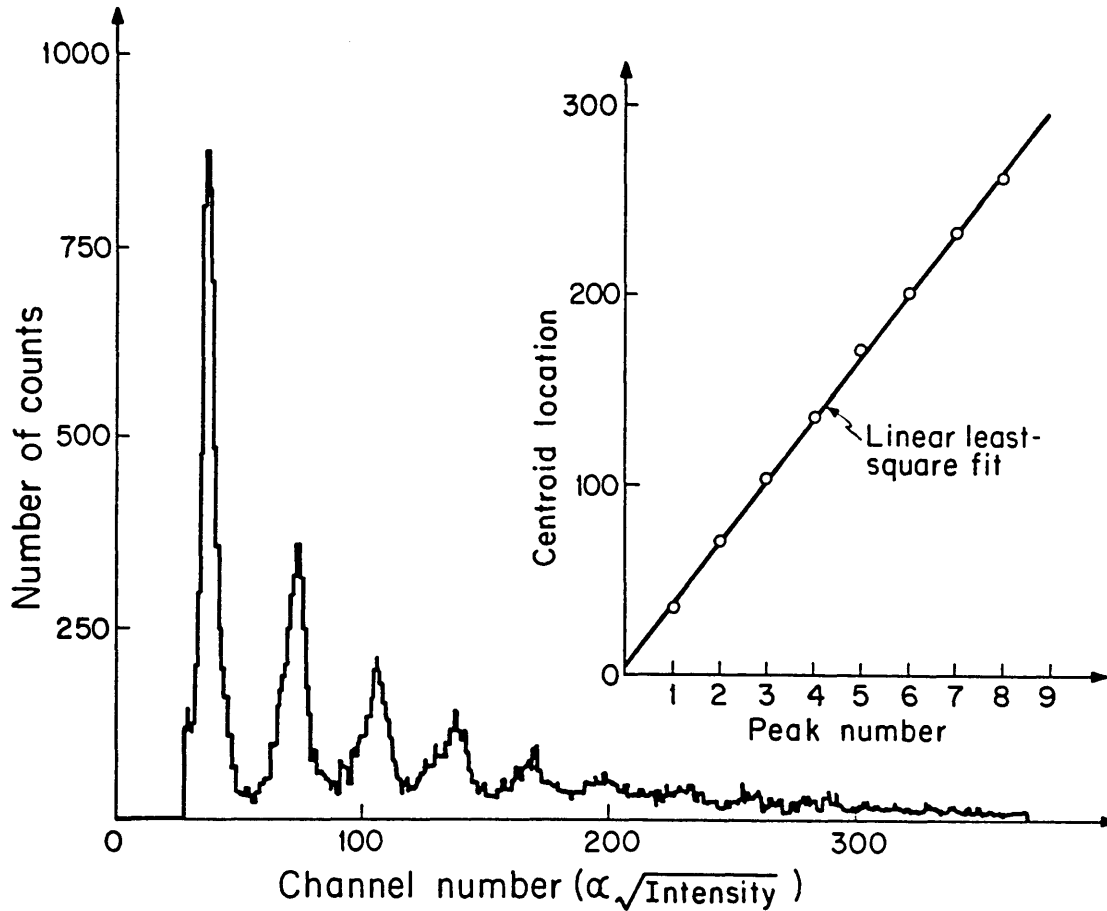


Figure 3.5
A histogram of aggregated 450 nm spheres.

smearing out of the peaks.

The histogram in Figure 3.6 displays one of the useful features of coherent light scattering or n^2 response that is not found with fluorescence detectors and other linear devices. It was collected in

the linear mode, using the laminar flow cell and 1,091 nm spheres. Halfway between the monomer and dimer peaks there lies a small peak which corresponds to the coincidence of two unattached monomers.

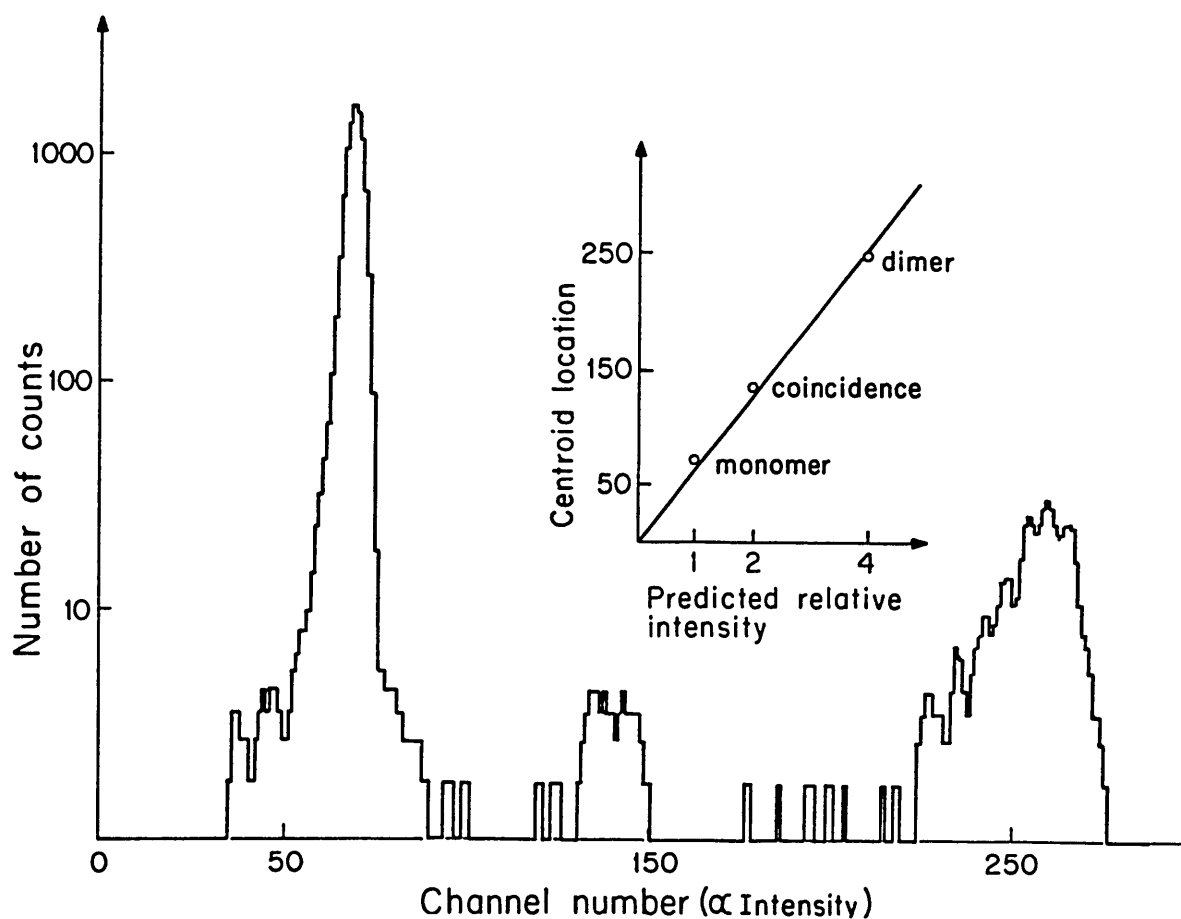


Figure 3.6
A histogram with a coincidence peak.

While a dimer scatters four times the intensity of a monomer, two unattached monomers scatter only twice the intensity of one. My explanation for this is that the relative motion of unattached monomers

must be significant during their transit time in the scattering volume. Enough relative motion would give rise to effectively incoherent scattering. Since free monomers always exist in greater concentration than any other species in solution, monomer-monomer coincidences are always the most probable. The presence of this peak indicates the need for a more dilute preparation or a smaller scattering volume. With linear instruments such as fluorescence detectors and resistive pulse analyzers, a coincidence of this sort would be indistinguishable from a dimer.

The widths of the peaks in Figure 3.6 may be fully explained by variations in particle size; the instrument causes little artifactual broadening. In this figure the coefficient of variation (CV) for the monomer and dimer peaks is 4.6% and 4.4% respectively, while the CV deduced from information supplied by the manufacturer is 4.5%.

Figure 3.7 was again obtained with the laminar flow cell, but this time in the square root mode. The three peaks in the histogram correspond to 480 nm, 710 nm and 1,091 nm polystyrene spheres respectively. In the inset, peak location - which in this case corresponds to the square root of intensity - is divided by the third power of the corresponding sphere radius and plotted against diameter. The solid line is the Mie prediction for zero degree scattering. For V^2 intensity dependence the points would fall on a horizontal line; however, the experimental points show deviations of approximately 13% in this size range, indicating Mie scattering.

Finally, Figure 3.8 demonstrates explicitly that n^2 intensity dependence results even when V^2 dependence breaks down. Here 710 nm

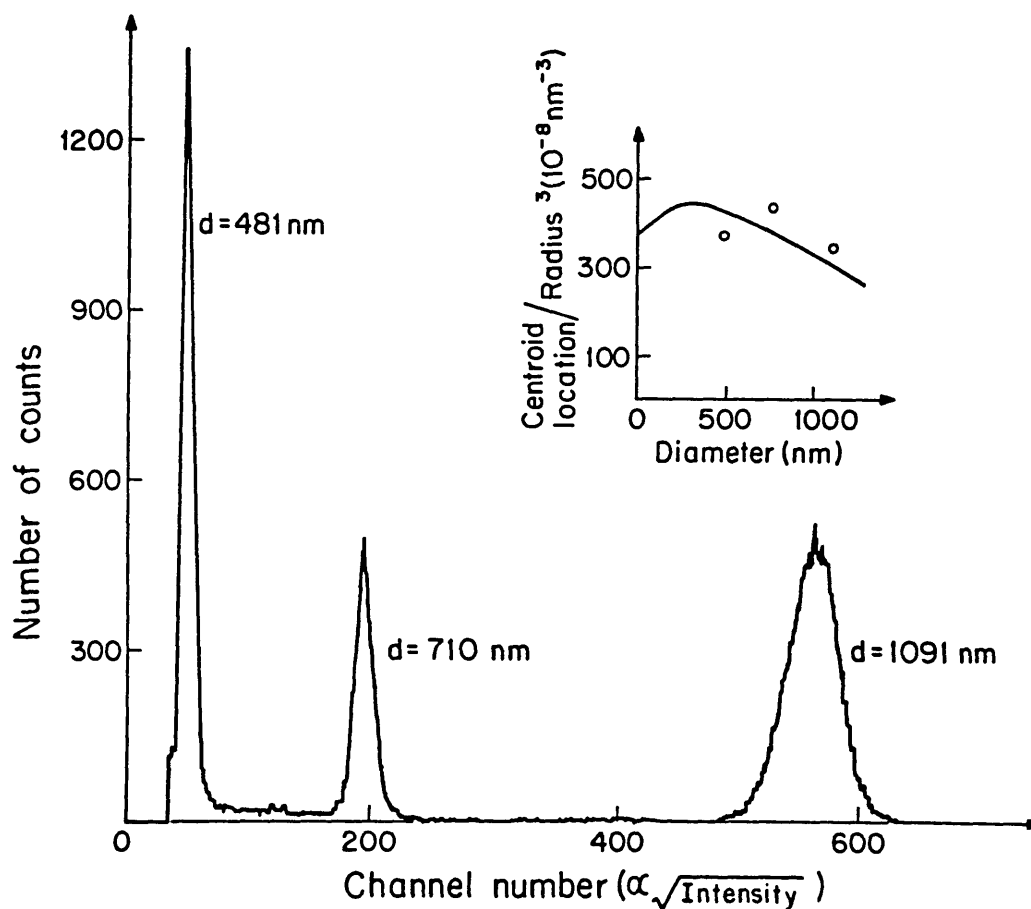


Figure 3.7
A histogram of three different sized spheres.

and 1,091 nm monomer peaks are shown with their corresponding dimer peaks on the same histogram, collected in the square root mode. The locations of the monomer peaks indicate a weaker than v^2 volume dependence, but in both cases the dimer peak location is precisely twice that of the monomer. This is surprising since these spheres fall in the range where secondary scattering should be significant; apparently

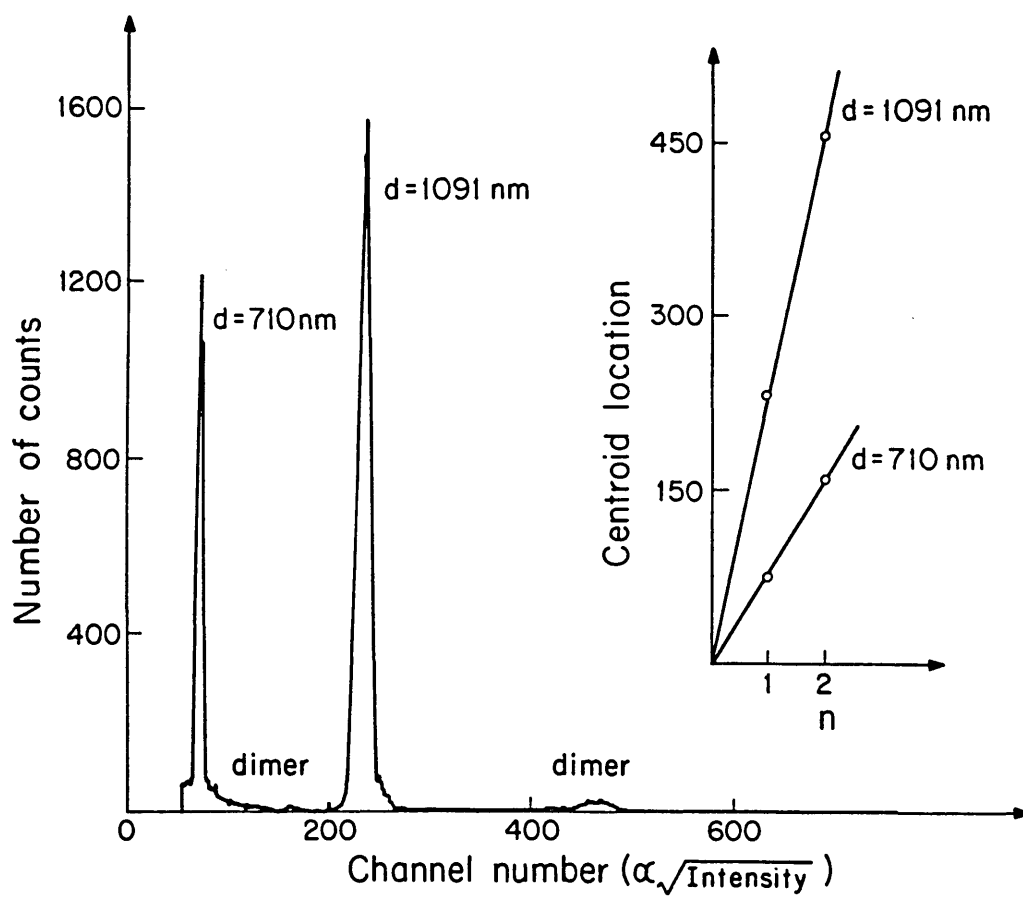


Figure 3.8
Monomer and dimer peaks of 710 nm and 1091 nm spheres.

criterion [3.7] is too stringent.

3.1.4 Discussion of the Instrument

These results demonstrate that coherent, low angle light scattering is a particularly useful method for probing cluster size distributions. It is superior to fluorescence and resistive pulse analysis for two reasons. First, it yields n^2 response even with monomeric units that are clearly in the Mie scattering regime. This actually leads to increasing peak separation (or resolution) with increasing n . It also permits the detection of coincidences (Figure 3.6), which are indistinguishable with linear systems. Second, low angle light scattering is quite insensitive to the orientation and configuration of individual clusters; without this insensitivity n^2 response does not guarantee good resolution. While linear systems, such as fluorescence detectors and resistive pulse analyzers, may be able to resolve smaller particles, they can not detect size differences between small particles with the resolution of low angle light scattering. In linear systems even the first and second peaks usually overlap, and more than four peaks are rarely discernible;^{12,21,22} but with our instrument it is possible to resolve eight or more clearly separate peaks before histograms become quasi-continuous (see Figure 3.5).

In two recent reports,^{21,22} Cummins et al. present an instrument very similar to ours, which detects both fluorescent (incoherent) and scattered (coherent) light. They demonstrate²² that low angle light scattering resolves cluster sizes better than fluorescence does,[†] and

[†] - Michael Broide has done the same in this lab.

they present flocculation data with the latter technique. I discuss this data in chapter V. They also explain the observed n^2 dependence at low angles as volume squared dependence even though, with a wavelength of 441.6 nm, a scattering angle of 4° , and 500 nm spheres, they are clearly observing Mie scatterers. They do show a low angle histogram with monomeric spheres of different sizes including 200 nm spheres - roughly half the size that I have been able to resolve.

Cummins et al. also demonstrate an experimental difficulty with fluorescence detection: it seems to be more difficult to produce uniform fluorescent coatings on polystyrene microspheres than it is to produce microspheres of uniform diameter. Estimating the widths of aggregate peaks purely on the basis of the experimental width of a fluorescent monomer peak, they show that even the fifth peak should be indistinguishable. We have done a similar calculation in this lab. The spheres I have used have standard deviations in diameter of roughly 0.5%. As I have pointed out, the widths of the peaks in Figure 3.6 are fully explained by this variation. I estimate that up to 33 peaks could be resolved if this variation in particle size was the only factor that contributed to resolution. Hence configuration is the most important factor determining the resolution of low angle light scattering.

In my theoretical analysis I found two relevant size limits for n^2 dependence (Equations [3.7] and [3.13]); the diameter of the individual spheres must be smaller than 580 nm, and the effective radius of gyration of the cluster must be smaller than 860 nm. Experimentally I find that I can exceed the first limit; but, without knowing

the detailed structure of clusters, the second is harder to verify. I can, however, examine the extreme cases of linear and hexagonal dense packed structures to estimate n_{\max} , the size of the largest cluster in the n^2 regime. With 450 nm spheres, the diameter I used to study coagulation, n_{\max} falls between 7 for linear clusters and 87 for dense packed clusters. This may explain why peaks in Figure 3.5 begin to overlap past $n = 8$. For each n , there will be at least a few roughly linear clusters, which will tend to make higher order peaks skew to the left; in other words, configuration becomes important at $n = 7$.

Since this bound on n will get larger as the ratio of sphere diameter to laser wavelength is decreased, it is advantageous to use smaller spheres. Assuming that photoelectron production is the major source of noise in the signal, the signal-to-noise ratio of an individual light pulse will be proportional to the square root of the number of photons it contains. I estimate the signal-to-noise ratio to be 10:1 for polystyrene spheres with a diameter of 100 nm. But the smallest spheres I have been able to resolve have been 380 nm in diameter. The signal-to-noise ratio should be roughly 50 times greater for these particles. I suspect that the major source of noise obscuring low level signals is background light - produced primarily by specular reflection with capillaries and by surface imperfections on the laminar flow cell. Despite its many optical advantages, the laminar cell is not superior to a capillary in this respect. The outside diameter of a capillary is actually smaller than the width of the laser beam, while the laminar cell is much wider. Therefore, a larger surface area is illuminated on the flow cell. Low angle scattered light from dust and scratches on this surface is harder to eliminate than specular

reflection from a capillary.

The major problem with the laminar cell, though, is not so much surface imperfections as it is shearing of clusters. Shearing could result from either a sharp edge that causes local turbulence in the path of the clusters or from an abrupt acceleration as the clusters are injected into the sheath fluid. We are presently looking into this problem. Although the capillary focusses the particle stream gently, it causes optical aberrations. The next stage of improvement here will involve surrounding the capillary with an index matched medium - either liquid or epoxy - that has optically flat exterior walls. This should eliminate specular reflection with the accompanying ripple it causes on the signal.

We could also improve the overall performance and flexibility of the instrument by digitizing the actual waveform of the current pulses - in real time. This would facilitate the use of parameters besides pulse-height to distinguish between particles. For instance, pulse-width could be monitored to filter out anomalously long or short pulses. Also, the area of a pulse might be less sensitive than height to small differences between clusters of the same size.

I will show in the next chapter that there are some very interesting questions in my experimental results involving the normalization of the cluster size distribution - in other words, the total number of spheres in the solution. One way to help get an estimate of this quantity would be to simply count the total number of clusters while collecting a particular histogram. This should be easily accomplished by placing a second phototube at a scattering angle of 90° . In

fact, it should be easier to detect very small spheres at this angle, since there will be little background light there.[†] The signal from the 90° phototube could also be used as a gate for the low angle pulses. Only while this signal is 'high' would the multichannel analyzer monitor the low-angle signal; hence it would count only one pulse during that time. This would help distinguish monomeric pulses from random background noise and would probably improve performance with highly aggregated samples.

Here I have attempted to remove the effects of cluster configuration and orientation by focussing exclusively upon low angle scattering. But, in light of the growing interest in the fractal nature of polymeric aggregates,^{4-7,10-12,32} it might be useful to examine the angular dependence (or q -dependence) of the scattered light as well. We see from Equation [3.11] that this should merely involve fitting the angular dependence of the scattered intensity to a parabola. This should necessitate perhaps three detectors on each (or perhaps only one) side of the low-angle phototube. Knowing cluster size n from low angle measurements, this might possibly yield the exponent p of Equation [2.44]. Angular anisotropy has already been used by other workers to estimate the size of individual cells and spheres.^{33,34}

In its present state, the instrument can be used to study aggregating systems other than the one considered here. Polystyrene microspheres may also be used as carrier particles in the study of agglutination reactions. Immunologists have studied the cross-linking of

[†] - Low angles are still better for detecting size differences, however.

antigen coated microspheres by antibody since the early 1960's.⁵³ Resistive pulse analysis has already been applied to this system,¹⁶⁻²⁰ but it might be useful to apply light scattering as well since it does not necessitate the use of high salt concentrations, which may denature the immunochemicals over time. The coagulation of red blood cells to form rouleaux has stimulated much theoretical interest lately.⁵⁶⁻⁶¹ With the gentle (non-shearing) flow characteristics of the capillary, it may be possible to observe this phenomenon in detail. I am also considering the feasibility of determining size distributions of blood platelets and cluster size distributions in colloidal gold sols.

3.2 Materials and Experimental Procedures

Each of these studies employed 450 ± 2 nm polystyrene spheres supplied by Polysciences, Inc., Warrington, PA (lot number 3-1217). Because samples taken straight from the bottle showed a high degree of aggregation, we first ultrasonicated the particles for up to 12 hours in order to obtain initial distributions with monomer weight fractions exceeding 95%.[†]

Solvents consisted of doubly distilled water containing appropriate concentrations of NaCl. We also added trace amounts (~1mM) of Sodium Azide to inhibit bacterial growth. Solvents were drawn through a 220 nm Millipore filter before spheres were added. We attached a

[†] - These experiments were conducted by Michael Broide and myself.

syringe containing the sample directly to the flow cell. Samples were always drawn from the bottom of the syringe. To determine absolute concentrations, we monitored the volume of fluid that passed through the cell as each histogram was collected.

For each syringe, we collected from ten to twenty histograms as the reaction progressed (Figure 3.9).

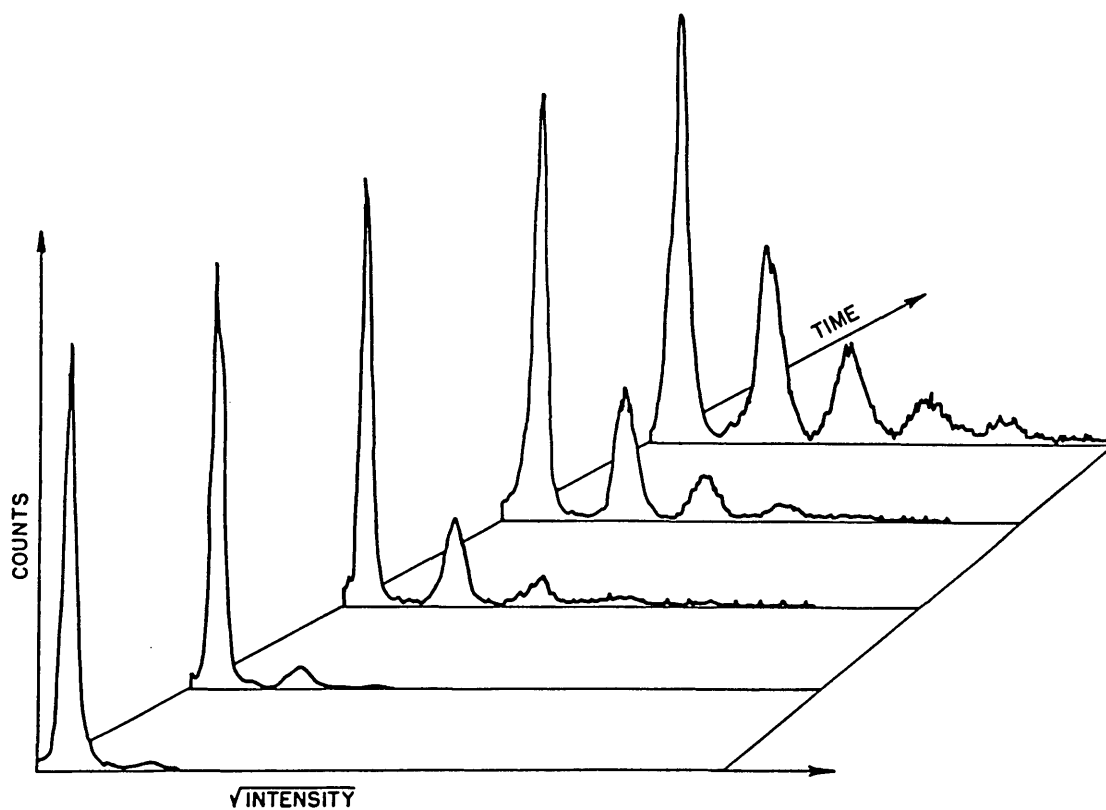


Figure 3.9
A sequence of histograms illustrating aggregation. Successive monomer peaks are normalized to facilitate comparison.

Histograms generally contained at least 10^4 counts and took less than 30 minutes to collect. Since characteristic aggregation times were at least nine hours, distributions remained essentially constant over the time histograms were collected.

Histograms generated by the multichannel analyzer had up to eight clearly discernible peaks, to the right of which the histogram became quasicontinuous (see Figure 3.5). To analyze a histogram we would divide it into partitions, taking the number of counts between partitions as the number of aggregates of a particular size. For the distinguishable peaks, the partitions coincided with the minima between peaks; while for the quasicontinuous portion, the partitions were determined by extrapolating a linear least-squares fit, as in Figure 3.5, to the peak locations of the discernible peaks.

After running a few preliminary experiments to determine the critical coagulation concentration (of salt - see Appendix I) for our particular batch of spheres, we ran four coagulation experiments, which I discuss in the next chapter. Three of these took place at a sphere concentration of $\sim 2.6 \times 10^6 \text{ cm}^{-3}$, and one took place at twice this concentration. Such low concentrations were dictated by the size of the scattering volume in the instrument. Other workers^{8,22,31} have recently published somewhat more preliminary results at higher concentrations by diluting the sample before observing it. We decided not to do this because it might have a profound effect upon the system. If the system does reach thermodynamic equilibrium, changing the concentration will cause cluster dissociation, according to Flory-Stockmayer theory.

As I mentioned in my discussion of the instrument, we evaluated two optical flow cells for this study. While, optically, the two were essentially on a par, the laminar flow cell would occasionally shear clusters apart. Therefore, we used exclusively glass capillaries to investigate colloidal flocculation.

REFERENCES - CHAPTER III

1. Lichtenbelt, W. Th., Pathmamanoharan, C., and Wiersema, P.H., J. Colloid Interface Sci., **49**, 281 (1974).
2. Lips, A., Smart, C., and Willis, E., Trans. Faraday Soc., **67**, 2979 (1971).
3. Lips, A. and Willis, E., J. Chem. Soc. Faraday, **69**, 1226 (1973).
4. Shaeffer, D.W., Martin, J.E., Wiltzius, P.W., and Cannell, D.S., in Reference 52.
5. Shaeffer, D.W., Martin, J.E., Wiltzius, P.W., and Cannell, D.S., Phys. Rev. Lett., **52**, 2371 (1984).
6. Shaeffer, D.W. and Keefer, K.D., Mat. Res. Soc. Symp. Proc., **32**, 1 (1984).
7. Shaeffer, D.W. and Keefer, K.D., "Origin of Fractals Structures in Amorphous Materials", preprint, 1984.
8. Cummins, P.G., Staples, E.J., and Thompson, L.G., J. Colloid Interface Sci., **92**, 287 (1983).
9. Barringer, E.A., Novich, B.E., and Ring, T.A., J. Colloid Interface Sci., **100**, 584 (1984).
10. Martin, J.E. and Schaefer, D.W., "Dynamics of Fractal Colloidal Aggregates", preprint, 1984.
11. Martin, J.E. and Ackerson, B.J., "Static and Dynamic Scattering from Fractals", preprint, 1984.
12. Weitz, D.A., Huang, J.S., Lin, M.Y., and Sung, J., Phys. Rev. Lett., **53**, 1657, (1984).
13. Coulter, W.H., U.S. Patent No. 2,656,508 (1953).
14. DeBlois, R.W. and Bean, C.P., Rev. Sci. Instrum., **41**, 909 (1970).
15. DeBlois, R.W., Bean, C.P. and Wesley, R.K., J. Colloid Interface Sci., **61**, 323 (1977).
16. von Schulthess, G.K., Benedek, G.B., and DeBlois, R.W., Macromolecules, **13**, 939 (1980).
17. von Schulthess, G.K., Benedek, G.B., and DeBlois, R.W., Macromolecules, **16**, 434 (1983).
18. von Schulthess, G.K., Ph.D. Thesis, M.I.T. (unpublished), 1979.
19. Johnston, D.F., Ph.D. Thesis, M.I.T. (unpublished), 1983.
20. Johnston, D.F. and Benedek, G.B., in Reference 52.
21. Cummins, P.G., Staples, E.J., and Thompson, L.G., J. Colloid Interface Sci., **92**, 189 (1983).
22. Gedan, H., Lichtenfeld, H., and Sonntag, H., Colloid Poly. Sci. **260**, 1151 (1982).
23. Walsh, D.J., Anderson, J., Parker, A., and Dix, M.J., Colloid Poly. Sci., **259**, 1003 (1981).
24. Mullaney, P.F., Van Dilla, M.A., Coulter, J.R. and Dean, P.N., Rev. Sci. Instr., **40**, 1029 (1969).
25. Melamed, M.R., Mullaney, P.F., and Mendelsohn, M.L., Eds., "Flow Cytometry and Sorting", Wiley, New York, 1979.
26. Mie, G., Ann. Physik., **25**, 377 (1980).
27. Kerker, M., "The Scattering of Light and Other Electromagnetic Radiation", Academic Press, New York, 1969, chapters 3 and 4.
28. van de Hulst, H.C., "Light Scattering by Small Particles", Dover, New York, 1981, chapter 9.
29. Reference 27, chapters 5 and 6.
30. Reference 28, chapters 15 and 16.

31. Levine, S. and Olafse, G.O., *J. Colloid Interface Sci.*, **27**, 442 (1968).
32. Twersky, V., *J. Math. Phys.*, **8**, 589 (1967).
33. Hodkinson, J.R. and Greenleaves, I., *J. Opt. Soc. Amer.*, **53**, 577 (1963).
34. Mullaney, P.F., *J. Opt. Soc. Amer.*, **60**, 573 (1970).
35. Mullaney, P.F., and Dean, P.N., *Biophys. J.*, **10**, 764 (1970).
36. Reference 27, section 3.9.2.
37. Gumprecht, R.O. and Sliepcevich, C.M., "Tables of Light Scattering Functions for Spherical Particles", Engineering Research Inst., University of Michigan, Ann Arbor, 1951.
38. Chu, C.M., Clark, G.C. and Churchill, S.W., "Tables of Angular Distribution Coefficients for Light Scattering Spheres", Engineering Research Inst., University of Michigan, Ann Arbor, 1957.
39. Clark, G.C. and Churchill, S.W., "Tables of Legendre Polynomials", Engineering Research Inst., University of Michigan Ann Arbor, 1957.
40. Denman, H., Heller, W., and Pangonis, W.J., "Angular Scattering Functions for Spheres", Wayne State University, Detroit, 1966.
41. Rayleigh, Lord, *Phil. Mag.*, **12**, 81 (1881).
42. Debye, P., *Ann. Physik.*, **46**, 809 (1915).
43. Gans, R., *Ann. Physik.*, **76**, 29 (1925).
44. Reference 27, chapter 8.
45. Reference 28, chapter 7.
46. Jackson, J.D., "Classical Electrodynamics", 2nd Ed., Wiley, New York, 1975, p. 421 ff.
47. Oster, G. and Riley, D.P., *Acta. Cryst.*, **5**, 1 (1952).
48. Tanford, C., "The Physical Chemistry of Macromolecules", Wiley, New York, 1961, p. 165 ff.
49. Reference 27, section 5.7.
50. Kachel, V. and Everhard, M., in Reference 25.
51. Cummins, P.G., Smith, A.L., Staples, E.J., and Thompson, L., in "Solid-Liquid Separation", J. Gregory, ed., Wiley, New York, 1984.
52. Family, F. and Landau, D.P., eds., "Kinetics of Aggregation and Gelation", North Holland, Amsterdam, 1984.
53. Mullaney, P.F. and Dean, P.N., *Appl. Opt.*, **8**, 2361 (1969).
54. Bartholdi, M., Salzman, G.C., Hiebert, R.D., and Kerker, M., *Appl. Opt.*, **19**, 1581 (1980).
55. Singer, J.M., Oreskes, I., Hutterer, F., and Ernst, J., *J. Ann. Rheumat. Disease*, **22**, 424 (1963).
56. Wiegel, F.W. and Perelson, A.S., *J. Stat. Phys.*, **29**, 813 (1982).
57. Perelson, A.S., and Wiegel, F.W., *Biophys. J.*, **37**, 515 (1982).
58. Samsel, R.W. and Perelson, A.S., *Biophys. J.*, **37**, 493 (1982).
59. Samsel, R.W. and Perelson, A.S., *Biophys. J.*, **45**, 805 (1984).
60. Hendriks, E.M. and Ernst, M.H., *J. Colloid Interface Sci.*, **97**, 176 (1984).
61. Perelson, A.S., and Samsel, R.W., in Reference 52.

CHAPTER IV

RESULTS

4.1 The Shape of the Distribution

Figures 4.1-4.6 all regard the shape of the cluster size distribution. They were all taken at the higher concentration ($5.2 \times 10^{-6} \text{ cm}^{-3}$), but the general results at this concentration are common to all four experiments. The reaction half-life calculated from von Smoluchowski theory ($\tau_A = 2/Ac_0 = 3\eta/4kTc_0$ - see [2.24]) is 9 hr, but the stability factor W is 2.0, as I show later (Sample 4, Table 4.1). Hence, the effective half-life, τ , for these figures is 18 hr.

I compared the shapes of experimentally obtained distributions to theoretical distributions A, B and C (see Table 2.1) using a two parameter fitting routine. By adjusting the values of c_0 and b , the routine minimized the error E :

$$E = \frac{1}{(p-2)\bar{c}} \sum_{k=1}^p \frac{(c_k^e - c_k^t)^2}{c_k^e} \quad [4.1]$$

where p is the size of the largest k -mer

c_k^e is the experimentally measured k -mer concentration

c_k^e is the theoretically predicted k-mer concentration

$$\text{and } \bar{c} = \frac{1}{p} \sum_{k=1}^p c_k^e. \quad [4.2]$$

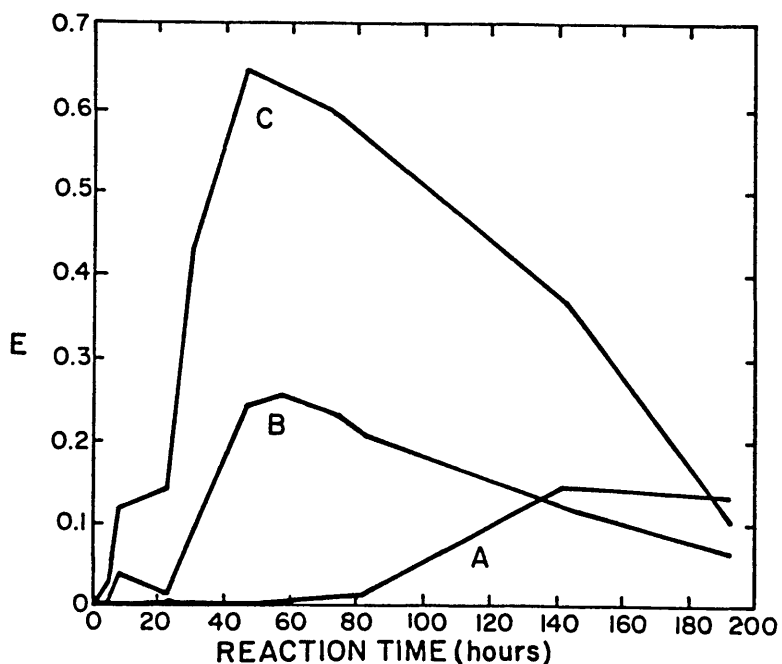


Figure 4.1
Time dependence of the goodness of fit, E, for cases A, B, and C.
 $\tau = 18$ hr.

In Figure 4.1 I plot the magnitude of E for Cases A, B and C as a function of reaction time. For times $t < 60$ hr (or roughly 3τ), distribution A (von Smoluchowski theory) provides an excellent fit to the data, while distributions B and C provide a poor fit. At times $t > 3\tau$ the fit for distribution A slowly deteriorates while fits for B and C slowly

improve. The three error curves cross at long reaction times ($t \approx 10\tau$).

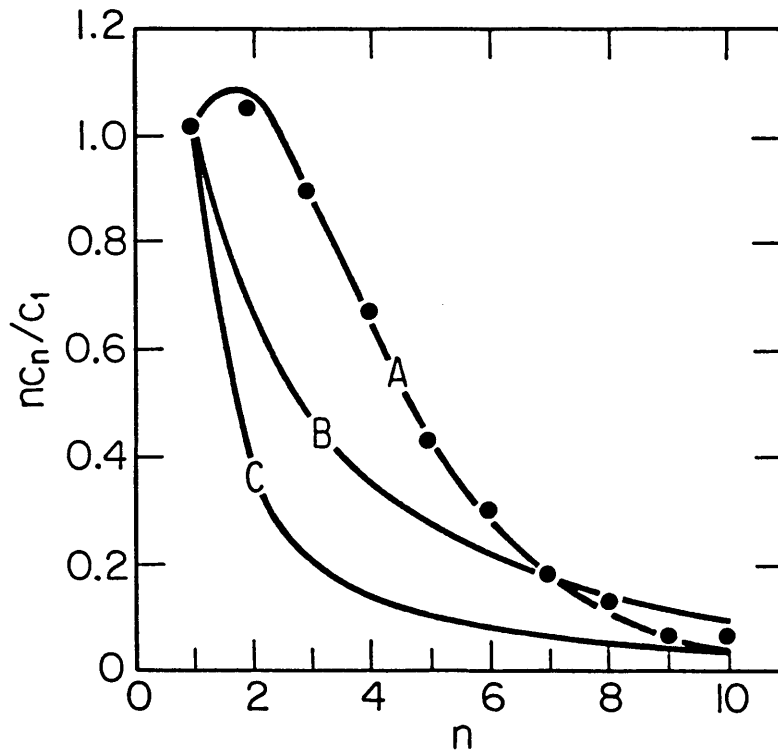


Figure 4.2
Normalized mass fraction, nc_n/c_1 , at short times ($t \approx \tau$). $b_A = 0.54$; $b_B = 0.64$; $b_C = 0.50$;

In Figure 4.2 I plot an illustrative mass fraction histogram, taken at $t = 21$ hr, with the fits for Cases A, B and C. Here distribution A fits quite well while distributions B and C fit poorly. One qualitative feature of distributions B and C makes it difficult to fit them to the experimental data: they require mass fraction to decrease monotonically with increasing n for all values of b . On the other hand, distribution A allows for the observed peak in this function.

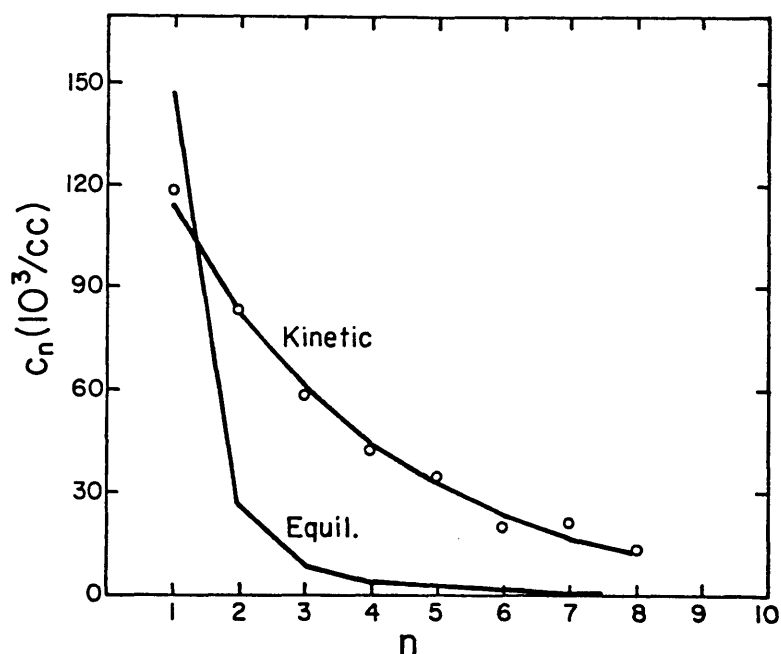


Figure 4.3
The cluster size distribution at $t = 2.6\tau$.

Figure 4.2 shows unambiguously that the shape of the cluster size distribution at small n is a sensitive indicator of the reaction mechanism. There is no need to go further out in the histogram to see that rapid coagulation is clearly diffusion limited. For case C in particular, most of the dynamic range of the cluster size distribution is spanned by the concentrations of the smaller species. Curve C in Figure 4.2 has saturated at its highest possible state of aggregation, $b = 1/2$. It has no possibility of fitting the data at short times. In fact it is the rapid decrease of the cluster size distribution with cluster size that leads to sol-gel phase separation in case C. The gel forms because of the

finite capacity of the gel phase. In all of the histograms I have ever collected, I have never found case A to saturate. Case B decays more rapidly than case A but less rapidly than case C. With very aggregated samples, I have found that case B appears to saturate at a b value of roughly 0.8; b_B never rose above this value even as the degree of aggregation increased in the experimental curve. I haven't investigated the mathematics of this, but my guess is that this unusual behavior results from the fact that I fit the theoretical curve only to a finite number of points.

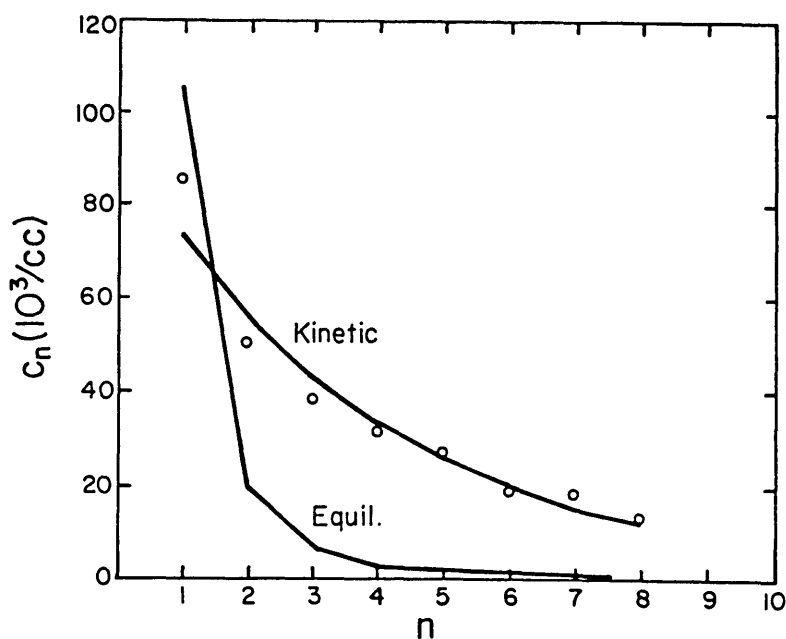


Figure 4.4
The cluster size distribution at $t = 4\tau$.

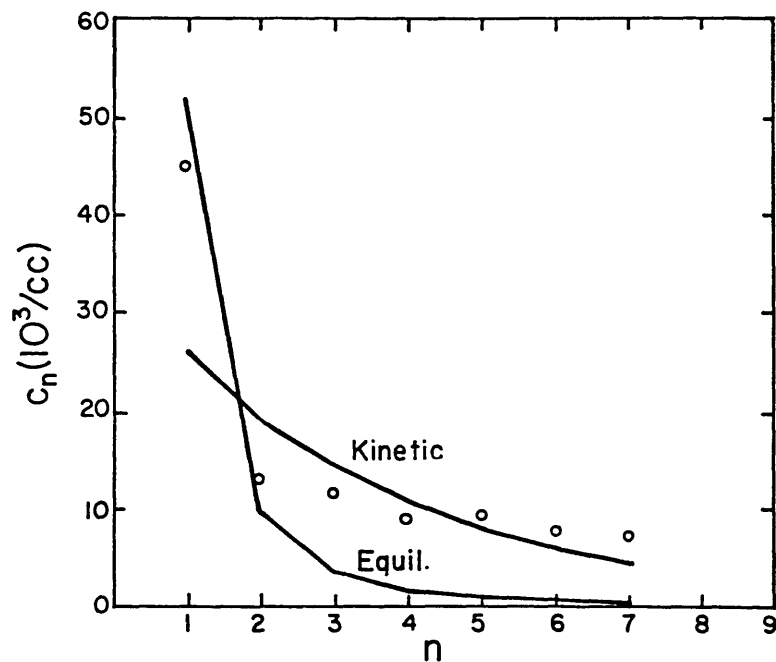


Figure 4.5
The cluster size distribution at $t = 7.9\tau$.

As I have emphasized: I expect Case A to apply while the reaction is kinetically controlled and Case C to apply at equilibrium. Therefore, I have compared the experimental cluster size distribution against these two theories in Figures 4.3-4.5. In all three of these figures b_C is $1/2$. In Figure 4.3 ($t = 47 \text{ hr} = 2.6\tau$; $b_A = 0.73$) the experimental data closely follows the von Smoluchowski distribution. In Figure 4.4 ($t = 72 \text{ hr} = 4\tau$; $b_A = 0.77$) I begin to observe a deviation from the kinetic theory: the

experimental points fall faster than predicted - but not as fast as in the equilibrium case. And finally, in Figure 4.5 ($t = 143 \text{ hr} = 7.9\tau$; $b_A = 0.75$) the experimental distribution falls much more rapidly than in the kinetic case and now agrees better with the equilibrium distribution.

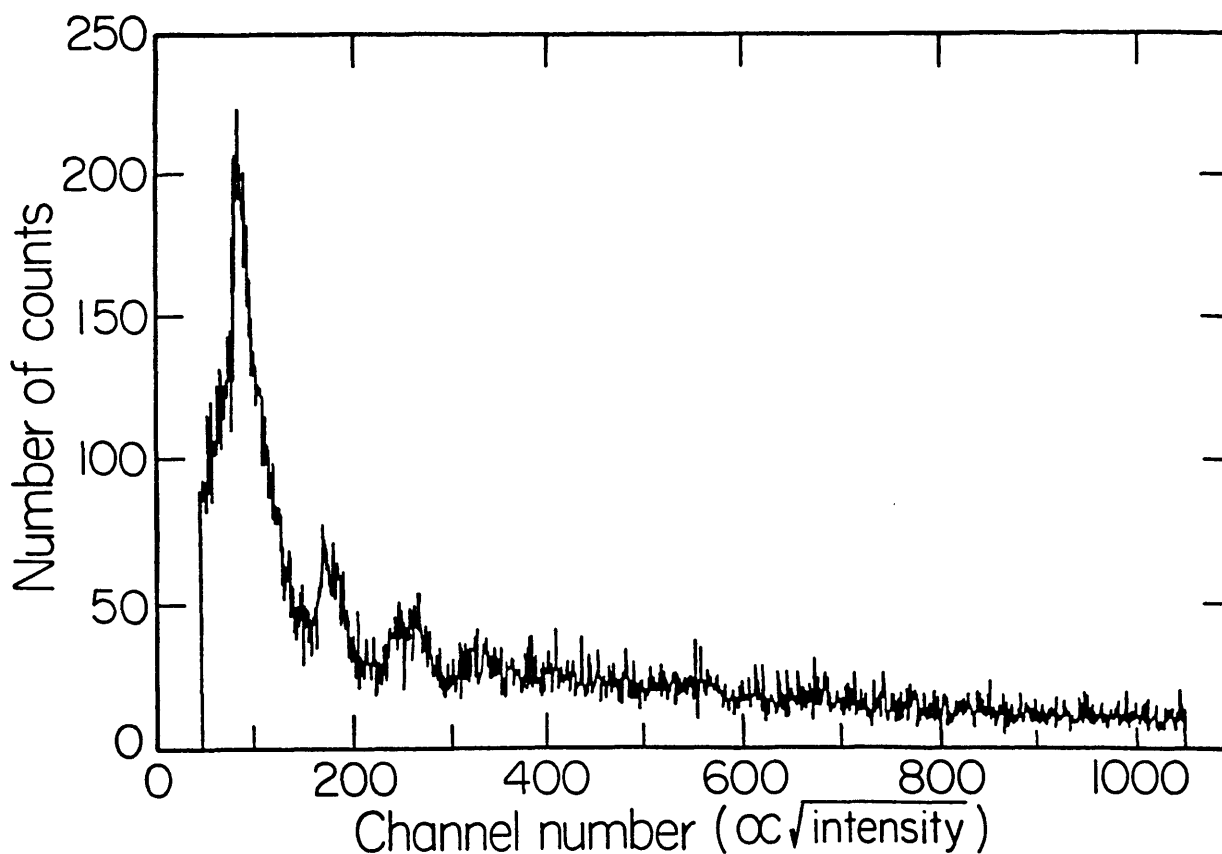


Figure 4.6
The raw histogram for Figure 4.5

The apparent discontinuity in the experimental points of Figure 4.5 is surprising. In fact, the unusual shape of this experimental distribution reflects the difficulty of observing highly aggregated sols more

than it reflects the true behavior of the system. At this point in time, the actual distribution was apparently bimodal; I discuss this point in section 4.3 below. The wild oscillations that characterized the very long pulses that appeared late in the reaction washed out the peaks in our observed histograms. Figure 4.6 depicts the actual histogram behind Figure 4.5. We see that the difference between the experimental points and the equilibrium curve in Figure 4.5 might be explained by the very noisy background, which adds a roughly uniform offset to each of the higher order peaks. I can not draw decisive quantitative information about the detailed form of the cluster size distribution from this histogram, but I can conclude that the ratio of monomers to dimers and trimers is much higher than I would expect from the von Smoluchowski distribution (case A) at such large reaction times ($t \simeq 8\tau$).

While quantitatively the cluster size distribution at long times does not compare well with the equilibrium theory, the excess of monomers in Figure 4.5 may be an indication of equilibrium kinetics. Cluster fragmentation may cause this excess of free monomers, in which case the change in shape of the distribution is a reflection of the finite capacity of the equilibrium sol phase.

4.2 Average Cluster Size and The Bond Parameter b

The mean cluster size \bar{n} is a good indicator of the extent of reaction in the sol phase. In Figures 4.7 and 4.8 I plot the temporal evolution of \bar{n} at both concentrations. Figure 4.7 depicts $\bar{n}(t)$ at the lower

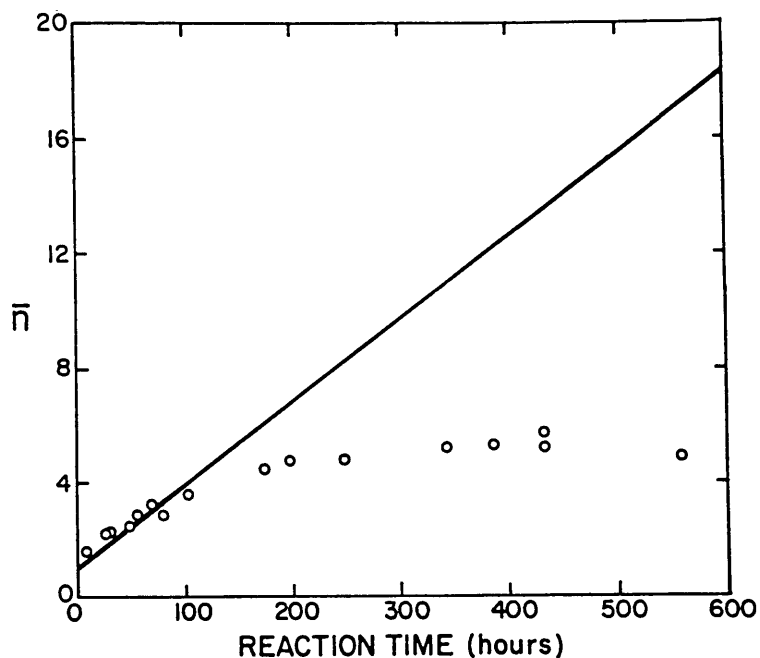


Figure 4.7

Time dependence of the average cluster size at the low concentration.
 $\tau = 36$ hr.

concentration, where τ is 36 hr (Sample 2, Table 4.1).

The optimized fits to the shape of the distribution (which give rise to Figure 4.1) allow me to estimate average cluster size through the relation $b = 1 - 1/\bar{n}$ (Equation [2.9]). In case A, \bar{n} should grow linearly with time. In both Figures 4.7 and 4.8, the experimental curves grow linearly at first, but at roughly 3τ they begin to plateau - as one might expect in a system approaching equilibrium. At the higher concentration of Figure 4.8, the average cluster size not only plateaus, but subsequently drops: the degree of aggregation in the sol appears to decrease.

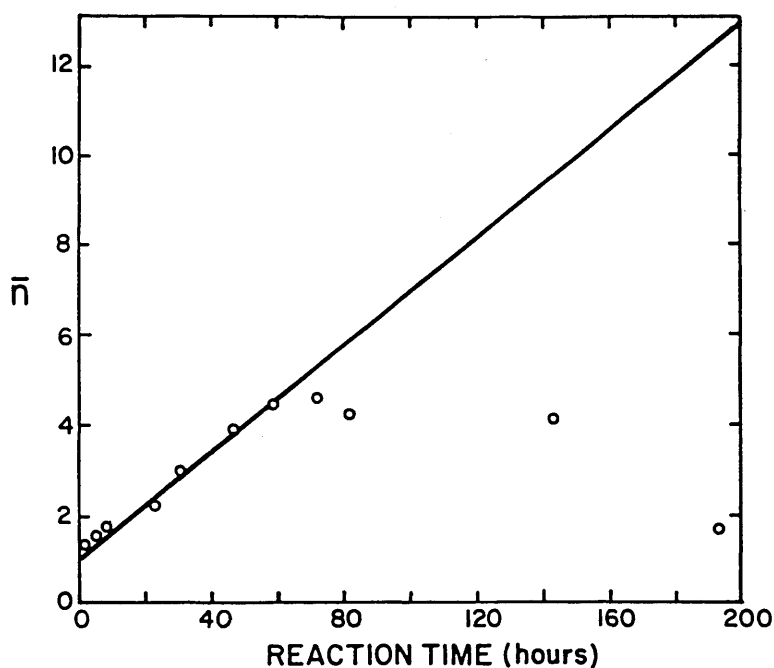


Figure 4.8
Time dependence of the average cluster size at the higher concentration.
 $\tau = 18$ hr.

As I have shown, \bar{n} is clearly related to b , the minimum number of bonds per monomeric particle in the sol. In Figures 4.9 and 4.10 I plot the fitted values of b versus time with the theoretical prediction for $b(t)$ according to distribution A ($b(t) = (t/\tau)/(1 + (t/\tau))$ - see Table 2.1). The value of τ was adjusted to optimize the fit; in fact, this is the way I determined the values of τ that I have been using throughout this section. As expected, experiment agrees with the kinetic theory for roughly three reaction half-lives, at which point bond formation appears to slow down. At the lower concentration (Figure 4.9) it merely levels off, but at the higher concentration (Figure 4.10) it actually decreases.

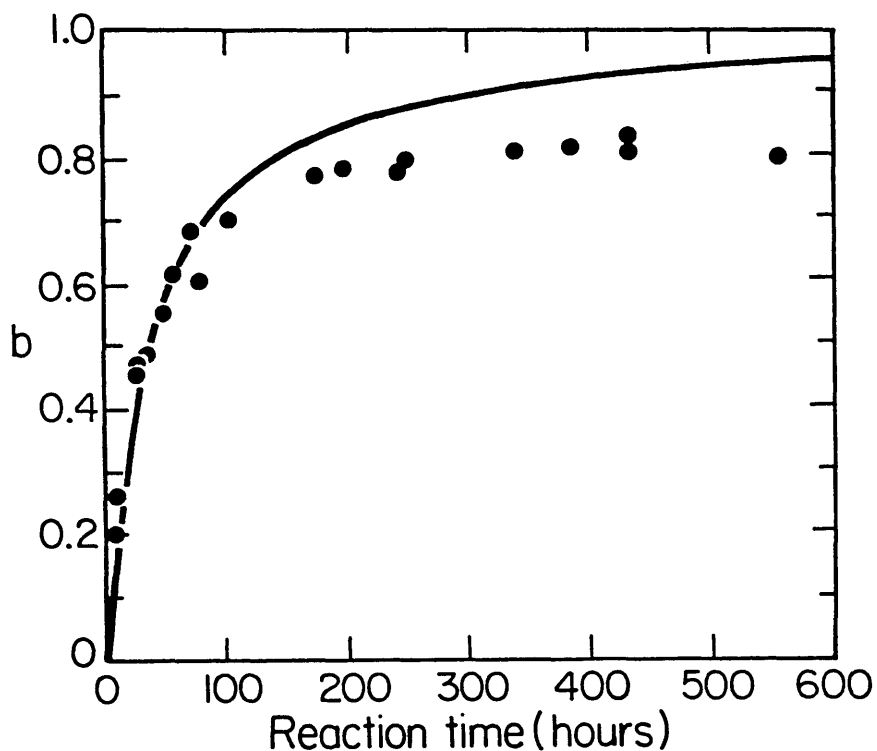


Figure 4.9
Time dependence of the bond parameter b at the low concentration.
 $\tau = 36$ hr.

The theoretical curves asymptotically approach unity at long times.

4.3 Total Sphere Concentration and the Growth of Very Large Clusters

As I stated in connection with Figure 4.1, I also estimated the parameter c_0 in optimizing the error function E . At the lower concentration there was a lot of scatter in the early points due to variations in

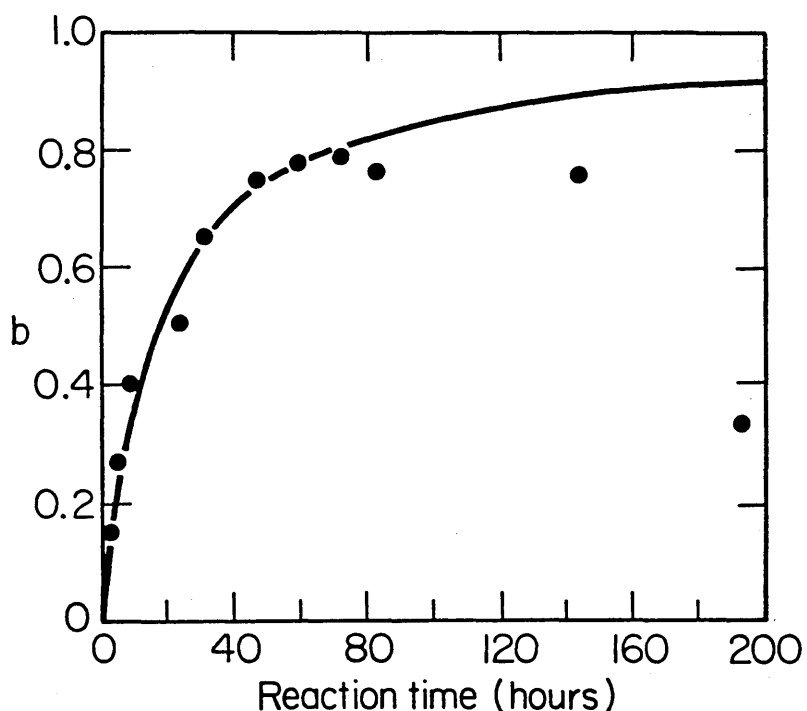


Figure 4.10
Time dependence of the bond parameter b at the higher concentration.
 $\tau = 18$ hr.

flow rate, but after three half-lives the points clearly indicated a steady decrease in c_0 . In Figure 4.11, which was taken at the higher concentration, we see that the fitted concentration stays roughly constant until $t = 60$ hr ($\sim 3\tau$) and then declines monotonically. While the applicability of the von Smoluchowski distribution is questionable at long times, the apparent loss of mass in the sol phase is especially intriguing in light of the sol-gel transition predicted by Flory-Stockmayer theory for the isomorphic $R-A_\infty$ system and by cluster-cluster aggregation.

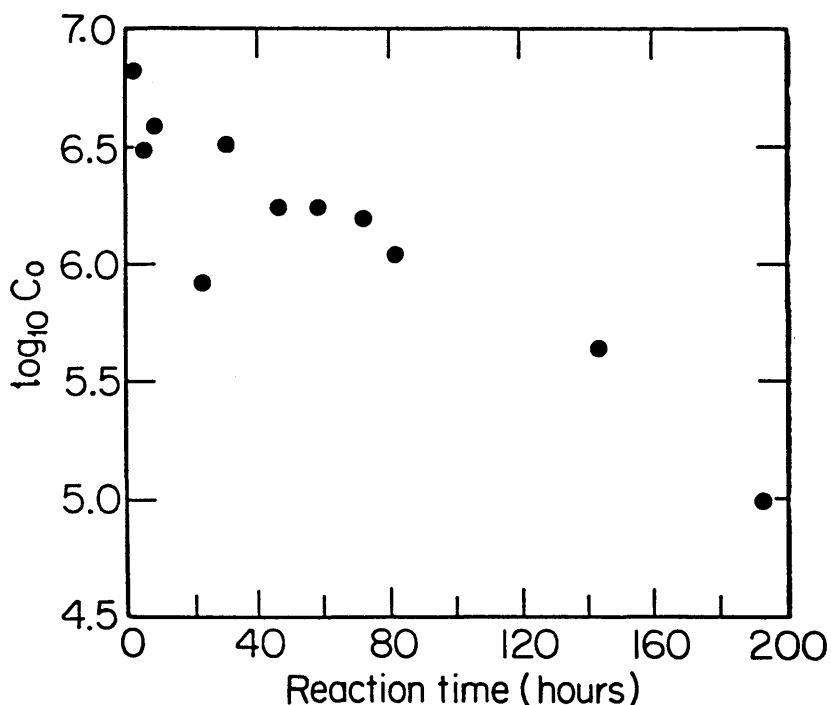


Figure 4.11
Time dependence of the total concentration c_0 .

Although no macroscopic precipitate ever became visible in any of my samples, I did observe (on the oscilloscope attached in parallel with the multichannel analyzer - see Figure 3.3) a number of striking and very unusual light pulses late in the reaction. These pulses generally exhibited a number of very large oscillations and took from 20 to 30 times as long as a pulse from a monomer. Assuming that pulse width is proportional to cluster radius, these pulses must have arisen from very large particles - many times the size of the scattering volume. I have already mentioned them in connection with the difficulty of obtaining thin peaks from highly aggregated samples (sections 3.1.3 and 4.1). The fact that

the pulses oscillated so strongly - often the scattered intensity appeared to shrink to zero - may indicate that these were highly ramified objects. The change in scattering angle as a cluster traverses the scattering volume is too small to explain the oscillations. Bacteria or other biological matter cannot explain the pulses, both because we added sodium azide to poison bacterial growth, and because we observed no such pulses in a control sample that contained no salt. Also, there were clearly too many anomalous pulses to be explained on the basis of extrapolation from the measured cluster size distribution: it appears that the distribution became bimodal.

4.4 Relative Concentrations

Although my evaluation of distribution shape is based upon an essentially unbiased chi-squared fit, my estimates of average cluster size, bond parameter, and total sphere concentration are biased, since they assume the validity of von Smoluchowski theory. The most direct evidence of the departure of my experimental data from von Smoluchowski theory is obtained by examining the temporal evolution of the n-mer concentrations themselves.

In Figures 4.12 and 4.13 I plot c_n/c_1 as a function of time at both concentrations. In both cases, I fit the theoretical curve for c_2/c_1 to the corresponding experimental points and used the resulting value of τ to generate the other theoretical curves. Again we see excellent agreement until $t = 3\tau$, at which point the course of the reaction changes

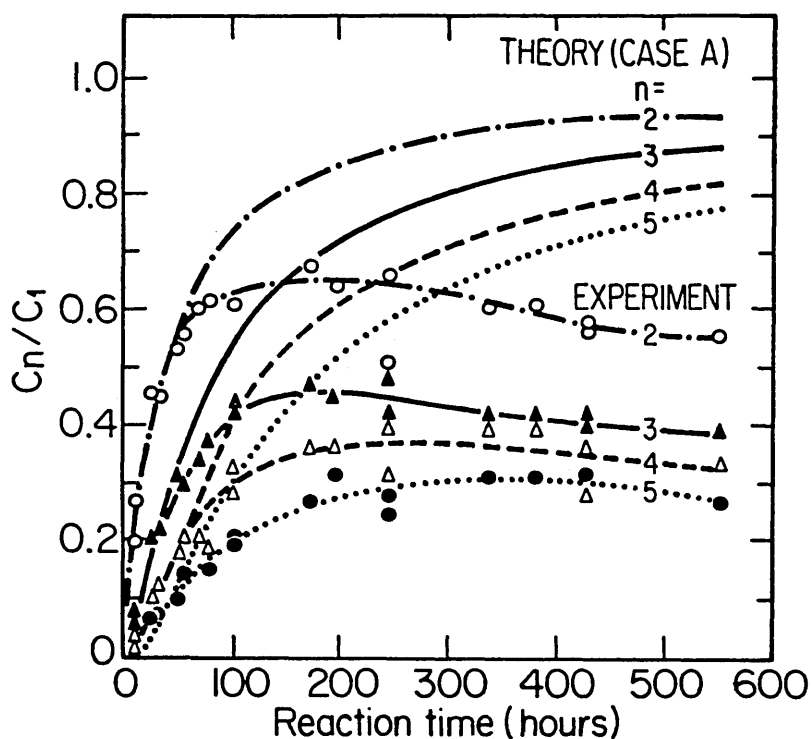


Figure 4.12
Time dependence of c_n/c_1 at the low concentration.

dramatically. As usual, the curves at higher concentration exhibit the more striking behavior. In Figure 4.12 relative concentrations essentially plateau, while in Figure 4.13 they decline quite abruptly. The sharp departure from von Smoluchowski theory may signal the onset of a sol-gel transition at the time $t = 3\tau$. The gel phase could consist of very large particles, invisible to the eye but beyond the range of our instrument - the same particles that caused the anomalously long light pulses mentioned above. I must stress that a decline in c_n/c_1 appears not to be a necessary prerequisite for a bimodal distribution, since

anomalous light pulses were observed at both concentrations.

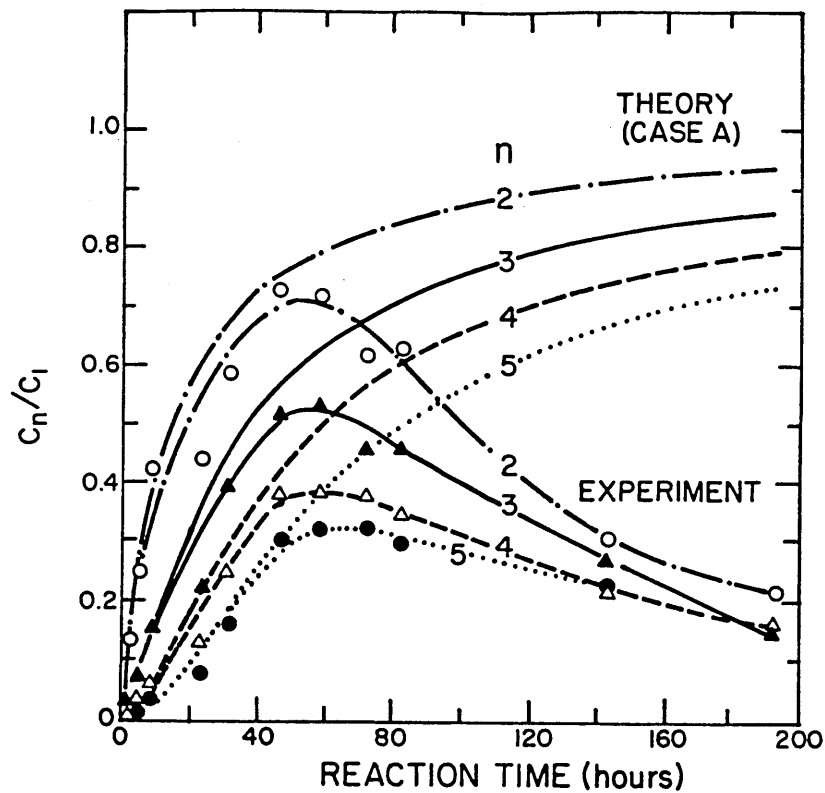


Figure 4.13
Time dependence of c_n/c_1 at the higher concentration.

4.5 Colloid Stability

Incidental to my principal efforts in determining the temporal evolution of the cluster size distribution, I also examined the effect of changing the concentration of salt. As predicted by DLVO theory, I found

that below a critical salt concentration significant coagulation did not occur. For the particular batch of latex particles I used, the critical coagulation concentration of NaCl was roughly 0.4M (see Appendix I).

I measured the stability factor W in two different ways. The first was to fit the theoretical curve $b(t)$ (as in Figures 4.9 and 4.10) to only those points with b less than 0.67 - since distributions fit best at low b values. This method yields the column labelled W_b in Table 4.1. The second method was to fit the theoretical curve $c_2(t)/c_1(t)$ (as in Figures 4.11 and 4.12) to early experimental points - for the same reason. From the τ values so obtained, I deduced W_2 . W_2 emphasizes the monomer-monomer interaction specifically, whereas W_b averages over all interactions.

Sample	$[\text{NaCl}]^\dagger$	c_o^*	τ_A (hrs)	W_b	W_2
1	1.0	2.7×10^6	18	1.4	1.7
2	0.5	2.6×10^6	18	2.0	2.1
3	0.5	2.6×10^6	18	1.8	1.9
4	0.5	5.2×10^6	9	2.0	1.8

Table 4.1

Experimental conditions, calculated time constants, and experimentally determined stability factors for four different preparations. All experiments took place at 298K.

\dagger - Salt concentration (mol/l).

* - Sphere concentration (cm^{-3}).

We see in Table 4.1 that the two methods lead to somewhat different results. As expected, both W 's decrease as salt concentration is raised, because increased salt provides greater shielding of electrostatic repulsion. While these results are hardly conclusive, they do suggest that in the future our single particle technique could prove useful in probing pair potentials between colloidal particles.

CHAPTER V

DISCUSSION AND FUTURE PROSPECTS

In this thesis I have described both a new, high resolution instrument and some new experimental results. I have also attempted to review the wide range of theory applicable to aggregation phenomena in general.

I have shown that our optical pulse particle size analyzer is particularly useful in resolving cluster size distributions of sub-micron particles. Its distinguishing feature is that it detects scattered light from individual clusters at very small forward angles. The intensity of this low angle light goes as n^2 , where n is the number of spheres in an aggregate, even when the spheres themselves are too large to have simple scattering properties individually. The scattered intensity is also quite insensitive to the shape and configuration of each cluster. It is these two features that make coherent, low angle light scattering an extremely sensitive probe of cluster size distributions - more sensitive, in particular, than resistive pulse analysis¹⁻³ and fluorescent (or incoherent) light scattering,^{4,5} because these methods yield linear response and are sensitive to cluster configuration and orientation. In fluorescence, it is also difficult to produce spheres with uniform scattering properties.⁶

Furthermore, low angle light scattering permits the detection of coincidences, which are indistinguishable in linear instruments. I have attempted to eliminate artifactual shearing of clusters with an appropriately designed optical flow cell.

This instrument has allowed me to measure n-mer concentrations, for n as large as 25, in the classical problem of colloidal flocculation. I have watched the size distribution evolve in time during so-called rapid coagulation, which takes place at high salt concentrations (see Appendix I).

At short times, $t < 3\tau$, where τ is the effective reaction time constant, both the shape and temporal evolution of the cluster size distribution closely follow von Smoluchowski's theory of diffusion controlled aggregation,^{6,7} corrected for the effects of inter-particle potentials⁸ and viscous interactions.^{9,10} At $t \simeq 3\tau$, apparently independent of initial sphere concentration, a sharp departure from von Smoluchowski theory takes place.

This departure is manifested most strikingly in the temporal evolution of the relative n-mer concentrations, c_n/c_1 , (Figures 4.12 and 4.13). Before $t \simeq 3\tau$ they follow their prescribed time courses very closely, but at $t \simeq 3\tau$ they veer sharply from their predicted trajectories. This deviation indicates that there are far fewer intermediate sized n-mers than we might expect. At the same time, the shape of the cluster size distribution changes, as evidenced by a progressive increase in the error function E (Figure 4.1). From actual histograms of the distribution (Figures 4.3 - 4.5) we see that, indeed, the greatest difference between the early and late distributions is a

sharp drop in the relative concentrations of the higher order species. In fact, the distribution approaches an equilibrium form proposed by Cohen and Benedek,¹¹ based upon Flory-Stockmayer polycondensation theory.¹²⁻¹⁷ Finally, c_0 , the inferred concentration of monomeric spheres in the sol, decreases for $t > 3\tau$ (Figure 4.11).

Shortly after the distribution changes shape I note the gradual appearance of a few anomalously large clusters, as evidenced by very long, oscillating scattering patterns on the oscilloscope. These clusters are too large to observe quantitatively with our instrument, but they are also too small to see with the un-aided eye. They indicate that the cluster size distribution becomes bimodal during the late stages of the reaction.

5.1 The Nature of the Transition

One of the most important qualitative features of my data is the clear evidence that a kinetically evolving system may change dramatically as it approaches equilibrium. Most theories of flocculation⁶⁻⁸ and polymerization¹²⁻¹⁸ have assumed that the functional form of the distribution must remain constant in time, even after gelation. In polymerization theory in particular, there has often been some confusion (see section 2.2.2) regarding the difference between kinetics and equilibrium because of the precise correspondence between kinetic solutions utilizing reaction limited kernels and equilibrium Flory-Stockmayer calculations.

Based upon experimental results involving antigen coated microspheres cross-linked by antibody,¹⁹⁻²¹ Cohen and Benedek¹¹ observed that there is no reason for the cluster size distribution to have the same form at equilibrium that it has while it evolves kinetically. They also pointed out that the Flory-Stockmayer R-A_∞ model is applicable to colloid flocculation at equilibrium. Up to this observation, flocculation had been treated almost exclusively from the kinetic standpoint, where von Smoluchowski's irreversible diffusion controlled model was essentially unquestioned.

In Chapter II, I analyzed both diffusion controlled flocculation (case A) and the R-A_∞ model in detail. I showed that the form of the association kernel ($a_{ij} = A$, a constant) precludes the possibility of gel formation in diffusion controlled coagulation. In the R-A_∞ model, on the other hand, gelation occurs at a specified degree of aggregation. Furthermore, the two models give different functional forms for the cluster size distribution. Hence only as the system approaches equilibrium is it possible for a gel to form. At the same time the shape of the distribution may change.

In fact, it is possible that the sharp departure of my experimental data from von Smoluchowski theory corresponds to the onset of a sol-gel transition as the system approaches equilibrium. Several observations support this interpretation. The total number of monomeric units in the sol phase, c_0 , decreases; at the same time very large clusters appear, generating off-scale pulse heights. It is also intriguing that the fit of distribution C, which corresponds to the proposed equilibrium distribution, progressively improves at long

times (Figure 4.1). The gel phase may consist of a population of very large clusters whose precise size is determined by a variety of factors not considered explicitly here - such as surface effects. The anomalously large pulses I observed may correspond to these 'gel clusters'. I cannot rule out, however, the possibility that the apparent disappearance of mass from the sol phase results from the formation of an adsorbed surface phase.

If a sol-gel transition is the explanation, the mechanism for gelation is, paradoxically, fragmentation. I mentioned in section 2.1.1, concerning reaction limited and mobility limited kernels, that aggregation always proceeds more slowly in the reaction limited case. In my system, this means that after the clusters diffuse towards each other, they may have to collide a few times before they stick. At equilibrium, not only would they have to finally stick, but at the same time, clusters would be breaking apart. Hence as equilibrium is approached, the apparent rate of bond formation decreases. If we assume on the basis of the short time behavior of my system that, in fact, every collision is fruitful, we can develop a rigorous theory to account for the behavior of the system at all times.

To do this we must utilize the reversible coagulation equations [2.78]. The association coefficients will be given by $a_{ij} = A$, as usual. If we require the system to approach the $R-A_\infty$ distribution (which is the same as that for the kinetic case C in Table 2.1), the dissociation coefficients are now completely determined. With equation [2.80] and the simplified degeneracy factor $D'_n = n^{n-2}/n!$ of the $R-A_\infty$ system, the expression for b_{ij} becomes:

$$b_{ij} = \lambda \frac{(i+j)! i^{i-2} j^{j-2}}{(i+j)^{i+j-2} i! j!} A \quad [5.1]$$

where $\lambda = c_{\text{solvent}} e^{g'/kT}$. The coefficients a_{ij} and b_{ij} are now fully determined by the parameters A and g' , the effective free energy of bond formation. Experimentally, A can be deduced from the short time behavior of the system, and g' can be measured from the equilibrium distribution or from the trajectories $c_n(t)$ in the transition regime. In this formulation, the only possible mechanism for gelation is cluster dissociation.

This formulation also provides an explanation for the observed excess of free monomers at times $t > 3\tau$. In Figure 5.1 I plot the fragmentation kernels b_{ij} for all sizes i and j in a 20-mer. These kernels reflect the rates at which the various sized clusters break free. The rate of monomer production from 20-mers is five times higher than even dimer production, and $b_{i,20-i}$ continues to drop very swiftly with increasing i .

To test this explanation quantitatively, it would be necessary to solve the reversible coagulation equations numerically with the indicated forms for a_{ij} and b_{ij} . The solutions would then predict the full temporal evolution of the relative concentrations c_n/c_1 as in Figures 4.12 and 4.13.

On the other hand, I have no hard experimental evidence that the R- A_∞ model actually describes equilibrium here. True, the distribution evolves in that direction, but in fact, even at late times, experimental distributions are so highly aggregated that the best fit for case

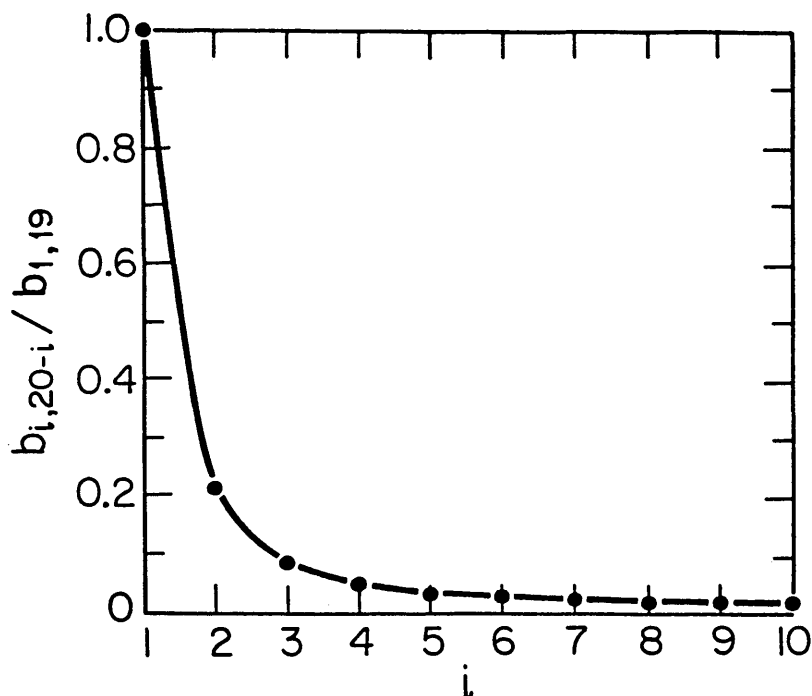


Figure 5.1
Fragmentation kernels for 20-mers when $a_{ij} = A$ and b_{ij} is given by equation [5.1]

C always saturates at its maximum possible value of $b = 1/2$. The most plausible explanation for this is that restructuring in large clusters allows cyclical bonds to form. This would increase the degeneracy factor for an n -mer, effect the form of the equilibrium distribution, and increase the capacity of the sol phase; hence, it would shift the critical point, and possibly effect the dynamics of the phase transition.

The method I have proposed for determining b_{ij} circumvents the very difficult problem of determining fragmentation terms directly. In my system fragmentation is complicated by the fact that diffusion undoubtedly plays a part for large clusters. In discussing reversibility in section 2.2.2, I mentioned that in reaction limited reactions, the assumption that every bond has an equal dissociation rate is essentially the converse of Flory's assumption of equal reactivity. It leads to reversible Flory-Stockmayer solutions. Even assuming that bonds break at equivalent rates, however, this reaction limited model misses an important factor in free cluster formation. Two large clusters formed as a bond breaks in a larger one will have an enhanced probability of recombining: they will diffuse apart very slowly, and they will have a very large collision cross-section. The model I have described takes this effect into account indirectly.

If a monomer were to break away from a large cluster it could diffuse out of reach more easily. Also, in the case where large clusters form cyclical bonds by restructuring, more than one bond would have to break to form a large fragment, so only small clusters near the surface of a large one will have any significant chance of breaking away. Both of these effects might explain the enhanced concentration of free monomers that I observe after three reaction half-lives.

It is also natural to ask whether sedimentation may play a role in the change of shape. Because the density of polystyrene is greater than that of the surrounding salt solution, clusters will tend to settle - larger ones settling more rapidly. An analysis of settling in the presence of diffusion²² shows that the relevant time scale for

settling is given by

$$t_{\text{settle}} \simeq 4D/C^2 \quad [5.2]$$

$$\text{where } C = (1-\rho_o/\rho) \frac{mg}{6\pi a\eta}$$

D is the diffusion coefficient given by [2.14], ρ_o is the particle density, ρ is the solvent density, m is the particle mass, a is its radius, and g is the gravitational constant. The specific density of polystyrene in salt water is roughly 1.02. This gives a settling time for monomeric spheres of roughly 204 hr - much longer than 3τ at both concentrations.

But uniform settling would not disturb von Smoluchowski's analysis significantly. Only differential settling, in which larger clusters move more rapidly through the sol than small clusters, would effect the form of the association coefficient, a_{ij} . The settling time in [5.2] has a strong dependence upon n, the cluster size:

$$t_{\text{settle}} \propto \frac{R_n^h}{n^2} \quad [5.3]$$

where R_n^h is the hydrodynamic radius of an n-mer, defined by the Stokes-Einstein relation [2.14]. If the cluster is fractal then $R_n^h \simeq n^{1/d_f}$ and

$$t_{\text{settle}} \simeq \frac{1}{n^{2-1/d_f}} \quad [5.4]$$

For a dense packed 10-mer ($d_f = 3$) the estimated settling time would be 4 hr 20 min; whereas, for a linear 10-mer it would be 20 hr. From Figures 4.7 and 4.8 we see that the distribution changes shape when the average cluster size is about four. The time limits at this size are about 21 hr and 50 hr respectively; hence I must conclude that settling may play a part in the change of shape.

Then it is important to know whether or not large settling clusters interact with the rest of the sol. In the extreme case, one could imagine a very large cluster settling quickly through the syringe and binding to every cluster in its path. This could lead to cascading growth, since the large cluster would develop a greater cross-section and settle more rapidly with every encounter. In my system we can rule out this possibility since the average distance between clusters is roughly 5×10^4 monomer radii.

It is difficult to explain the observed decrease in the relative concentration of larger clusters on the basis of pure settling. Recall that I always drew the sample from the bottom of the reaction vessel. It would seem that larger clusters - and I did measure concentrations for up to 25-mers - would congregate there. In fact, the bimodal distribution at long times may be evidence that large clusters settle too quickly to interact appreciably with the sol. My results could be explained if some sort of cascading growth takes place in the absence of settling, and the very large clusters so formed precipitate quickly. This is in obvious parallel to Stockmayer's model for gelation, in which the cluster size distribution 'sticks' at the gel point, and there is no interaction between sol and gel. Although it is

interesting to note that case C does 'stick' in these experiments, my results are not quantitative enough to distinguish between the Flory and the Stockmayer gelation models.

To attempt a rigorous analysis of coagulation with settling would be computationally intensive. It would be also complicated by the fact that settling rate depends not only upon a cluster's mass, but also its geometry. To answer the question of settling from an experimental standpoint, it would be desirable to conduct experiments at higher concentrations, where coagulation takes place at a much faster rate than sedimentation. In this case it would be necessary to dilute the sample in order to observe the reaction.[†]

In section 2.1.7.1 I pointed out that cluster-cluster aggregation,²³ which as of now ignores both fragmentation and restructuring, exhibits the same general features as my experimental system: distributions do change shape, and anomalously large clusters do appear. Unfortunately, there is little quantitative information on the cluster size distribution in the regime $\omega > 1/2$, in which gelation occurs.

Another promising theoretical explanation lies in the work of Donoghue and Gibbs²⁴⁻²⁶ on finite systems. Here, once again, the cluster size distribution is calculated numerically. It would be useful to determine the temporal evolution of intermediate sized clusters in this model after the distribution becomes bimodal.

[†] - In fact, Cummins et al.⁵ have performed preliminary experiments at high concentrations. They note an apparent decrease in the rate of aggregation even earlier than 3τ .

5.2 Other Experimental Results

Recently, other workers have used single particle counting techniques to study colloidal coagulation. Cummins et al.^{4,5} describe an instrument that measures fluorescence and low angle light scattering, but they have studied salt induced flocculation only with fluorescence. They discuss the time dependence of the zeroth and first moments of the distribution and the concentration of monomers, but they do not discuss the shape of the distribution. They note an excess of monomers over the von Smoluchowski prediction - just as I do - and observe that this implies that particles beyond the range of their instrument must be larger on the average, but they mention no anomalous pulses, nor do they allude to a possible bimodal distribution at long times. Also, the fluorescent coating on the spheres seems to reduce bond strength.

Gedan et al.²⁷ use low angle light scattering to calculate the magnitudes of a_{11} , a_{12} , and a_{13} on the basis of data obtained at short times. They find that a_{1j} is not constant, even early in the reaction - in contradiction with my results. I note that their laminar flow cell, which caused occasional shearing in my tests, may explain this contradiction.

Neither of these studies indicates case A kinetics. This may be the result of three- and four-body interactions, which become increasingly important at high sphere concentrations and are ignored in the coagulation equations [2.1]. Both Cummins et al. and Gedan et

al. use at least 100 times the initial sphere concentration that I chose for these studies; they also diluted the sample before observing it. As I have mentioned, diluting the sample will lead to cluster fragmentation if the bonds are not strong. Fragmentation will be enhanced with the weak bonds between fluorescent particles.

In a system somewhat different than mine, von Schultess et al.¹⁹⁻²¹ and Johnston et al.^{28,29} use a resistive pulse analyzer to investigate antigen-antibody agglutination - the antibody mediated cross-linking of antigen coated microspheres. They find that aggregation in this system is both kinetically controlled and unidirectional. However, the reaction rate is several orders of magnitude lower than von Smoluchowski's theory of diffusion controlled coagulation would predict. Furthermore, they find that distribution B fits the shape of the experimental distributions and that the shape does not change with time.

Most other studies have measured bulk properties of the dispersion. Until recently, they have been concerned primarily with measuring stability factors^{8,30-32} and have not critically examined the shape of the cluster size distribution. In fact, the key to understanding $\log(W)$ vs. $\log(C)$ plots at low salt concentration C (see Appendix I) may lie in a change in the shape of the distribution.³³ As I indicate in Appendix I, our instrument may answer important questions in this area.

Recently, there have been a number of attempts to estimate and measure the fractal dimension of large colloidal aggregates.³⁴ Shaeffer et al.^{35,36} measure the structure factor of colloidal

silicates with light scattering and low angle X-ray scattering. They find that $d_f \sim 2.12$. Weitz et al.³⁷⁻³⁹ study colloidal gold spheres, which aggregate when pyridine is added to the solution. They estimate the fractal dimension to be 1.75 using electron microscopy. In yet a third set of experiments, Sinha et al.⁴⁰ employ small angle neutron scattering to measure the structure of Cab-o-sil powders. They find $d_f \sim 2.5$. Of these studies, only the first can be considered a true in situ measurement, since the aggregates were deposited upon a substrate in the first case,[†] and compressed or suspended in a fluid in the second.

To my mind, structure is most interesting from the point of view of how it effects and is in turn effected by the coagulation kernel a_{ij} . The cluster-cluster aggregation model draws a clear connection between the two (see Equation [2.62]). Furthermore, the pair potential certainly effects a_{ij} and might also effect structure. The question of how to control structure is very important in the development of ceramics, where dense structures have higher strength, and in sol-gel glasses, where it may be possible to control refractive index and mechanical properties by tuning the early stages of the sol growth process.

[†] - Weitz et al. do not propose a detailed mechanism for bonding in the gold/pyridine system, yet in order to justify their experimental procedure they assert that the gold particles essentially weld after aggregating. It seems more likely that they are witnessing so-called polymer flocculation,⁴¹ in which first a pyridine molecule adsorbs on the surface of a sphere and then another sphere collides at the same spot. The pyridine molecule forms a bridge between the two spheres by adsorbing to each. The bonds in this system would be much weaker than a gold-gold bond and might easily break or restructure as an aggregate is deposited for microscopic observation.

Shaeffer et al.³⁶ argue that a balance of entropic and energetic effects causes an equilibrium structure to depend upon the ratio of the height of the potential barrier to the depth of the primary minimum (see Figure A.1.2). As this ratio increases, they conclude that an aggregate will assume the comparatively ramified, self-avoiding walk structure of a lattice animal.

On the other hand, computer simulations⁴² show that in reaction limited reactions structures become more dense. This can be understood in the following way: If the reaction is diffusion limited, every time a small particle touches a large one, it will adhere. If the reaction is reaction limited, the small cluster will collide a few times before finally adhering. In the second case, it will have a chance to diffuse farther toward the center of a ramified cluster than it will in the first, where it will most likely be caught at the perimeter. In fact, Weitz et al.³⁹ have investigated diffusion limited and reaction limited aggregation in the gold/pyridine system with quasi-elastic light scattering. Preliminary results show that reaction limited structures are indeed more dense.

Although he never used the word 'fractal', Overbeek himself actually noticed such effects as early as 1941.⁴³ He states that structures are "relatively dense...when the repulsive action of the double layer is not completely discarded" and that "when the repulsion is completely absent, the flocs are very irregular, rather loose, and scatter little light." More recently, Giles and Lips⁴⁴ have also shown that low ionic concentrations lead to denser structures.

Overbeek⁴³ also notes that the valency of the ions used to shield the electrostatic repulsion between colloids has an effect upon aggregate structure: "In very rapid coagulations, the primary particles are connected in the completely haphazard way in which they first touched each other. If there is just a little repulsion left, rearrangements in the position are still possible which will lead to a lower energy, better contact and thus a denser structure. The polyvalent ions seem to act as cementing centres, preventing this type of stabilization." Experiments with high valency salts would provide a good test of cluster-cluster aggregation, which does not incorporate restructuring.

5.3 Future Experiments

Colloidal aggregation is a very rich phenomenon. These experiments answer a few questions concerning rapid coagulation, but they raise quite a few more.

The greatest questions concern the precise nature of the 'gel' clusters. Using the value determined by Shaeffer et al.^{35,36} ($d_f \sim 2.12$) for their fractal dimension, we can estimate from the temporal width of the anomalous photopulses that these clusters contain at least 1000 monomers. They also seem to be ramified, judging from the strong oscillation of the photopulses, but, clearly, I have little direct knowledge of their properties. Since their diameter seems to be roughly 20 μ m, it might be possible simply to look at them through a microscope. It will most likely necessitate bulk scattering of some

kind - either quasielastic or static - in order to characterize them quantitatively, but it will be difficult to probe such large structures with the wavelengths of visible light. Quantitative information of this sort will be a prerequisite in differentiating between any of the gelation theories I have discussed.

To resolve the question of settling, it is important to extend these studies to higher concentrations. This might also suggest a mechanism behind the change in shape at $t = 3\tau$.

At the end of the last section I discussed the interconnections between pair potentials, cluster structure, and kinetics. It could be quite rewarding - and not too difficult - to investigate this exact system under conditions of slow coagulation. By varying salt concentration (and hence the height of the potential barrier) during slow coagulation and by changing the valency of the electrolyte, a detailed study of the effect of potential and structure upon coagulation kernels could be made. Also so-called reversible flocculation in the secondary minimum of the potential (see Figure A.1.2) presents a possibility for studying truly equilibrium cluster size distributions.

While I have focussed primarily upon the detailed shape of the evolving cluster size distribution, in order to elucidate the mechanisms governing aggregation phenomena in general, our single particle counting technique also provides a direct means of testing theories of colloidal interactions. Theories of interparticle potentials and viscous effects deal exclusively with monomer-monomer interactions. Yet nearly all experimental analyses of the effects on the potential of salt, particle size, temperature and dielectric constants of

particles and solvent, have relied upon measurement of bulk sol properties. To interpret these bulk measurements it has been generally necessary to assume that von Smoluchowski theory is valid. By directly measuring the temporal evolution of concentrations of low order n-mers, a more precise test of these theories is now possible.

REFERENCES - CHAPTER V

1. Coulter, W.H., U.S. Patent No. 2,656,508 (1953).
2. DeBlois, R.W. and Bean, C.P., *Rev. Sci. Instrum.*, **41**, 909 (1970).
3. DeBlois, R.W., Bean, C.P. and Wesley, R.K., *J. Colloid Interface Sci.*, **61**, 323 (1977).
4. Cummins, P.G., Staples, E.J., and Thompson, L.G., *J. Colloid Interface Sci.*, **92**, 189 (1983).
5. Cummins, P.G., Smith, A.L., Staples, E.J., and Thompson, L., in "Solid-Liquid Separation", J. Gregory, ed., Wiley, New York, 1984.
6. von Smoluchowski, M., *Phys. Z.*, **17**, 585 (1916).
7. von Smoluchowski, M., *Z. Phys. Chem.*, **92**, 129 (1917).
8. Verwey, E.J. and Overbeek J. Th. G., "Theory of the Stability of Lyophobic Colloids", Elsevier, Amsterdam, 1948.
9. Spielman, L.A., *J. Colloid Interface Sci.*, **38**, 376 (1972).
10. Honig, E.P., Roeberson, G.J. and Wiersema, P.H., *J. Colloid Interface Sci.*, **36**, 562 (1971).
11. Cohen, R.J. and Benedek, G.B., *J. Phys. Chem.*, **86**, 3696 (1982).
12. Flory, P.J., *J. Am. Chem. Soc.*, **63**, 3083 (1941).
13. Flory, P.J., *J. Am. Chem. Soc.*, **63**, 3091 (1941).
14. Flory, P.J., *J. Am. Chem. Soc.*, **63**, 3096 (1941).
15. Flory, P.J., "Principles of Polymer Chemistry", Cornell University Press, Ithaca, 1953.
16. Stockmayer, W.H., *J. Chem. Phys.*, **11**, 45 (1943).
17. Stockmayer, W.H., *J. Chem. Phys.*, **12**, 125 (1944).
18. Ziff, R.M. and Stell, G., *J. Chem. Phys.*, **73**, 3492, (1980).
19. von Schulthess, G.K., Benedek, G.B. and De Blois, R.W., *Macromolecules*, **13**, 939 (1980).
20. von Schulthess, G.K., Benedek, G.B., and De Blois, R.W., *Macromolecules*, **16**, 434 (1983).
21. von Schulthess, G.K., Ph.D. Thesis, M.I.T. (unpublished), 1979.
22. Chandrasekhar, S., *Rev. Mod. Phys.*, **15**, 1 (1943), p 57 ff.
23. Jullien, R., Kolb, M., and Botet, R., in Reference 34.
24. Donoghue, E. and Gibbs, J., *J. Chem. Phys.*, **70**, 2346 (1979).
25. Donoghue, E., *J. Chem. Phys.*, **77**, 4236 (1982).
26. Donoghue, E., in Reference 34.
27. Gedan, H., Lichtenfeld, H., and Sonntag, H., *Colloid Poly. Sci.* **260**, 1151 (1982).
28. Johnston, D.F., Ph.D. Thesis, M.I.T. (unpublished), 1983.
29. Johnston, D.F. and Benedek, G.B., in Reference 34.
30. Lichtenbelt, W. Th., Pathmamanoharan, C., and Wiersema, P.H., *J. Colloid Interface Sci.*, **49**, 281 (1974).
31. Lips, A., Smart, C., and Willis, E., *Trans. Faraday Soc.*, **67**, 2979 (1971).
32. Lips, A. and Willis, E., *J. Chem. Soc. Faraday*, **69**, 1226 (1973).
33. Alexander Lips, personal communication.
34. Family, F. and Landau, D.P., eds., "Kinetics of Aggregation and Gelation", North Holland, Amsterdam, 1984.
35. Shaeffer, D.W., Martin, J.E., Wiltzius, P.W., and Cannell, D.S., in Reference 34.
36. Shaeffer, D.W., Martin, J.E., Wiltzius, P.W., and Cannell, D.S., *Phys. Rev. Lett.*, **52**, 2371 (1984).
37. Weitz, D.A. and Oliveria, M., *Phys. Rev. Lett.*, **52**, 1433 (1984).

38. Weitz, D.A. and Huang, J.S., in Reference 34.
39. Weitz, D.A., Huang, J.S., Lin, M.Y., and Sung, J., Phys. Rev. Lett., **53**, 1657 (1984).
40. Sinha, S.K., Freltoft, T., and Kjems, J., in Reference 34.
41. Hogg, R., J. Colloid Interface Sci., **102**, 281 (1984).
42. Botet, R., Jullien, R., and Kolb, M., J. Phys. A: Math. Gen., **17**, L75 (1984).
43. Overeek, J.Th.G., in "Colloid Science", Vol. I, H.R. Kruyt, ed., Elsevier, Amsterdam, 1952, pps. 298-299.
44. Giles, D. and Lips, A., J. Chem Soc. Faraday Trans. I, **74**, 733 (1978).

APPENDIX I

A SHORT REVIEW OF COLLOID STABILITY THEORY

As I stated in the introduction, since the early part of this century one of the major concerns of colloid science has been to explain the stability of sols. The potential between particles is the basis of this explanation, and coagulation rate turns out to be a very sensitive indicator of the strength and shape of this potential. But potentials are not the only source of modification to von Smoluchowski's original theory. The relative diffusion coefficient of equation [2.18] must also be modified since viscous forces oppose the approach of diffusing particles - especially at small separations. And of course one of the major points of this thesis is that fragmentation terms must be included in the coagulation equation if the change in shape of the cluster size distribution is to be explained. Only potentials and viscous interactions are considered in this Appendix.

To calculate the contribution of these effects, one must rewrite the diffusion equation to include the effect of inter-particle forces:¹

$$\frac{\partial \tilde{c}_j}{\partial t} = -\vec{\nabla} \cdot \vec{J} = \frac{1}{r^2} \frac{\partial}{\partial r} r^2 \left[D_{ij} \frac{\partial \tilde{c}_j}{\partial r} + \frac{D_{ij}}{kT} \frac{dV}{dr} \tilde{c}_j \right] \quad [A.1.1]$$

where $V(r)$ is the two-particle potential and $j(r)$ is given by:

$$j(r) = - \left[D_{ij} \frac{\partial \tilde{c}_j}{\partial r} + \frac{D_{ij}}{kT} \frac{dV}{dr} \tilde{c}_j \right] \quad [A.1.2]$$

For now I will use a general potential that goes to zero at infinite particle separation and is infinitely deep at $r = r_i + r_j$. Considering only stationary ($\partial \tilde{c}_j / \partial t = 0$) solutions to [A.1.1], which will be established over times on the order of $(r_i + r_j)^2 / D_{ij}$ (see [2.20]), we find after multiplying by r^2 and integrating once that

$$r^2 \left[D_{ij} \frac{\partial \tilde{c}_j}{\partial r} + \frac{D_{ij}}{kT} \frac{dV}{dr} \tilde{c}_j \right] = -r^2 j = \alpha \quad [A.1.3]$$

where α is an integration constant. This first order linear equation must be solved with the boundary conditions

$$V = -\infty, \quad \tilde{c}_j = 0 \quad \text{at } r = r_i + r_j \quad [A.1.4.a]$$

$$V = 0, \quad \tilde{c}_j = c_j \quad \text{at } r = \infty \quad [A.1.4.b]$$

The solution is

$$\tilde{c}_j = \alpha \int_{r_i+r_j}^r \frac{1}{D_{ij}} \frac{e^{V/kT}}{r^2} dr \quad [A.1.5]$$

with

$$\alpha = \frac{c_j}{\int_{r_i+r_j}^{\infty} \frac{1}{D_{ij}} \frac{e^{V/kT}}{r^2} dr}$$

So that the rate at which j -mers collide with a given i -mer is

$$-4\pi r^2 j = 4\pi\alpha = \frac{4\pi c_j}{\int_{r_1+r_j}^{\infty} \frac{1}{D_{ij}} \frac{e^{V/kT}}{r^2} dr} \quad [\text{A.1.6}]$$

Recognizing that $D_{ij}(\infty) = D_i + D_j$ and defining $s = r/r_1$, this equation becomes

$$-4\pi r^2 j = 4\pi D_{ij}(\infty) R_{ij} c_j / W \quad [\text{A.1.7}]$$

where

$$W = (1 + r_1/r_j) \int_{(1+r_1/r_j)}^{\infty} \frac{D_{ij}(\infty)}{D_{ij}} \frac{e^{V/kT}}{s^2} ds \quad [\text{A.1.8}]$$

and $R_{ij} = r_1 + r_j$, von Smoluchowski's sphere of influence.

Now, making von Smoluchowski's original assumption that collision rate is independent of i and j , we find the modified rate coefficient:

$$a_{ij} = A/W \quad [\text{A.1.9}]$$

where

$$W = 4D_1 \int_2^{\infty} \frac{1}{D_{11}} \frac{e^{V/kt}}{s^2} ds \quad [\text{A.1.10}]$$

and A is given in [2.23]. Since half-life is inversely proportional to A , it increases by a factor W , the stability factor. Von Smoluchowski gave the particles a square well interaction potential, with

infinite depth out to the sphere of influence, where it rises to zero. If the relative diffusion coefficient is also assumed constant, it is easy to verify that $W = 1$. Due to the complexity of the modern estimates of D_{11} and V , the integral in [A.1.10] is generally evaluated numerically.

The Interaction Potential

In the 1940's, Derjaguin and Landau² in the Soviet Union and Verwey and Overbeek³ in the Netherlands, simultaneously developed a quantitative model, based upon a superposition of electrostatic double-layer repulsion and van der Waals attraction, for the two-particle interaction potential. This model is commonly known as DLVO theory. Although continuum theories developed by Lifshitz⁴ and extended by Parsegian and Ninham⁵ show that the problem is rigorously a single electrostatics problem, the simpler phenomenological approach of DLVO theory has worked very well. The attractive potential falls off as an inverse power of particle separation and is essentially independent of ionic strength; whereas, the repulsive potential falls off exponentially over a Debye length, which varies inversely with ionic strength. Therefore, by adjusting electrolyte concentration, it is possible to mask or reveal the attractive force.

Hamaker⁶ first calculated the attractive potential V_A between two spheres, assuming strictly additive van der Waals potentials between pairs of molecules. He integrated the molecular potential given by

$$V_{\text{van der Waals}} = -\lambda/r^6 \quad [\text{A.1.11}]$$

where r is the distance between the molecules, over the volumes of two identical spheres of radius a to obtain

$$V_A = -A/6 \left[\frac{2a^2}{4aH+H^2} + \frac{2a^2}{(2a+H)^2} + \log \left[\frac{4aH+H^2}{(2a+H)^2} \right] \right] \quad [\text{A.1.12}]$$

where $A = \pi^2 q \lambda$, q is the number density of molecules in the spheres, and H is the shortest distance between the surfaces of the spheres (see Figure A.1.1).

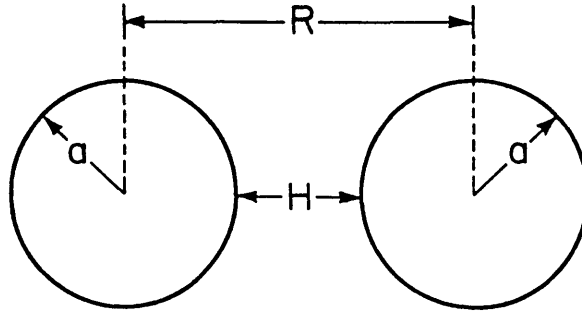


Figure A.1.1
Geometry for DLVO theory.

For small separations ($H/a \ll 1$), [A.1.12] becomes

$$V_A \simeq -Aa/12H \simeq 1/H \quad [\text{A.1.13}]$$

and for large separations ($R/a \gg 1$):

$$V_A \simeq -\frac{16}{9}A(a/R)^6[1 + 6(a/R)^2] \simeq -\frac{[qV_{\text{sphere}}]^2}{R^6} \lambda \quad [\text{A.1.14}]$$

as we would expect for point particles.

The value of the Hamaker constant A depends upon the material comprising the spheres and upon the solvent. Typically it is about 10^{-13} ergs. The most accurate estimates of A are obtained using Lifshitz theory^{4,5}

The repulsive force results from the surface charge that is found on most colloidal particles. This charge induces a double-layer of charge separation in ionic media near the surface. No exact formula for the charge distribution exists, but useful approximations have been made at low ionic strength for double-layers that are either very thick or very thin relative to the radius of the particle. In our system the double layer is thin:

$$a/\lambda_D \gg 1 \quad [\text{A.1.15}]$$

Here λ_D is the Debye length⁷ in the solvent:

$$\lambda_D = \left[\frac{8\pi e^2}{\epsilon kT} \frac{N_A}{1000} \frac{1}{2} \sum_i c_i z_i^2 \right]^{-1/2} \quad [\text{A.1.16}]$$

where e is the elementary charge (in electrostatic units), ϵ is the static dielectric constant of the solvent, N_A is Avogadro's number, c_i

is the concentration of ions i in moles/liter, and z_i is the charge on ions i . The quantity $1/2 \sum_i c_i z_i^2$ is known as the ionic strength. In our experiments total ionic strengths were roughly 1.0 mole/liter, giving a Debye length of 0.4 nm. Since sphere radius was approximately 225 nm, the approximation of thin double-layers is justified.

If we now specialize to the case of a single symmetric counter ion with valency z , the approximate repulsive potential is given by:³

$$V_R = \frac{ea}{2} \left[\frac{4kT\gamma}{ze} \right]^2 \log |1 + \exp(-H/\lambda_D)| \quad [A.1.17]$$

$$\text{or} \quad V_R = \frac{ea}{2} \left[\frac{4kT\gamma}{ze} \right]^2 e^{-H/\lambda_D} \quad [A.1.18]$$

$$\text{where} \quad \gamma = \tanh(z\phi e/4kT) \quad [A.1.19]$$

and ϕ is the surface potential of the spheres.

In the DLVO model the total interaction potential is simply a superposition of the attractive and repulsive potentials:

$$V = V_A + V_R \quad [A.1.20]$$

For analytical purposes this expression is useful, but physically it must be corrected because it leads to an infinite attraction as the spheres touch. This is accounted for in a rather ad hoc fashion by invoking the Born repulsion, which arises as the electronic shells of surface atoms interpenetrate.³ In fact, other difficulties with the theory also appear at small H ; the reader is referred to recent review

articles by Ninham⁸ and Overbeek⁹ for discussions of these.

Figures A.1.2, A.1.3, and A.1.4 depict the potential V at three increasing salt concentrations. At low concentrations (Figure A.1.2), the potential presents a barrier to coagulation. Still, if the height of the barrier is roughly the order of kT , a few particles will diffuse over it. This is the regime of so-called slow coagulation, where the stability factor W is greater than unity. The deep well near the origin and the shallow well just outside of the barrier are known as the primary and secondary minima, respectively.

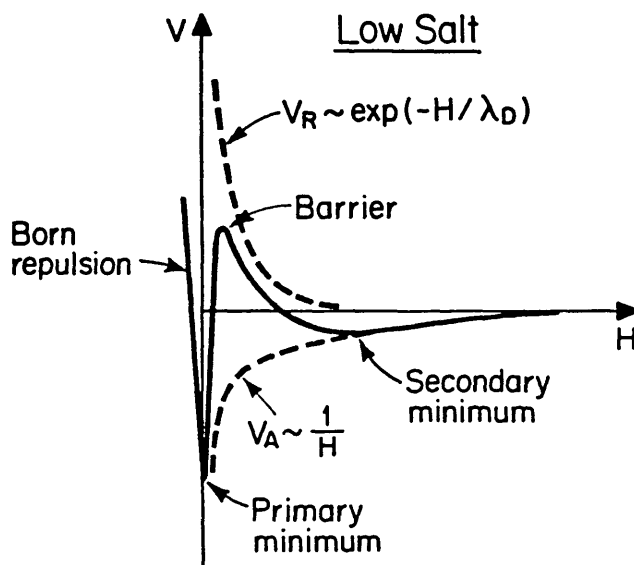


Figure A.1.2
The pair potential at low ionic strength.

The concentration at which the barrier disappears (Figure A.1.3)

is known as the critical coagulation concentration (c.c.c.), because at this point coagulation rate increases sharply to roughly its von Smoluchowski value (the regime of rapid coagulation).

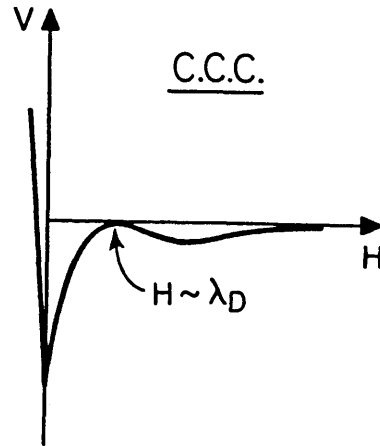


Figure A.1.3
The pair potential at the critical coagulation concentration.

The condition for this to occur is

$$V = 0 = dV/dH \quad [A.1.21]$$

Using the approximate expressions [A.1.13] and [A.1.18], we find that the maximum occurs at approximately $H = \lambda_D$:

$$V_{\max} \simeq -\frac{Aa}{12\lambda_D} + \frac{\epsilon a}{2} \left[\frac{4kT\gamma}{ze} \right]^2 \exp(-1) \quad [A.1.22]$$

Setting V_{\max} to zero, we find the c.c.c.:

$$\text{c.c.c.} = 49.6 \times 10^3 \frac{\epsilon^3 (kT)^5 \gamma^4}{N_A A^2} (ze)^{-6} \quad [\text{A.1.23}]$$

This z^{-6} dependence of the c.c.c. was one of the earliest phenomenological discoveries of colloid science and is known as the rule of Schulze and Hardy.³

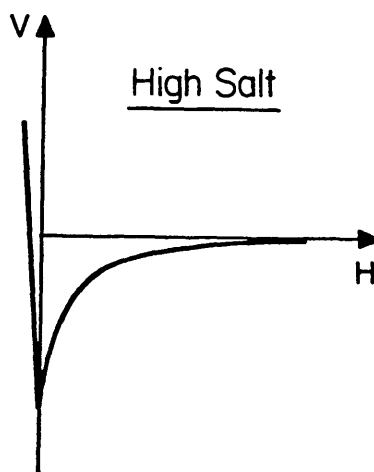


Figure A.1.4
The pair potential at high ionic strength.

In Figure A.1.4, high salt concentration has effectively shielded the surface charge so that all that remains is the van der Waals force. In this case, the attractive potential may be relatively long range, and stability factors may fall below unity: von Smoluchowski's

sphere of influence may extend beyond the radius of the sphere.

Accurate determination of W usually requires numerical integration. We can, however, estimate W at very low salt concentrations, where the interaction potential exhibits a definite peak (see Figure A.1.2). Note that V enters as an exponential factor in the integral expression [A.1.10] for W . Since the value of the integral is relatively insensitive to the pre-exponential factor $1/D_{11}$, we may approximate the factor $\exp(V/kT)$ as a delta function located at H_{\max} , and [A.1.10] becomes

$$\begin{aligned} W &\simeq 4D_1 \int_2^{\infty} \frac{1}{D_{11}} e^{V/kT} \delta(s-s_{\max}) \frac{ds}{s^2} \\ &\simeq 4 \frac{D_1}{D_{11}(s_{\max})} \frac{1}{s_{\max}^2} \exp\left[\frac{V_{\max}}{kT}\right] \end{aligned} \quad [A.1.24]$$

Substituting expression [A.1.21] for V_{\max} , we see that W has the form

$$W \simeq A' e^{-B'C^{1/2}} \quad [A.1.25]$$

where A' is a constant, C is salt concentration, and

$$B' = A/6 \left[\frac{2\pi e^2}{\epsilon kT} \frac{N_A}{1000} \right]^{1/2} \quad [A.1.26]$$

So, for small C :

$$\partial \log(W) / \partial \log(C) \simeq -\frac{1}{2} B' C^{1/2}$$

$$\approx -A/12 \left[\frac{2\pi e^2}{\epsilon kT} \frac{N_A}{1000} \right]^{1/2} az \left(1 + \frac{1}{2}C \right) \quad [A.1.26]$$

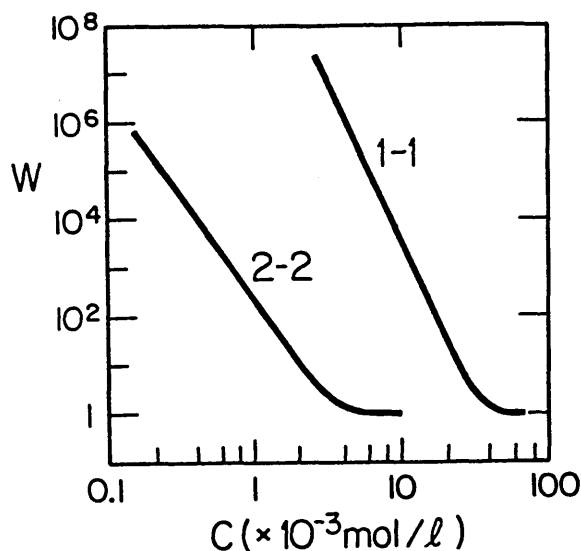


Figure A.1.5

A log-log plot of stability factor W versus salt concentration C . The two curves are identified by the valency of the ionic species giving rise to them.

The slope of a $\log(W)$ vs. $\log(C)$ curve is directly proportional to both sphere radius and z at low salt concentration.[†] Even though

[†] This is one of the few quantitative predictions of colloid stability theory that has not been substantiated experimentally. There is a question as to whether theory or experiment is to blame for this discrepancy.⁹ Since the experiments in question have been performed using bulk measurements of the dispersion, we expected that our single particle technique might help to answer this question. From a theoretical standpoint it may turn out that three body interactions are important, since recent experiments with unshielded latex spheres¹⁰ show that the locations and Brownian motions of dispersed particles may be highly correlated when long

larger clusters are not spherical, this radial dependence of W leads us to expect enhanced coagulation rate (or reactivity) at large cluster size with low salt. This would cause a_{ij} to depend upon i and j , thereby effecting the shape of the distribution. At high concentrations, V and W are both independent of concentration, and W approaches its rapid coagulation value of unity. With these two results, we are able to graph $\log(W)$ vs. $\log(c)$ (Figure A.1.5). The general shape of this curve has been confirmed in a number of systems.⁹

Viscous Interactions

Experimental values of the stability factor are important to condensed matter theory, because they test estimates of the Hamaker constant A . Until the introduction of viscous interactions by Spielman in 1970¹¹ and Honig et al. in 1971,¹² however, deduced values of A based solely upon DLVO theory were often greatly in error. The surprising accuracy of von Smoluchowski's coagulation time is based upon a cancellation of errors during rapid coagulation: repulsive viscous forces offset attractive van der Waals forces at close range.

The viscous correction is based upon an exact solution of Stokes's equations for the motion of two spherical particles in a viscous medium.¹³ With spherical particles, the relative radial motion decouples from the motion along other coordinates, and an exact form

range repulsive forces act between them.

for the relative diffusion coefficient may be found. The expression is rather complicated, but it is worth while here to summarize some of its important features.

At large separations, D_{ij} approaches its von Smoluchowski value $D_i + D_j$. At small separations ($H \rightarrow 0$) it approaches an asymptotic form estimated by lubrication theory:

$$D_{ij} \simeq \frac{kT(1 + r_i/r_j)^2 H}{6\pi\eta r_i^2} \quad [\text{A.2.28}]$$

and it varies monotonically between these two limits. The fact that D_{ij} goes to zero as the particles approach each other indicates an effectively infinite viscous force at close range. In this ideal model, the particles would never touch, but in a real physical system, non-Newtonian fluid effects remove the singularity.

The effect of hydrodynamic forces is particularly important in slow coagulation. In this regime, the viscous correction to classical DLVO theory involves a simple factor of $D_{11}(s_{\max})$ as seen in Equation [A.2.24].¹¹

Bond Strength

As I show in section 2.2.1.1, bond strength is an important parameter in Flory-Stockmayer theory. In this theory, one first

assumes that bond strength is finite and then assumes that each new particle binding to a cluster produces the same change in the free energy of the system. It is difficult to examine the second assumption in the context of colloid stability theory, because of the complications of entropy, the ad hoc nature of the Born force, and the effect of non-spherical clusters; but, it is possible to probe bond strength.

The finite strength of the bonds will be felt at high states of aggregation. According to Flory-Stockmayer theory, the shape of the equilibrium cluster size distribution may provide a quantitative estimate of that strength. According to DLVO theory, it is also possible to estimate the bond strength by lowering the salt concentration in a previously flocculated system. At very low salt concentrations - much lower than the c.c.c. - the repulsive force may become strong enough to remove the primary minimum altogether, in which case clusters will dissociate.¹⁴ This is known as reptization.

As I have stated, irreversible coagulation corresponds to effectively infinite bond strength. The reason that von Smoluchowski's irreversible theory has become so firmly entrenched in colloid science is that bonds in the primary minimum of the interaction potential (Figure A.1.2) are strong enough that little dissociation occurs during the early stages of aggregation. In fact, flocculation in the primary minimum is commonly called irreversible flocculation.

Flocculation in the secondary minimum is known as reversible flocculation. Once a system of this sort has reached equilibrium it is possible to change the degree of aggregation simply by adjusting particle concentration.³ Since it is clear that this process does reach

equilibrium, reversible flocculation presents an interesting system for study.

REFERENCES

1. Fuchs, N.A., Z. Physik, **89**, 763 (1934).
2. Derjaguin, B.U. and Landau, L., Acta Physiochim. URSS, **14**, 633 (1941).
3. Verwey, E.J. and Overbeek J. Th. G., "Theory of the Stability of Lyophobic Colloids", Elsevier, Amsterdam, 1948.
4. Lifshitz, E.M., Dokl. Akad. Nauk. SSSR, **97**, 643 (1954).
5. Parsegian, V.A. and Ninham, B.W., Nature, **224**, 1197 (1969).
6. Hamaker, H.C., Rec. Trav. Chim., **55**, 1015 (1936) **56**, 3 (1937).
7. Debye, P., and Huckel, E., Physik, Z., **24**, 185 (1923).
8. Ninham, B.W., Adv. Colloid Interface Sci., **16**, 1 (1982).
9. Overbeek, J. Th. G., Adv. Colloid Interface Sci., **16**, 17 (1982).
10. Pusey, P.N. and van Megen, W., J. Physique, **44**, 285 (1983).
11. Spielman, L.A., J. Colloid Interface Sci., **38**, 376 (1972).
12. Honig, E.P., Roeberson, G.J. and Wiersema, P.H., J. Colloid Interface Sci., **36**, 562 (1971).
13. Stimson, M., and Jeffery, G.B., Proc. Roy. Soc. London Ser. A, **111**, 110 (1926).
14. Frens, G. and Overbeek, J. Th. G., J. Colloid Interface Sci., **36**, 286 (1971).

APPENDIX II

SOLUTION OF CASE A WITH ARBITRARY INITIAL CONDITIONS

Since it is difficult to produce strictly monomeric samples, I present here a solution to the irreversible coagulation equations with a constant association kernel and an arbitrary initial cluster size distribution. I follow the usual approach of first solving for the zeroth moment M_0 and then finding the cluster size distribution by iteration. In this case the coagulation equations become

$$\frac{dc_n}{dt} = 1/2 \sum_{k=1}^{n-1} A c_{n-k} c_k - \sum_{k=1}^{\infty} A c_n c_k \quad [\text{A.2.1}]$$

with $c_n(t=0) \equiv c_n^0$.

Summing over n and changing the order of summation and differentiation:

$$\frac{d}{dt} \sum_{n=1}^{\infty} c_n = \frac{A}{2} \sum_{n=1}^{\infty} \sum_{k=1}^{n-1} c_{n-k} c_k - A \sum_{n=1}^{\infty} c_n \sum_{k=1}^{\infty} c_k \quad [\text{A.2.2}]$$

With the identity

$$\sum_{n=1}^{\infty} \sum_{k=1}^{n-1} c_{n-k} c_k = \sum_{n=1}^{\infty} c_n \sum_{k=1}^{\infty} c_k \quad [\text{A.2.3}]$$

this becomes

$$\frac{dM_0}{d\tau} = -M_0^2 \quad [\text{A.2.4}]$$

$$\text{where} \quad \tau = At/2$$

In the case of diffusion controlled coagulation $\tau = (4kT/3\eta)t$ (see [2.24]). M_0 is just the total concentration of clusters of all sizes. The solution to [A.2.4] is

$$M_0(\tau) = \frac{M_0^0}{1 + M_0^0 \tau} \quad [\text{A.2.5}]$$

where $M_0^0 = \sum_n c_n^0$. To find $c_1(\tau)$ we return to [A.2.1]:

$$\frac{dc_1}{d\tau} = -2c_1 M_0 \quad [\text{A.2.6}]$$

Using the explicit expression [A.2.5] for M_0 and separating variables:

$$\frac{dc_1}{c_1} = -2 \frac{M_0^0}{1 + M_0^0 \tau} d\tau \quad [\text{A.2.7}]$$

Integrating with the appropriate initial conditions we find $c_1(\tau)$:

$$c_1(\tau) = \frac{c_1^0}{(1 + M_0^0 \tau)^2} \quad [\text{A.2.8}]$$

The expressions for $M_0(\tau)$ and $c_1(\tau)$ can be used to find $c_2(\tau)$.

With [A.2.1]:

$$\frac{dc_2}{d\tau} = c_1^2 - 2c_2M_0 \quad [A.2.9]$$

Upon substitution this becomes

$$\frac{dc_2}{d\tau} + \frac{2M_0^0}{1 + M_0^0\tau} c_2 = \frac{c_1^{02}}{(1 + M_0^0\tau)^4} \quad [A.2.10]$$

This first order linear equation may be solved straightforwardly, and after some algebra:

$$c_2(\tau) = \frac{c_2^0}{(1 + M_0^0\tau)^2} + \frac{c_1^{02}}{(1 + M_0^0\tau)^3} \tau \quad [A.2.11]$$

In the same fashion we can find $c_3(\tau)$:

$$c_3(\tau) = \frac{c_3^0}{(1 + M_0^0\tau)^2} + \frac{2c_1^0c_2^0}{(1 + M_0^0\tau)^3} \tau + \frac{c_1^{03}}{(1 + M_0^0\tau)^4} \tau^2 \quad [A.2.12]$$

After a few more iterations, which, naturally, get more complicated at each step, one soon convinces oneself that the general solution for $c_n(\tau)$ is:

$$c_n(\tau) = \frac{c_n^0}{(1 + M_0^0 \tau)^2} + \frac{\sum_{i+j=n} c_i^0 c_j^0}{(1 + M_0^0 \tau)^3} \tau + \frac{\sum_{i+j+k=n} c_i^0 c_j^0 c_k^0}{(1 + M_0^0 \tau)^4} \tau^2 + \dots$$

$$+ \frac{c_1^0{}^n}{(1 + M_0^0 \tau)^{n+1}} \tau^{n-1} \quad [A.2.13]$$

This result can be understood in the following way. For monodisperse initial conditions ($c_n^0 = c_0 \delta_{n,1}$) all terms but the last drop out of [A.2.13] giving

$$c_n(\tau) = \frac{c_0^n}{(1 + c_0 \tau)^{n+1}} \tau^{n-1} \quad [A.2.14]$$

Each term in [A.2.13] has this precise form, except that the numerator c_0^k becomes a sum over all possible combinations of particles that would add up to an n-mer. The first term, which is strictly decreasing in time, looks exactly like $c_1(\tau)$ in the monodisperse case (Table 2.1). It traces the disappearance of the c_n^0 original n-mers as they combine with other particles and with each other to make larger clusters. The higher order terms can be looked upon as contributions to the formation of n-mers by the aggregation of two original clusters, three original clusters, etc.; each term looks like its monodisperse counterpart, because with this kernel all clusters behave identically as far as coagulation is concerned. In a certain sense, the second term describes doublet formation, the third triplet formation, and so on; so that, in retrospect, we could almost have written down the polydisperse solution immediately after solving the monodisperse case.

Appendix III

COINCIDENCE ANALYSIS

If two particles pass through the scattering volume at the same time they will be counted as one particle. It seems intuitively obvious that a significant number of these coincidences will occur if the average volume per particle in solution is roughly equal to the scattering volume. The purpose of this appendix is to investigate this question quantitatively. I follow the approach of von Schultess.¹

To determine the probability that a particular pulse is a coincidence, I first define τ as the transit time of a particle through the scattering volume and $t_0 \equiv 1/\alpha$ as the average time between pulses. First we need the probability $p(n, \alpha\tau)$ that n clusters enter the scattering volume within a time τ of a certain 'test particle'. Since uncorrelated arrival times of this sort are a Poisson process, this probability is given by²

$$p(n, \alpha\tau) = \frac{(\alpha\tau)^n}{n!} e^{-\alpha\tau} \quad [\text{A.3.1}]$$

The probability that no other particle enters the scattering volume while the test particle passes through it will be given by $p(0, \alpha\tau)$:

$$p(0, \alpha\tau) = e^{-\alpha\tau} \quad [\text{A.3.2}]$$

The total probability that there is no coincidence must also include the possibility that the test particle itself may have entered the scattering volume before the proceeding particle left it. Hence [A.3.2] must be squared to give the probability that the test particle is not involved in a coincidence:

$$p(\text{no coincidence}) = e^{-2\alpha\tau} \quad [\text{A.3.3}]$$

We might arbitrarily choose an average of one coincidence every 1000 counts as an acceptable level; then

$$\begin{aligned} p(\text{coincidence}) &= 1 - p(\text{no coincidence}) \\ &= 1 - e^{-2\alpha\tau} < 1/1000 \end{aligned} \quad [\text{A.3.4}]$$

Expanding the exponential to first order:

$$\alpha\tau < 1/2000 \quad [\text{A.3.5}]$$

We can also look at the dimensionless quantity $\alpha\tau$ in another way. First define the flow rate Q (cc/sec), scattering volume V_s (cc), and the particle concentration C (particles/cc). The concentration C is the zeroth moment of the cluster size distribution, not the total concentration of monomeric spheres. Clearly,

$$V_s = Q\tau \quad [A.3.6]$$

and $\alpha = t_o^{-1} = QC \quad [A.3.7]$

Thus $\alpha\tau = V_s C \quad [A.3.8]$

From [A.3.5] we see that the maximum observable particle concentration is inversely proportional to the size of the scattering volume, which is intuitively reasonable. Since typical scattering volumes in our instrument are roughly 10^{-9} cc, the maximum observable particle concentration is roughly $10^6/\text{cc}$.

REFERENCES

1. von Schulthess, G.K., Ph.D. Thesis, M.I.T. (unpublished), 1979, p. 169 ff.
2. Villars, F.M.H. and Benedek, G.B., "Physics with Illustrative Examples from Medicine and Biology", Vol. 2, Addison-Wesley, Reading, 1974.

Mark Stander Bowen was born November 23, 1954 in New York, New York. He grew up in Port Chester and Rye, New York and graduated from the Rye Country Day School in 1972. After four years of travelling and working odd jobs in construction, he entered college: first the New School for Social Research in New York City, where he focussed upon creative writing, then Columbia University, and finally the Massachusetts Institute of Technology, where he graduated with a bachelor's degree in physics in 1980. In the same year he married Craigen Weston, a conservator of works of art on paper. They presently live in Newton, Massachusetts.

Publications

- "Experimental Analysis of Diffusion Controlled Coagulation Using an Optical Pulse Partical Size Analyser", M.S. Bowen, M.L. Broide, and R.J. Cohen, in "Kinetics of Aggregation and Gelation", F. Family and D.P. Landau, eds., North Holland, Amsterdam (1984).
- "Temporal Evolution of the Cluster Size Distribution During Brownian Coagulation", M.S. Bowen, M.L. Broide, and R.J. Cohen, Journal of Colloid and Interface Science, in press.
- "Determination of Cluster Size Distributions Using an Optical Pulse Particle Size Analyser", M.S. Bowen, M.L. Broide, and R.J. Cohen, Journal of Colloid and Interface Science, in press.